

Integrated Measurements of Stress, Motion Capture and Environmental Parameters for Ambient Assisted Living Scenarios



Matteo Zanetti

Supervisors: Prof. M. De Cecco

Prof. G. Nollo

Department of Industrial Engineering
University of Trento

This dissertation is submitted for the degree of

Doctor of Philosophy

June 2019

I would like to dedicate this thesis to my grandparents Stefano and Maria.

Declaration

I hereby declare that except where specific reference is made to the work of others, the contents of this dissertation are original and have not been submitted in whole or in part for consideration for any other degree or qualification in this, or any other university. This dissertation partially includes scientific articles of which I am a co-author and that were published in journals or presented at international conferences. This dissertation contains fewer than 65,000 words including appendices, bibliography, footnotes, tables and equations and has fewer than 150 figures.

Matteo Zanetti
June 2019

Acknowledgements

Firstly, I would like to express my sincere gratitude to my supervisors Prof. Mariolino De Cecco and Prof. Giandomenico Nollo for bringing me into direct with the research world. Thanks for their patience, motivation, and immense knowledge. Their guidance helped me in all the time of research and writing of this thesis.

Besides my supervisors, I would like to thank Prof. Luca Faes for teaching me everything I know about Network Physiology and Information Dynamics.

I would also like to thank the occupational therapists of Villa Rosa led by Dr. Giovanni Guandalini. They provided insight and expertise that greatly assisted my research.

A special thanks to Alberto, Paolo, and Martina with whom I have enjoyed the closest possible cooperation during the AUSILIA project and my PhD. It was a pleasure working with them.

I also want to thank all the other members of the Measurements Instrumentations and Robotics (MIRO) lab: Mattia, Nicola, and Alessandro. I want to make special mention of Luca with whom I shared many moments of my university life and beyond. Thanks for his friendship.

I am also grateful to all my friends who have supported me along the way and in difficult times. In particular, the “Renault 5 Official Group” for the endless Saturday nights and Jacopo, Paola and Stefano for the magnificent trip in New York.

I would like to thank my parents Gianpaolo and Silvana and my brother Davide for supporting me spiritually throughout writing this thesis and my life in general.

Last but not least, I would like to spare a thought for my grandparents Maria and Stefano, who left me during the years of my PhD. They will be always in my heart.

Abstract

Chronic diseases and their consequent impairment of the cognitive and motor functions are becoming considerable problems for modern societies that are undergoing rapid demographic changes. Advanced technologies are supposed to be determinant to enable new services and provide assistive devices for patient home care. However, the real-life applicability of these technologies needs to be proved in real settings and their efficacy needs to be tested as regards the environment and patient. In this context, accurate measurement of stress and effort (performed at any level, i.e., muscular, cardiovascular, or cerebral) combined with the subject behaviour (motion of the subject while interacting with the assistive device) and the environment status is determinant for assessing the cost/benefit ratio of each specific assistive technology. The final goal of this project was the implementation of a multi-sensorial platform able to collect multivariate biological signals, motion capture, and environment-related interaction parameters and to elaborate them to provide physicians with a measurable indicator of the user point of view and performances achievable. Operating in the context of integrated system physiology, evaluation of effort and adaptation to a task are assessed as whole on the entire body response thus providing a holistic estimation of potential improvement of life condition.

The following thesis partially includes scientific articles that were published in journals [55, 180] or presented at international conferences [33, 179, 54]. These articles, which partially summarize the work carried out during my PhD, were here revised and presented organically to the reader. Part of the work presented in this thesis was developed inside the AUSILIA project financed by Provincia Autonoma di Trento and partially developed with the support of the IEEE Smart Cities Initiative - Student Grant Program.

Table of contents

| | |
|--|-------------|
| List of figures | xiii |
| List of tables | xvii |
| Nomenclature | xix |
| 1 Introduction | 1 |
| 1.1 Motivation | 1 |
| 1.2 Health in smart cities | 3 |
| 1.3 Ambient Assisted Living | 5 |
| 1.4 Occupational therapy | 6 |
| 1.5 The AUSILIA project | 8 |
| 1.5.1 The measurement framework | 10 |
| 1.5.2 The protocol | 14 |
| 1.5.3 Project impact | 16 |
| 2 Supporting technologies | 19 |
| 2.1 Wearable devices | 19 |
| 2.1.1 Used wearable equipment | 20 |
| 2.1.2 Synchronization of the devices | 21 |
| 2.2 Environmental monitoring | 25 |
| 2.2.1 Weight distribution | 25 |
| 2.2.2 Local pressure | 26 |
| 2.2.3 Inertial measurement unit | 28 |
| 2.2.4 Load cell | 29 |
| 2.2.5 Flow-meter | 30 |
| 2.3 Motion capture system | 31 |
| 2.3.1 Calibration framework | 36 |

| | | |
|----------|---|------------|
| 3 | Stress assessment | 55 |
| 3.1 | The mechanism of stress | 55 |
| 3.2 | Physiological measures for stress detection | 56 |
| 3.2.1 | Cardiovascular system activity | 58 |
| 3.2.2 | Respiratory system activity | 61 |
| 3.2.3 | Electrodermal activity | 62 |
| 3.2.4 | Muscle activity | 63 |
| 3.2.5 | Cerebral activity | 64 |
| 3.3 | The Network Physiology paradigm | 65 |
| 3.4 | Data acquisition | 67 |
| 3.5 | Time series extraction | 68 |
| 3.6 | Information Dynamics during different levels of mental stress | 73 |
| 3.6.1 | Information decomposition | 73 |
| 3.6.2 | Statistical analysis | 77 |
| 3.6.3 | Results | 78 |
| 3.6.4 | Information produced and stored in the nodes of the human physiological network | 86 |
| 3.6.5 | Information transfer across the nodes of the human physiological network | 87 |
| 3.7 | Stress classification | 89 |
| 3.7.1 | Results | 91 |
| 4 | Virtual Reality interface | 97 |
| 4.1 | Reality-virtuality continuum | 97 |
| 4.2 | Mixed Reality in healthcare systems | 98 |
| 4.3 | Possible means to provide VR for occupational therapy | 99 |
| 4.4 | Integration of body and environmental data | 103 |
| 4.4.1 | Magnification | 107 |
| 4.4.2 | Direct time management | 109 |
| 4.4.3 | Average trend | 109 |
| 4.4.4 | Potential of the proposed solution | 110 |
| 5 | Conclusion and future developments | 111 |
| | References | 115 |

List of figures

| | | |
|------|---|----|
| 1.1 | World population aged 60-79 years and aged 80 years or over in 2000, 2015, 2030 and 2050. | 2 |
| 1.2 | The user-centred design model. | 5 |
| 1.3 | The domotic apartment inside the Villa Rosa Hospital. | 10 |
| 1.4 | The living lab with different reconfigurable environments. | 11 |
| 1.5 | Framework, sensing infrastructure of the apartment. | 12 |
| 1.6 | Framework, interconnection and management structure. | 13 |
| 1.7 | Framework, data visualization. | 14 |
| 1.8 | The AUSILIA paradigm inside the de-hospitalization process. | 16 |
| 2.1 | The potential given by technology for health monitoring. | 20 |
| 2.2 | Wearable devices used to acquire the physiological signals. | 22 |
| 2.3 | Used wearable devices connected to a rigid bar for time synchronization. . . | 23 |
| 2.4 | Temporal synchronization of the wearable devices by mean of the acceleration signals. | 24 |
| 2.5 | Pressure sensor matrix used to monitor the weight distribution. | 26 |
| 2.6 | Local pressure sensors. | 27 |
| 2.7 | IMU installed under a glass. | 28 |
| 2.8 | The installed load cell. | 29 |
| 2.9 | The installed flow-meters. | 30 |
| 2.10 | The Kinect V2 camera. | 31 |
| 2.11 | The layout of the domotic apartment showing where the Kinect cameras have been installed. | 32 |
| 2.12 | Example of the motion capture setup. | 33 |
| 2.13 | NTP vs. device internal time. | 35 |
| 2.14 | Behaviour of retro-reflective surfaces in the infrared and depth domain. . . | 39 |
| 2.15 | Example of first RGB-D image from each calibration set used for colour initialization. | 40 |

| | | |
|------|---|-----|
| 2.16 | Manual initialization of the circular ROI. | 41 |
| 2.17 | Models used for the definition of spatial uncertainty. | 44 |
| 2.18 | Spatial distribution of the uncertainties. | 45 |
| 2.19 | Result of RANSAC fitting. | 46 |
| 2.20 | Identified trajectories of the calibration tool and covariances. | 47 |
| 2.21 | Trajectory projection to FoV invariant kernel and synchronization in frame domain. | 49 |
| 2.22 | Graph structure for a set of N devices. | 51 |
| 2.23 | Alignment of the trajectories resulting from graph optimization. | 52 |
| 2.24 | Example of the acquisition sequence of a moving subject. | 54 |
| | | |
| 3.1 | Function of the autonomic nervous system. | 57 |
| 3.2 | ECG signal. | 59 |
| 3.3 | An example of a tachogram. | 59 |
| 3.4 | Comparison between a PSD of an RR time series during rest and during mental arithmetic. | 60 |
| 3.5 | An example of a respiratory signal acquired by a piezoresistive sensor. | 62 |
| 3.6 | SC signal. | 63 |
| 3.7 | The network physiology perspective. | 66 |
| 3.8 | Schematic representation of the experimental protocol adopted. | 68 |
| 3.9 | Time series extraction procedure from the acquired physiological signals. | 69 |
| 3.10 | ECG, respiratory signal and BVP acquired from the wearable sensors. | 70 |
| 3.11 | RR interval, respiratory and PAT time series measured for a representative subject. | 71 |
| 3.12 | Brain wave amplitude. | 72 |
| 3.13 | Boxplots of the information storage S_j | 79 |
| 3.14 | Boxplots of the new information N_j | 81 |
| 3.15 | Boxplots of the total information transfer T_j | 83 |
| 3.16 | Information transfer for the cardiorespiratory-brain network using the conditional information transfer $T_{i \rightarrow j k}$ | 85 |
| 3.17 | Classification results for different classifiers. | 92 |
| 3.18 | Classification results for different classifiers without EEG. | 95 |
| | | |
| 4.1 | Reality-virtuality continuum. | 97 |
| 4.2 | Domotic scenario with the following relevant data acquired: patient shape, motion (estimated via skeletonization), pressure on the floor. | 100 |
| 4.3 | Different viewpoints available in 3D. | 102 |

| | | |
|-----|--|-----|
| 4.4 | Comparison of occupational therapy support/interaction. | 104 |
| 4.5 | The general scheme of the developed GUI. | 106 |
| 4.6 | Examples of GUI in action for the augmented virtualized visualization of hidden physical variables. | 108 |

List of tables

| | | |
|-----|---|----|
| 1.1 | Overall clinical observation requirements. | 15 |
| 2.1 | Wearable sensors characteristics. | 20 |
| 2.2 | Coefficients of the semi-lobes. | 43 |
| 2.3 | Identified extrinsic parameters and uncertainties (3σ , 99 % ci). | 53 |
| 3.1 | Time series and information dynamic indices analysed. | 77 |
| 3.2 | Median values of S_j for the seven time series under consideration during rest (REST), mental arithmetic (MA), and serious game (SG). | 80 |
| 3.3 | Median values of N_j for the seven time series under consideration during rest (REST), mental arithmetic (MA), and serious game (SG). | 82 |
| 3.4 | Median values of T_j for the seven time series under consideration during rest (REST), mental arithmetic (MA), and serious game (SG). | 84 |
| 3.5 | Top 10 feature importance of Random Forest classifier. | 93 |
| 3.6 | Feature importance of Random Forest classifier without Emotive EPOC features. | 94 |
| 3.7 | Comparison of the obtained results with respect to similar works in the literature. | 96 |

Nomenclature

Acronyms / Abbreviations

AAL Ambient Assisted Living

ABP Arterial Blood Pressure

ADL Activity of Daily Living

AIC Akaike Information Criterion

AMPS Assessment of Motor and Process Skills

AR Augmented Reality

AV Augmented Virtuality

BP Blood Pressure

BVP Blood Volume Pulse

DFA Detrended Fluctuation Analysis

ECG Electrocardiogram

EDA Electrodermal Activity

EEG Electroencephalogram

EMG Electromyography

FoV Field of View

GSR Galvanic Skin Response

HF High Frequency

| | |
|-------|--|
| HRV | Heart Rate Variability |
| ICT | Information and Communications Technology |
| IMU | Inertial Measurement Unit |
| IoT | Internet of Things |
| LF | Low Frequency |
| LPP | Lagged Poincaré Plot |
| LR | Logistic Regression |
| MA | Mental Arithmetic |
| MR | Mixed Reality |
| NTP | Network Time Protocol |
| OT | Occupational Therapy |
| PAT | Pulse Arrival Time |
| PPG | Photoplethysmographic |
| PQRS | Performance Quality Rating Scale |
| PSD | Power Spectral Density |
| REST | Rest |
| RF | Random Forest |
| RMS | Root Mean Square |
| RMSSD | Root Mean Square of the Successive Differences |
| RQA | Recurrence Quantification Analysis |
| RSA | Respiratory Sinus Arrhythmia |
| SCL | Skin Conductance Level |
| SCR | Skin Conductance Response |
| SC | Skin Conductance |

SDNN Standard Deviation of Normal-to-Normal intervals

SFS Shape-From-Silhouette

SG Serious Game

SMNA Sudomotor Nerve Activity

SVC Support Vector Classification

SVD Singular Value Decomposition

SVM Support Vector Machine

TEB Thoracic Electrical Bioimpedance

ToF Time of Flight

VE Virtual Environment

VH Visual Hull

VR Virtual Reality

WWS Wearable Wellness System

Chapter 1

Introduction

1.1 Motivation

The demographic studies underline how life expectancy has increased significantly, thanks to higher life quality and the progress in the medical field. According to [157], the number of people in the world aged 60 years or over is projected to grow by 56% from 901 million to 1.4 billion between 2015 and 2030. By 2050, the global population of older people is projected to more than double its size in 2015, reaching nearly 2.1 billion. Projections [158] indicate that in 2050 the number of people aged 80 years or over in the world will be 434 million. Such a number is more than triple concerning 2015 when there were 125 million people over age 80 (Fig. 1.1). This phenomenon is leading to an exponential growth of chronically ill people with disabilities at the motor and/or cognitive level, accompanied by progressive lengthening of life expectancy in chronic conditions and disabilities. For this reason, there is a rapid increase in demand for healthcare, while healthcare systems are facing the depletion of resources. For these reasons, a major challenge is to ensure equity of access to healthcare services for everyone. There is, therefore, a need for low-cost and efficient solutions without compromising care.

Elderly people that are fragile and characterized by reduced independence need assistance by families and, in the worst cases, hospitalization in specialized structures. The result is an overload of the social assistance system. This is partly due to the fact that the patient's house is not sufficiently safe and is not able to send to the caregiver emergency signals in case of need. It also does not facilitate the social inclusion of the person and his/her family, causing progressive isolation. These conditions imply depression and a spirit of renunciation, leading to a higher burden on the social assistance system. For these reasons, the problem is to give back to the person the most possible self-sufficiency. In this scenario, technology plays

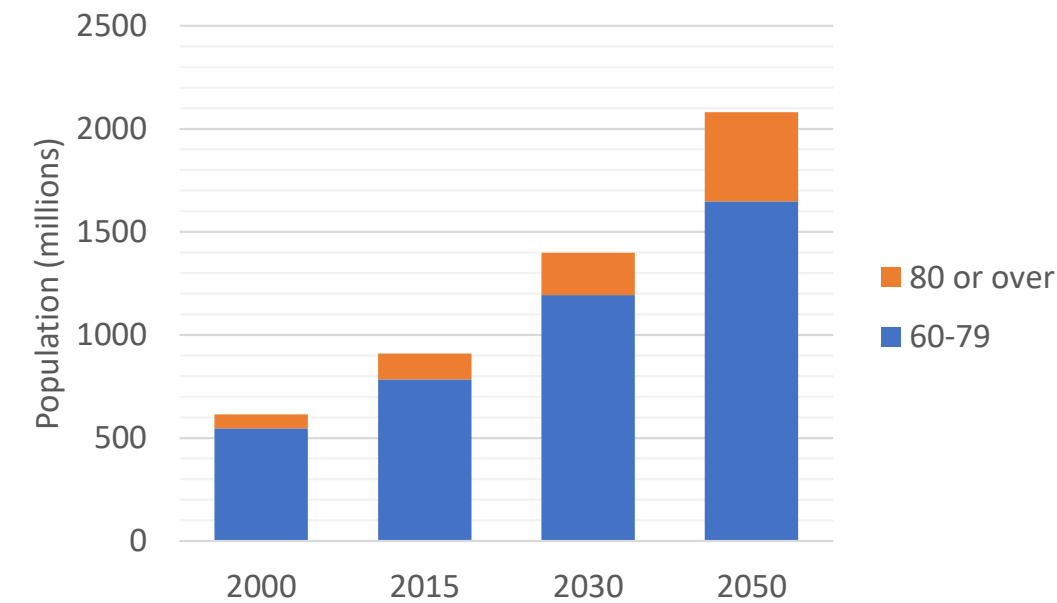


Fig. 1.1 World population aged 60-79 years and aged 80 years or over in 2000, 2015, 2030 and 2050 [158].

an important role, making available solutions and aids. It can compensate for the limited abilities of the user, enhancing the residual capabilities.

The development of assistive technologies is an issue that in recent years has received wide interest [62]. Besides problems and risks intrinsic in the application of devices and new procedures in hospital settings, the proposed technologies should be assessed concerning their impact and acceptability by users, relatives, and caregivers. Indeed, testing of the interaction of these technologies with the patient and his/her living environment is a poorly developed area. Furthermore, the identification of solutions capable to solve the specific needs of a patient is still an unresolved issue. An accurate assessment of patient status and needs is also required, both from a physical and cognitive point of view. Also, assistive technology should be customized on personal needs and wishes and a range of new services designed to encourage healthy lifestyles and an active ageing process should be created [56]. This thesis tries to answer to these emerging needs, presenting an innovative framework for testing aids and therapies in real settings, providing to clinicians and caregivers a measurable indicator of the performance achievable by users, with special regard to their point of view in the usage of the various aids. For this reason, part of this thesis focuses on studies relative to physiological stress assessment and the development of algorithms for stress detection. An innovative manner for presenting all the acquired data to clinicians was also developed based on Virtual Reality (VR) technologies that will be presented in Ch. 4.

1.2 Health in smart cities

As stated in [173], a “smart community” is “a community in which government, business, and residents understand the potential of information technology, and make a conscious decision to use that technology to transform life and work in their region in significant and positive ways”. In the field of health, this concept can be translated into structures, processes and social behaviours that act to improve the health of community and well-being. Health systems have to assure dignity, autonomy, and independence for a longer time to frail and ageing citizens. Indicators of “smartness” are quality of life, access to high-quality healthcare services, remote healthcare monitoring, and home automation to improve autonomy. It is important to develop a citizen-centred innovation system, in which citizens play an active role. They have to be aware of services they have the right to expect, having a simple interaction even with complex structures.

A first step is to align the health system to the new age-related challenges, developing and ensuring access to services for older people and training an appropriate health workforce. There is a need to develop long-term care services, ensuring quality and improving the autonomy of patients. To achieve these goals, it is important to improve measuring, monitoring, and understanding of healthy ageing, relying on agreed metrics and using analytical approaches.

A key factor for assuring autonomy and dignity to frail individuals is their home environment. In this context, ICTs can play an important role in providing new forms for communication and interaction and developing new assistive tools. The proper use of ICT in this context can significantly contribute to the reduction of costs and increase efficiency.

ICT technologies help to eliminate distance and may allow access to medical services, otherwise inaccessible to distant rural communities. One of the results is telemedicine, which is the use of telecommunication and information technology to provide clinical healthcare at a distance. Mobile technology can allow healthcare professionals to share information and discuss patient issues as if they were in the same place. Moreover, remote patient monitoring can reduce outpatient visits and enable remote prescription verification and drug administration oversight. All of this could result in a reduction of costs for the healthcare system. The drawbacks are the necessity to have specialized staff in the use of technology and the risk to decrease the human interaction between patients and medical professionals.

Internet of Things (IoT) made possible the connection between objects and people. The connection with the network allows objects to take a proactive role and enable new possibilities for detection, remote control, and monitoring. Examples of applications in healthcare are the management of medical devices, i.e. the precise location of the devices, state of use, level of obsolescence, maintenance status, and functional verification. Moreover,

Internet-connected devices can help to reduce the need for direct patient-clinician interaction and the caregivers can focus better their effort: for example, IoT technology can be used to track health information, such as electrocardiograms, body temperature or blood glucose level. These technologies facilitate also the replica of the hospital environment in the patient's home.

New technologies such as virtual, augmented reality and serious game applications find increasing expressions in healthcare. Examples of applications are in the medical simulation, telemedicine, medical and healthcare training, pain control, visualization aid for surgery, rehabilitation and promotion of healthy lifestyles. Besides the use of virtual reality, the modelling of biological phenomena is widely used as an aid for better understand the disease, interaction and plan possible interventions.

In the current years, there has been a shift to a patient-centred care approach and the interest in health in the population is growing. The increase in technology is transforming the entire healthcare industry, which has to reassess its business models.

Social media are offering a great opportunity to improve information and support from healthcare entities. Furthermore, there is an increase in data demands by clinicians and administrative leaders to optimize patient care. Data sharing could bring innovation and better communication among healthcare services: the analysis of such data can allow to identify common health needs and help to create innovative solutions. In this context, particular attention must be paid to privacy concerns and data security, avoiding misuse of private health data.

In the design process of new technologies and services, the user gained a central role in the last years. The user-centred approach (Fig. 1.2) allowed to develop systems that better-matched users' needs, improving the user experience. In this kind of approach, the focus is on the product or service being designed and the aim is to ensure that the users' requirements are fulfilled. In the user-centred approach, the design of the product is conducted by researchers and professionals and the user's needs are investigated through interviews, researches, and observations. In the current years, we are seeing a shift toward a participatory design approach, in which the attitude changes from design for users to design with users [6]. In this new approach, the user is asked to participate proactively in the design development processes, taking an active role in the group of stakeholders. As reported in [127], the relationship between clinicians and patients is changing. The patient is becoming an active partner that wants to be involved and influence his/her treatment and care. Participatory design in the field of healthcare allows achieving more effective services and sustainable programs, improving user's satisfaction.

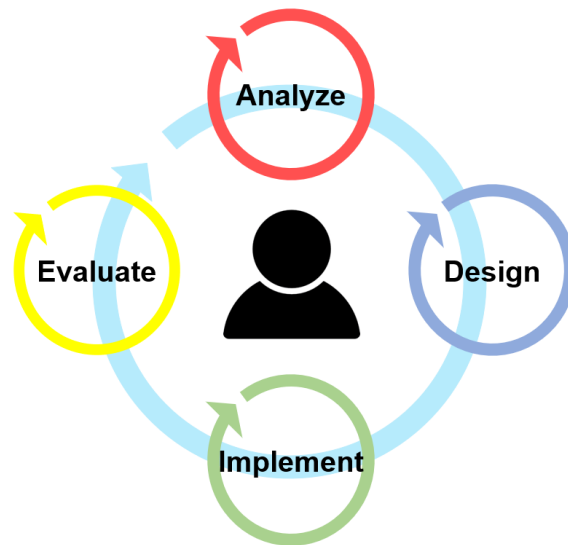


Fig. 1.2 The user-centred design model. An iterative design process in which designers focus on the users and their needs in each phase of the design process.

1.3 Ambient Assisted Living

Ambient Assisted Living (AAL) [123] is a term that encapsulates a set of technological solutions to make the environment in which a person lives smarter and cooperative. The main objectives are:

- to increase the period during which people can live in their favourite places, enhancing their self-sufficiency and mobility;
- to maintain the health and the functional capabilities of elderly people;
- to encourage healthy lifestyles for people at risk;
- to increase safety, prevent social exclusion and maintain the relational network of people;
- to support family members and care organizations;
- to improve the efficiency and productivity of resources in ageing societies.

AAL solutions can help to recognize dangerous situations, monitor health, and environmental conditions, and support the rehabilitation processes. To design effective solutions, key aspects are the best knowledge of the real needs of the user and facilitation of the work of the caregivers.

It is important to underline that AAL technologies should support the caregivers but not replace their fundamental role: AAL tools should be designed to simplify the work of the caregivers and allow them to follow the patients efficiently. A powerful AAL system should be able to support the rehabilitation processes, offering to the caregivers monitoring tools, able to recognize dangerous situations, monitoring the health and environmental conditions. For this reason, it is important that all the AAL stakeholders (among which the most important are the patients, their families, and the caregivers) are involved from the beginning of the design process.

The areas of interest of AAL technologies are:

- prevention, that is all the actions that can be taken to limit and, when possible, eliminate the causes and the complications of the disease, focusing on how to avoid chronic pathologies. An example is the prevention of the degeneration of cognitive disease using apps and interfaces for brain training and serious games;
- support, that is the compensation of physical or cognitive disability to prolong the independent living and to facilitate the work of the caregivers. In this context, we can cite the support for social inclusion and interaction, management of the house and mobility;
- independent and active ageing, that is all the solutions that can provide a safer and a more age-friendly environment, such as the use of service robots and smart appliances or intuitive interface to maintain the contact with the family and the community, proposing social and leisure activities;

In this context is situated the AUSILIA (Assisted Unit for Simulating Independent Living Activities) project [119]. This project aims to merge common skills in the medical and rehabilitation field with the best technologies in the areas of ICT, automation, architecture, and ergonomics. The aim is to provide innovative and user-centred solutions.

1.4 Occupational therapy

The ability or inability of a person to perform Activities of Daily Living (ADLs) [108, 84] is considered by health care professionals as a measure of functional status, especially regarding individuals with disabilities or the elderly. ADLs include personal care, such as hygiene, bathing, showering, dressing, functional mobility (walk, sit, standing up), and self-feeding, productivity (household management, paid/unpaid work) and leisure (socialization, quiet or active recreation activities).

The only health care branch that has as a primary focus ADLs throughout the entire rehabilitation process is Occupational Therapy (OT), and its' main objective is to enable individuals to participate in activities of everyday life they want to, need to, or are expected to do. This can be achieved by teaching or rebuilding those skills required to engage in daily activities allowing a person to achieve the independence that has been lost after a trauma or caused by a pathological status. Moreover, OT considers the environmental (social, physical, economic) and biological reasons that cause (or are associated with) the difficulties in independence. Hence, a person's engagement in everyday life can also be supported by modifying the daily activities or the individuation and elimination of environmental barriers. During the OT process, the person is actively involved in every step of the rehabilitation process, and the focus of OT is the daily activities considered important for that person, which is why the profession is considered client-centred.

An OT process consists of specific steps: initial interview to identify problematic daily activities, observation, and assessment of the performance of those daily activities, agreement on goals and treatment plan, carrying out of the treatment plan, monitoring and modifying the plan as needed, and reassessment. The first step typically includes the Canadian Occupational Performance measure [20], a standardized semi-structured interview of the person used to identify the everyday activities that he/she needs to, wants to, or is expected to do, but can not do, does not do, or is not satisfied with the way he/she does them.

The individual is subsequently asked to rate his level of performance and satisfaction on a 10-point scale for each activity. After that, the therapist observes and analyses the person while performing the activities identified in the interview. A standard evaluation method helps the therapist in identifying the factors that support or limit the correct performance. The occupational therapist takes into consideration the quality of the performance in terms of efficacy, safety, physical effort, and physical or verbal assistance provided. Also, a 10-point observation-based rating scale is used, the Performance Quality Rating Scale (PQRS). 1 indicates that no activity criteria are met, and 10 indicates that all activity criteria are met with good quality. Usually, two versions of the rating scales are considered: PQRS-G and PQRS-OD [97]. The PQRS-G is the generic rating scale, which provides the therapist with a table to guide the evaluation based on the percentage of completed activities and the overall quality of the performance. PQRS-OD, on the other hand, uses operational definitions.

The next step considers the definition of specific measurable metrics and goals to evaluate clinical intervention. The goals are always related to the daily activities identified in the initial interview and subsequently observed. For example, the improvement in the performance of specific everyday activities in a particular environment, increasing the quality of life or also social inclusion.

The last step verifies the progress of the individual. The therapist constantly verifies and re-evaluates the intervention plan, which can be adjusted if the established treatment plan is not effective. At the end of the process, either modified, interrupted or positively concluded, the therapist performs a reassessment to compare to the initial assessment.

During the OT process, the therapist mainly uses his/her clinical eye to evaluate the quality of an activity in terms of efficacy, safety, assistance, and effort. This makes his/her judgment valid only based on his/her experience since in practice no instrumentation is used. The AUSILIA project aims to overcome such limitations, defining more reliable assessment scales based on objective parameters, increasing the effectiveness of clinical observation for more effective rehabilitation programs.

1.5 The AUSILIA project

As stated in Sec. 1.3, it is important that a user-centred approach is followed in the design and implementation of AAL solutions. Indeed, to reduce the necessity of assistance and hospitalization, key conditions are:

- the choice of personalized assistive device. The aids and the environment should be designed on the specific needs of the patient;
- the patient should be trained in the transition phase from the hospital to his/her home, to help him/her in the use and acceptance of the assistive technologies.

If these two conditions are not verified, the risk is that the use of the various technological aids results in limited and ineffective. This is particularly true in the case of elderly people because they are generally unfamiliar with technology.

In the literature, several studies in the field of domotic and service robotics for elderly and disabled have been done [68, 93, 22, 103, 12, 125]. The main problem is how to find solutions that fit specific needs. Given, from one side, the high variability of syndromes and diseases, environmental and personal contexts, and, on the other side, the high number of possible assistive solutions, it is necessary to think of personal solutions [37]. This approach is essential to optimize the cost/benefit ratio [86]. The process of detection and allocation of the various aids should then be based on personalized and specific studies for every single user. In such a manner, it is possible to design solutions that perfectly fit the individual needs most effectively.

Technology can help people with chronic disabilities to live in their own homes, leaving hospitalization as a last resort. This is the goal of AUSILIA, a joint project between the University of Trento and the local health service of the Province of Trento. A main target of

AUSILIA is the customization of assistive solutions for users with physical and/or cognitive impairments. The disciplines involved in this project are:

- smart architecture: environmental solutions, furnishings, and objects designed according to ergonomic principles to meet the needs of different categories of users;
- ambient intelligence: innovative cognitive environments, capable of supporting a secure, well-equipped and monitored space.
- physiological status monitoring: devices to measure the main vital signs and physiological parameters, ensuring a better understanding of the interaction among patients, environment and assistive tools. These devices can give also information about reactions and mood of patients;
- innovative interfaces: the aim is to provide a more natural interaction of users with the smart environment, enhancing usability and acceptability of the technological assistive tools;
- inclusion: studying solutions not only able to passively satisfy the individual's needs but also to promote a healthy and active lifestyle. The aim is to support daily activities, communication, rehabilitation, and social involvement.
- safety and monitoring: systems for the automatic analysis of the proper use of assistive tools, sensors for the user's safety, such as fall-prevention sensors, and tools for the evaluation of adaptation and customization of the assistive solutions.
- user-based assessment: definition of metrics and objective measurements of user satisfaction in the use of technologies and the effectiveness of the proposed solutions.

AUSILIA consists of a domotic apartment and a living lab, both realized inside the Villa Rosa hospital in Pergine, Trento (Italy). Users can spend some days in the domotic apartment (Fig. 1.3) to try various aids during their normal daily activities. In this manner, users realize their limits and how aids and ergonomic and architectural solutions can solve some of their problems.

The domotic apartment can accommodate patients with different cognitive and/or motor impairments and different needs. For such a reason, the apartment, as far as possible, is designed to cover various types of situations and certain flexibility has been required to allow the clinicians to evaluate and choose the solutions that best fit the specific needs. However, since the apartment is too small to have all the possible solutions that are available in a normal house, a living lab of 400 m² was realized (Fig. 1.4). In this living lab, there are some



Fig. 1.3 The domotic apartment inside the Villa Rosa Hospital in Pergine, Trento (Italy).

prototypes of “environments” that are highly reconfigurable. In this manner, users can verify how they live with different types of configurations of the same environment, choosing the one that best fits their needs, improving their autonomy and quality of life.

The AUSILIA living lab can also be a great opportunity for enterprises that are interested in sponsoring their products and solutions. They will have the possibility to have a real test-bench, enabling an effective understanding of problems and a design that takes into consideration the proposed solutions.

1.5.1 The measurement framework

The framework is realized as three independent elements able to share information. The first is the sensing infrastructure (Fig. 1.5), which is constituted by a set of sensors and technologies distributed inside the apartment for the acquisition and the recording in real time of data.

Such data concern the status evaluation of patients and their interaction with the environment and the various aids. They are useful for:

- providing a tool for active monitoring to prevent possible health and safety risks;



Fig. 1.4 The living lab with different reconfigurable environments.

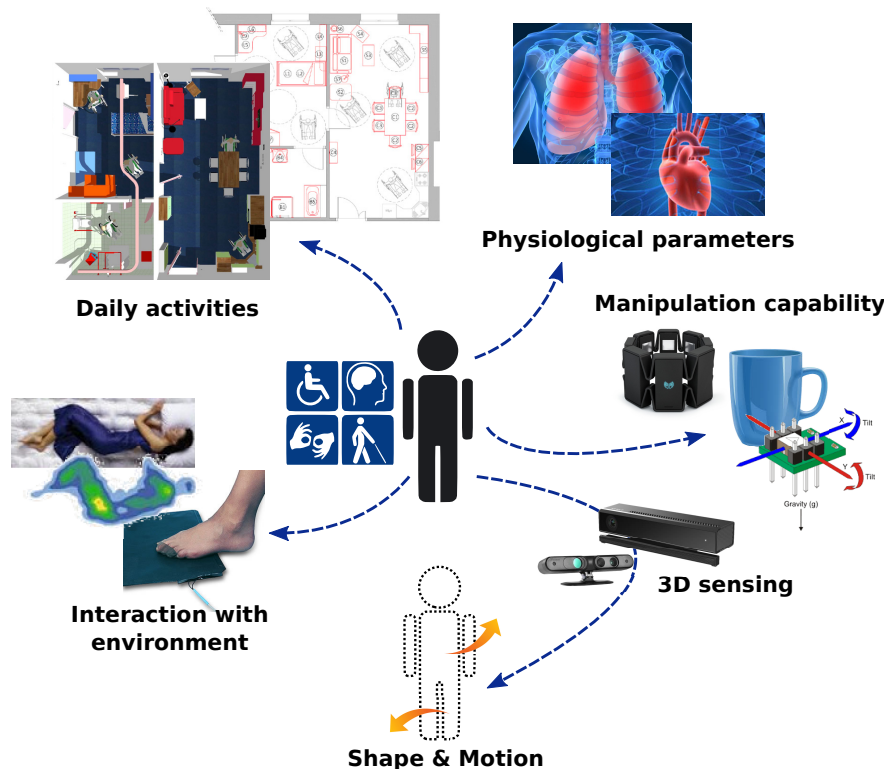


Fig. 1.5 Framework, sensing infrastructure of the apartment.

- providing a basis for the evaluation of the facilities: in this manner, clinicians and designers can determine the solutions that best fit the patient's needs;
- evaluating the degree of confidence acquired by the patient in using the various aids and his/her stress level;
- making a historical record on the use of the territorial lab. This could be helpful for further analysis and research, such as identify possible models, repetitive situations and user profiles.

Examples of systems used for monitoring are cameras, occupancy sensors, pressure and force sensors, and fall detection sensors. Motion capture systems are also present. These systems are helpful to evaluate the body posture of the patient during daily life or specific exercises for rehabilitation. The state of health of patients is monitored through wearable sensors. Acquired physiological signals are electrocardiogram (ECG), the respiratory signal, blood volume pulse (BVP), electrodermal activity (EDA), skin temperature and electroencephalogram (EEG).

The collectors of the information are a set of PCs placed in proper locations to provide the best coverage and thus allow a proper connection with the sensors. These are connected by a local network to a router.

The second element of the framework is the main data collection unit (Fig. 1.6), represented by a displaced server and a database. This is connected as the master to the local network of the apartment. It manages:

- the supervision on the state of the apartment;
- the activation of the area/zones concerning the status/actions/motions of the user;
- the time synchronization between PCs, devices, and data;
- the data collection and transit from the PC and sensors to the database (NTP based).

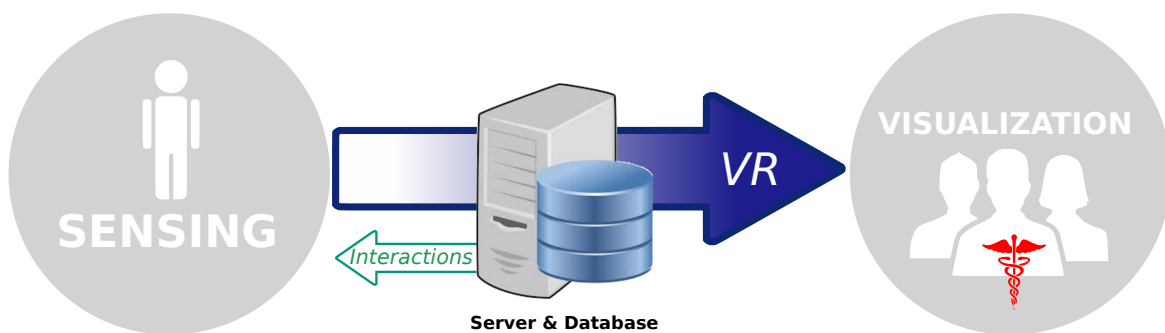


Fig. 1.6 Framework, interconnection and management structure.

The third part of the framework is the one related to the fruition of the data, which are rendered in a Virtual Reality (VR) scenario. The therapists can view the acquired data on a flat display or using a virtual reality headset (Fig. 1.7).

Through this type of visualization, the therapists can merge the information already provided by their eyes with a series of parameters that are usually “hidden”. Examples are quantities regarding environmental interaction, such as 3D movements, interaction forces, weight distribution, and object manipulation, or physiological parameters. This type of data visualization enables to estimate physical state and state of stress of the patient, in the context of the particular situation under examination, enabling a fully empathic interaction with the clinicians.

This is a revolution in the diagnostic methods currently in use for physical/cognitive rehabilitation. Indeed, this methodology will increase the efficiency and objectivity of therapists and enable more effective rehabilitation programs.

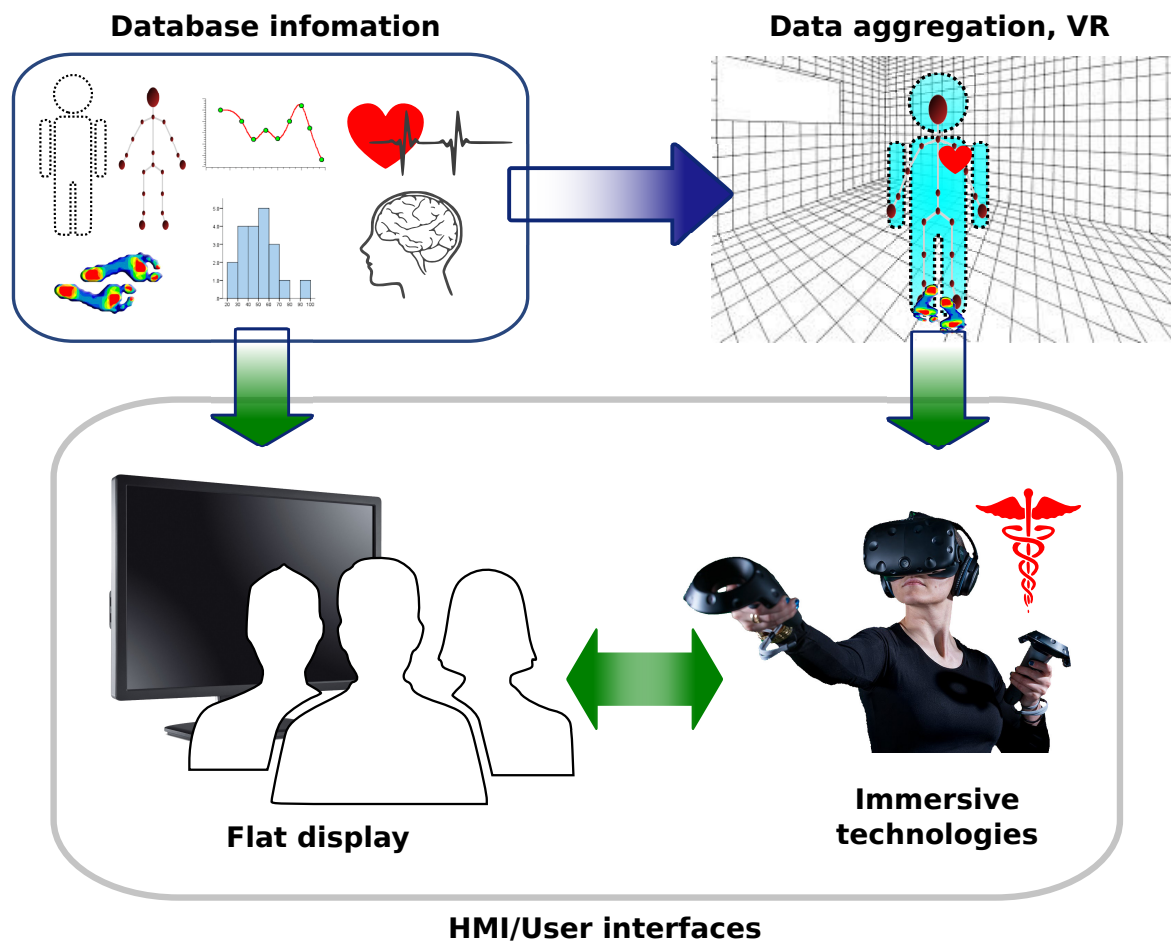


Fig. 1.7 Framework, data visualization.

1.5.2 The protocol

The protocol foresees that, after an initial psychiatrist assessment, the individual is observed in the domotic apartment performing the self-chosen activities of daily living important to him/her, identified with an occupational therapist using the Canadian Occupational Performance Measure [20]. The occupational therapist's observation assesses the individual's level of independence, efficacy, physical effort, and safety, using the Assessment of Motor and Process Skills (AMPS) [53] and the PQRS [97]. Tab. 1.1 shows the main observation scenarios (bathroom, kitchen, bedroom, house management, and safety) for the domotic apartment with the associated daily activities. It was up to the engineers to translate such requirements into technological solutions to monitor the performance in carrying out such activities.

After this preliminary clinical assessment, the second phase foresees that the interdisciplinary team of AUSILIA shares with the individual and his/her caregiver a preliminary

Table 1.1 Overall clinical observation requirements.

| Observation Scenario | Relevant daily activities |
|------------------------------------|---|
| 1. Bathroom | 1.1 I want to use the toilet for bodily needs; 1.2 I want to wash my hands, face, teeth, head, upper arms/arts underarms, shave with a razor blade and foam; 1.3 I want to wash up: shave with an electric razor, comb my hair, get dressed, put on makeup; 1.4 I want to wash my whole body (bath, shower ...). |
| 2. Kitchen | 2.1 I want to eat; 2.2 I want to drink; 2.3 I want to prepare meal; 2.4 I want to fix/tidy up the kitchen. |
| 3. Bedroom | 3.1 I want to go to/get up from bed; 3.2 I want to manage the activities in bed; 3.3 I want to get dressed / undress; 3.4 I want to make the bed. |
| 4. House management, safety | 4.1 I want to do the laundry; 4.2 I want to clean the rooms; 4.3 monitor the house environment; 4.4 security of the house environment; 4.5 patient safety. |

personalized project, which can exploit innovative technological and/or personalized assistive solutions appropriate for them. This phase foresees the possibility that for the individual and his/her caregiver to try the identified solutions in the domotic apartment. This project may include spending up to 8 hours a day for a maximum of five days in the domotic apartment that is able to collect the augmentative parameters/measurements and then feed them back in VR to the clinician, providing the more complete/objective picture regarding the individual's day, his/her routine and performance, and his/her physiological state in relation to with the different technological solutions employed. At the end of the testing period, the clinician, enabled by the VR HMI, reassesses to determine if the identified technological solutions identified in the preliminary project improved the level of independence, efficacy, physical effort and safety during the performance of daily activities, or if other solutions shall be identified and tested. This makes possible to realize tailored projects, designing and producing custom architectural solutions and custom assistive components or devices (Fig. 1.8) to help patients in daily activities. They can then adapt their own houses accordingly to these projects.

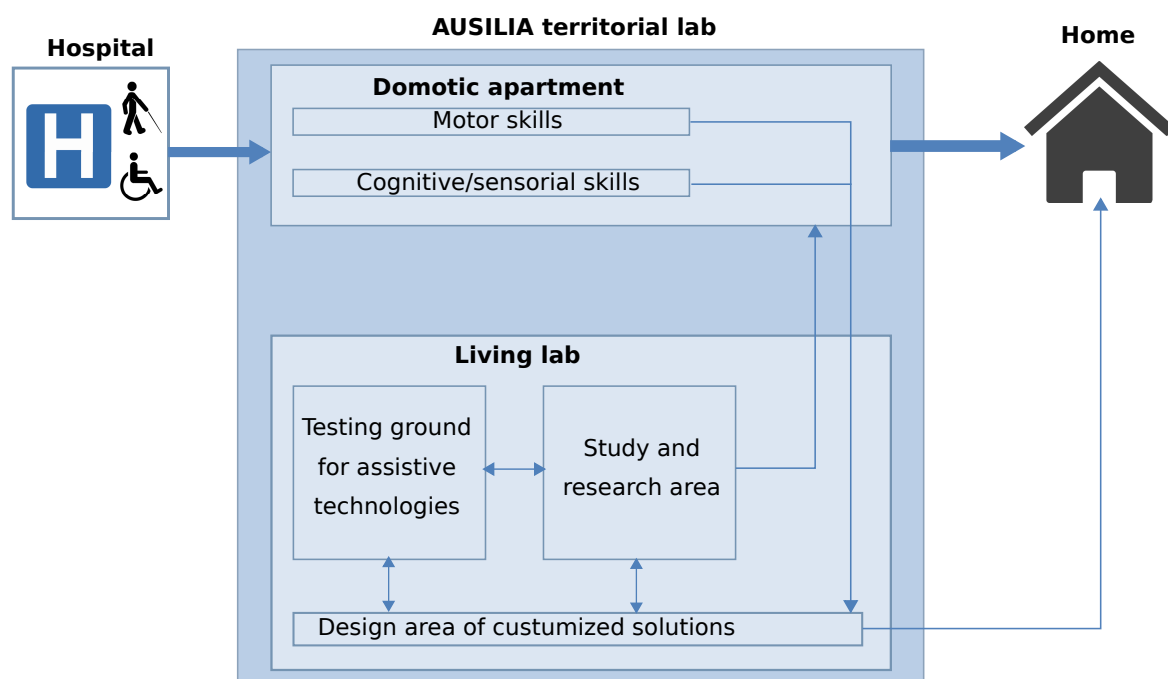


Fig. 1.8 The AUSILIA paradigm inside the de-hospitalization process.

1.5.3 Project impact

AUSILIA offers a great opportunity for the development of a new form of public-private cooperation. In particular, this project enables us to move from a market mechanism based on

the “technology push” approach to a “market pull” model. Indeed, the government will have the possibility to try and introduce technologies that are effectively meeting the user needs. On the other side, the business community will have the possibility to develop innovative products and verify their potential on the ground.

AUSILIA foresees important benefits in terms of the development of new tools and services by local and national enterprises. The latter will have the opportunity to validate and enhance their products. Moreover, enterprises can gather new ideas and new technological challenges. They will have also the possibility to transfer the “know-how”, generated in the laboratory, in innovative projects. This territorial laboratory could also be a reference point for enterprises involved in the health sector; in particular for what concerns investments in research and development. This fact is due to the possibility to test and validate the various aids on the user, adopting an approach that is “user-centred”. Moreover, AUSILIA can contribute to the definition of standard and best practice in a field in which there are still gaps in the definition of rules, standards, compatibility, and interoperability of facilities.

From a research point of view, AUSILIA will effectively contribute to the progress of knowledge in the involved areas. This progress will not only interest the development of new technologies but also the possibility to develop an interdisciplinary field of research. Indeed, the research will focus also on behavioural models of users and their needs. The analysis will be performed on the interaction of the users with the environment, with the possibility to exploit in the best manner their residual capabilities, trying to recover impaired functions when possible.

AUSILIA will have also a great impact on the education and training of specialist staff. First of all, the project will create increased awareness and knowledge about the availability and the features of the various technological aids. AUSILIA will help the staff to deal with the various tools and to be informed on the state of technology. The project will also create a space for interaction among clinicians, technicians, and producers. This space will enable faster and more effective communication. AUSILIA will then offer to researchers and innovators the possibility to communicate, without intermediaries, with domain experts. This possibility will create the opportunity to have mutual contamination in different fields: medicine, rehabilitation, cognitive sciences, ICT, mechanical and automation engineering, biomedical engineering, architecture, and design.

The major impact of AUSILIA is in the healthcare context. The customization of the solution and the training that will be offered to disabled users will enable the possibility of a more autonomous life inside their homes. The benefit is double. Citizens will experience a better quality of life on one side; the government will see a reduction of the expenditures for

health on the other. This fact is mainly due to a lower need to recur to hospitalization or to care services provided by specialist staff.

The AUSILIA project has great potential. Its added value is due to the interdisciplinary collaboration between clinicians and technicians. AUSILIA will enable us to expand the set of the possible aids that a person with cognitive and/or motor impairments can have. In particular, the various solutions will be designed in a manner that will fit appropriately the specific user needs. Indeed, AUSILIA will enable us to come up with new technologies that are customizable, implementable and adaptable to different situations in a low-cost manner. With this kind of approach, there will be a reduction of the burden on the health-care system, especially for what concerns the hospitalization.

AUSILIA will ensure the suitability of the proposed solutions. Patients and caregivers can try these solutions, to verify if they are really useful and capable to enhance the quality of life of users and their relatives. The reduction of the health-care burden, the greater autonomy and safety, and the possibility to have more integration in the society will increase the well-being of the patients, of their families and of the community in which they live.

Chapter 2

Supporting technologies

2.1 Wearable devices

There are descriptions of several technologies with the aim of health monitoring in the literature. One of them is the new phenomenon of Wearable Sensors [115]. These devices can be accessories or clothes and may comprise various sensors for measuring physiological parameters, such as heart rate, respiratory rate, blood pressure, brain activity, body temperature, skin conductance, physical activity, sleep patterns and calorie consumption.

Wearable sensors and systems are gaining an ever-growing interest both from consumers and from companies. Smart wearable system applications are emerging in the sport, entertainment, healthcare, and military domains. The general trend goes towards the development of less invasive, low consumption and low-cost devices, ensuring certain freedom of movements.

One of the biggest advantages of these systems is the ability to monitor an increasing number of individuals with problematic conditions even in places difficult to reach, while still providing a prompt intervention in case of emergency. Indeed, they can establish a continuous connection between the patient and caregivers (Fig. 2.1), guaranteeing non-invasive 24-hour monitoring. The patient's physiological parameters during daily activities can be easily monitored, identifying potential situations of stress or overexertion. Indeed, such devices have the potential to give to healthcare providers real-world assessments of their patients' daily life at a time when we are seeing a transition of care outside hospitals, due to increasing chronic diseases.

However, there are some critical challenges in the use of these devices, such as the limited battery life, privacy concerns, improvement of efficiency and non-invasiveness, clinical validation and standardization [114].

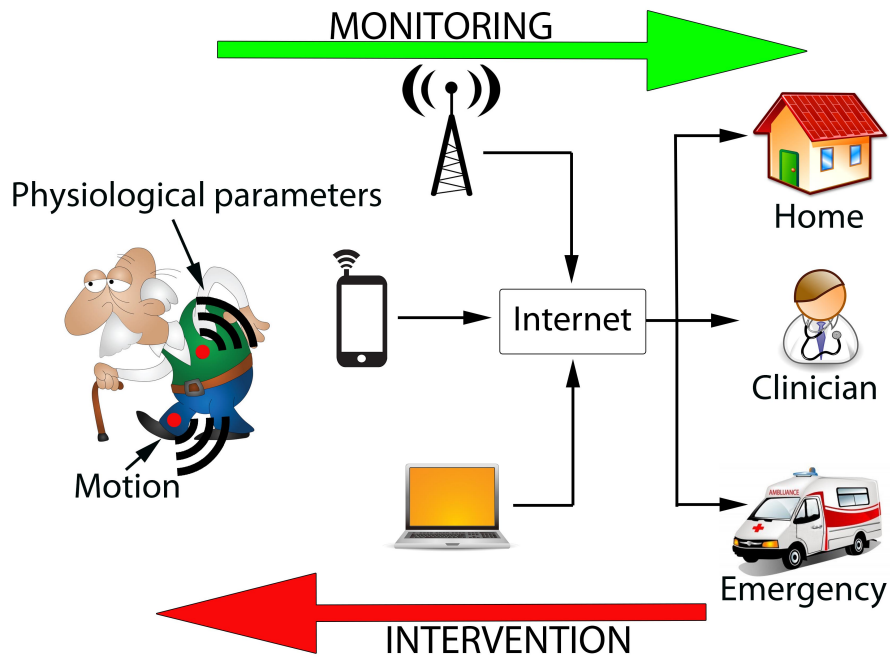


Fig. 2.1 The potential given by technology for health monitoring, ensuring emergency services regardless of physical location [115].

2.1.1 Used wearable equipment

During this project, the various physiological signals were acquired using low-invasive wearable devices (Fig. 2.2). Tab. 2.1 shows the monitored physiological signals and the wearable sensors used.

Table 2.1 Wearable sensors characteristics.

| Sensor name | signal | unit | Sampling frequency [Hz] |
|--------------|----------------------|--------------------|-------------------------|
| Smartex WWS | ECG | mV | 250 |
| | Respiratory signal | mV | 25 |
| | 3-axis accelerometer | m s^{-2} | 25 |
| Empatica E4 | BVP | nW | 64 |
| | EDA | μS | 4 |
| | Temperature | $^{\circ}\text{C}$ | 4 |
| | 3-axis accelerometer | m s^{-2} | 32 |
| Emotiv EPOC+ | EEG | mV | 256 per channel |
| | 3-axis accelerometer | m s^{-2} | 64 |
| | 3-axis gyroscope | dps | 64 |
| | 3-axis magnetometer | μT | 64 |

The Wearables Wellness System (WWS) t-shirt by Smartex (Prato, Italy) provides the ECG signal (lead II) and the respiratory signal, obtained with a sampling frequency of 250 Hz and 25 Hz respectively. The t-shirt provides also the respiratory signal, recorded by a piezo-resistive sensor situated at the level of the ribcage. The output is a voltage signal proportional to the sensor stretch, which was not calibrated to yield measurements of the respiratory volume in l/min. However, since the analysis will focus on the dynamic variations of the signal rather than on its absolute value, this was not an issue for the present project.

The Empatica (Milano, Italy) E4 wristband is used to record the BVP signal using its photoplethysmographic (PPG) sensor; BVP data are acquired at a sampling frequency of 64 Hz. The Empatica wristband provides also the EDA signal and the skin temperature at 4 Hz.

The Emotiv (San Francisco, USA) EPOC+ wireless headset is used to record the EEG. It collects 14 EEG signals with a sampling frequency of 256 Hz for each channel. The battery life of the Smartex, Empatica and Emotiv devices in streaming mode is respectively of 12h, 24h, and 12h.

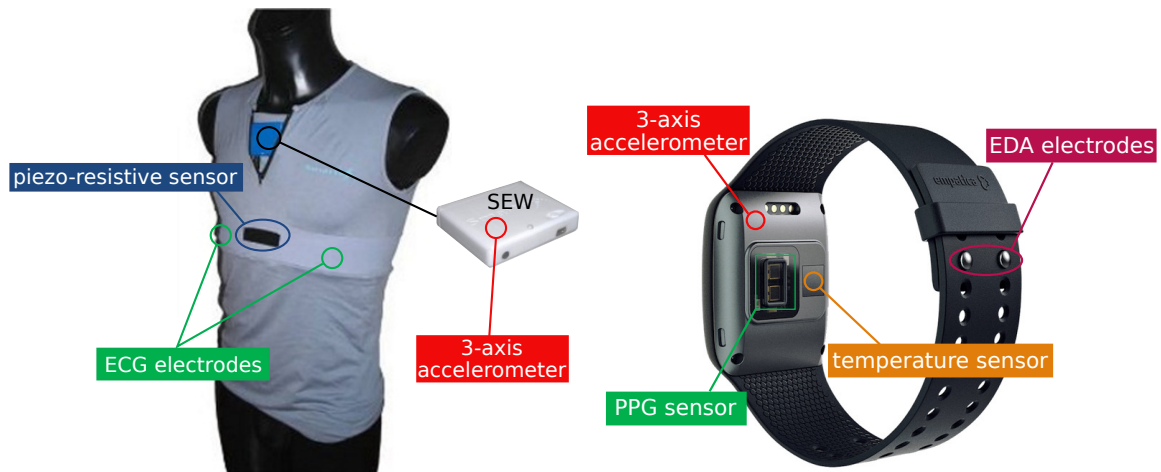
For what concerns problems in the correct wearing [179] to obtain high accuracy vital signs acquisition, it is important that the t-shirt is the right size to have good contact with the ECG electrodes and not to have the piezo-resistive sensor too much stretched or loose. The wristband should be worn reasonably snugly (but not uncomfortably tight) in order not to be able to see any light escaping from the PPG sensor on the back of the wrist. For the EEG headset, special attention must be paid to the correct positioning of the EEG electrodes. However, thanks to the fixed configuration, the setup time of the EEG headset is about 3-5 min. Smartex and Emotiv devices provide also an interface for verifying the acquired signal quality. The various devices were connected to a PC through a Bluetooth connection.

2.1.2 Synchronization of the devices

The main issue in the combination of multiple independent devices is the lack of a hardware driven synchronization method. The data must then be managed and analysed, devising software solutions to perform the temporal alignment of the various signals. That is critical since errors could occur in the generation of the clock of the electronics, thus potentially affecting the processing with temporal shifts in the recorded data. Such an element was here solved by running a custom designed synchronization method that foresees the usage of the quantity that is available from all devices: the acceleration.

The process can be subdivided into the following steps:

1. the identification of the principal motion directions for each device;



(a) Smartex WWS composed by a sensorized t-shirt and an electronic device (SEW).

(b) Empatica E4 wristband.



(c) Emotiv EPOC+, 14 channel wireless EEG headset.

Fig. 2.2 Wearable devices used to acquire the physiological signals.

2. the alignment and fastening of devices on rigid support: the industrial Velcro achieved very good performances both in term of stability of the mount and removability capabilities, Fig. 2.3;
3. the motion of the rigid support (together with the sensors) to define a non-uniform acceleration pattern: a sinusoidal path is suggested since it is periodic and easy to be performed;
4. the synchronization of the collected, low-pass filtered, acceleration signals with the one used as the reference ($a(t)_r$).

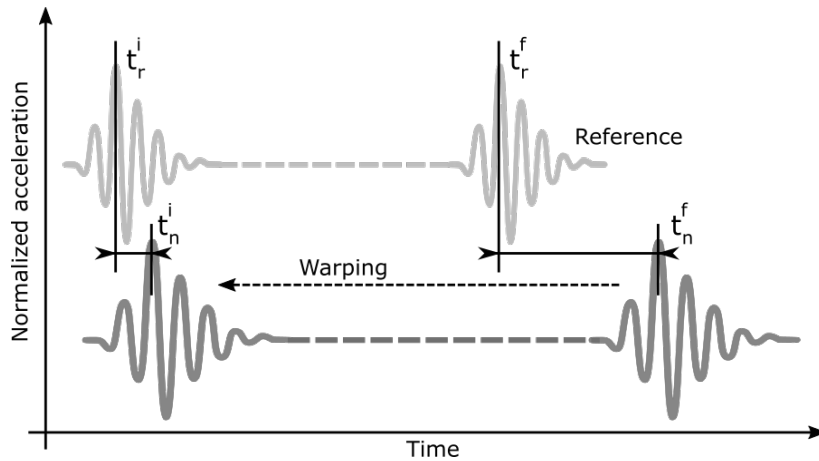
The last two are performed both at the beginning and the end of the recording sessions. This is fundamental to compensate for any modifying factor that can cause dilatations of the time bases. The synchronization is performed as a linear warping of the time to a reference signal, in this case, the one provided by the Smartex sensor. Eq. 2.1 reports the formulation, where $t_{r,n}^{f,i}$ stands respectively for a time instant t collected from the reference or n -th series, aligned at the initial or final phase of the data record. The modified temporal instant \tilde{t}_n can be computed as:

$$\tilde{t}_n = \frac{(t_r^f - t_r^i)}{t_n^f - t_n^i} \cdot (t_n - t_n^i) + t_r^i \quad (2.1)$$

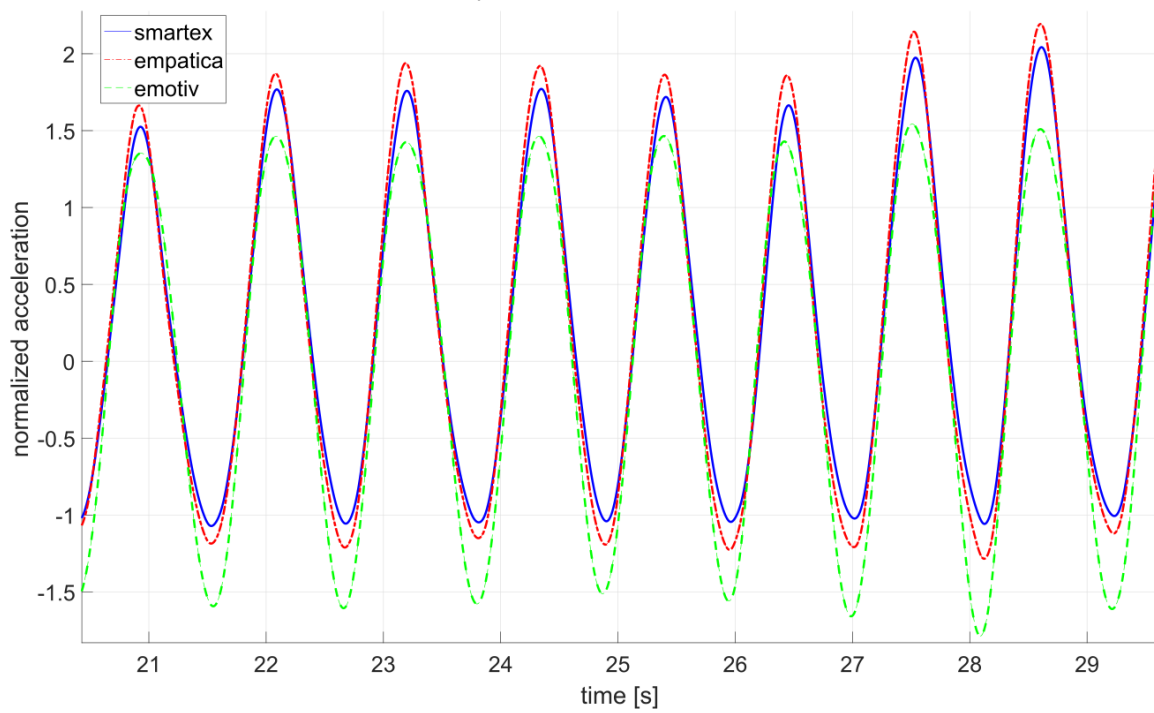


Fig. 2.3 Used wearable devices connected to a rigid bar for time synchronization.

Alternative quantities than the acceleration can be considered, the method is general and can be adapted accordingly to the required hardware configuration with no major modifications.



(a) Synchronization scheme.



(b) Example of synchronized data from the considered hardware architecture.

Fig. 2.4 Temporal synchronization of the wearable devices by mean of the acceleration signals.

2.2 Environmental monitoring

The sensors installed in the domotic apartment are the following:

- Sa.Ni. Corporate “Ultrasensor” (pressure sensor matrix);
- Interlink “FSR 400 Series” (local pressure);
- Lp-Research “LPMS-B2” (Inertial Measurement Unit (IMU));
- Phidgets “0-100 kg S Type Load Cell”;
- Adafruit “Water Flow Sensor (1/2 inch)”;

To synchronize the data provided by the environmental and physiological sensors (the Smartex device is taken as reference), the time at which the data arrive at the PC is taken. The synchronization accuracy (in the range of 0.1 s) is enough for the project. The synchronization among the physiological sensors still follows the procedure described in Sec. 2.1.2.

2.2.1 Weight distribution

To monitor the weight distribution of the user, a pressure sensor matrix was installed in front of the sink (Fig. 2.5). Such a measure is useful to determine the correct posture of the user while performing daily activities such as washing, shaving, combing his/her hair, get dressed or putting on makeup. The device specification are the following:

- data transmission rate: 30-200 Hz;
- size: 0.5×0.5 m;
- spatial resolution: 42 dpi;
- max pressure: 150 N cm⁻²;
- pressure resolution: 0.02 N cm⁻²;
- accuracy ±5 %.

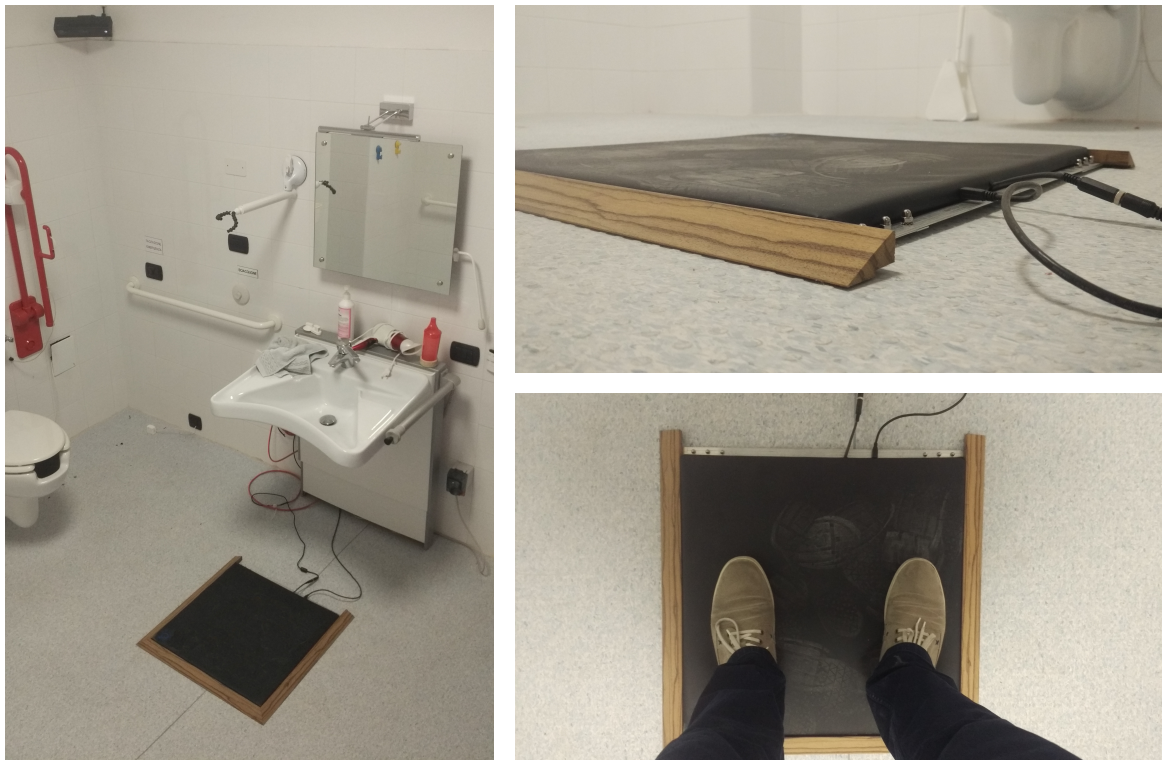


Fig. 2.5 Pressure sensor matrix used to monitor the weight distribution.

2.2.2 Local pressure

Local pressure measurements are performed using the Interlink “FSR 400 Series” sensors. Such sensors were installed under the table in the kitchen (Fig. 2.6a) to monitor how the user leans against it. They were also installed under the toilet seat and on the bars (Fig. 2.6b) to assess the balance and thus the stability of a subject in the transfer from and to the wheelchair so as the correctness of the seat.

The specifications are the following:

- force sensitivity range: 0.2-20 N;
- force resolution: 1024 point;
- force repeatability single part: $\pm 2\%$;
- standing load durability 2.5 kg for 24 h: -5% average.

Since the force sensitivity range was too low for the project requirements, a calibration was performed to obtain an operative range that spans from 0 to 300 N.



(a) Local pressure sensors installed under the table.



(b) Local pressure sensors installed under the toilet seat and on the bars.

Fig. 2.6 Local pressure sensors.

2.2.3 Inertial measurement unit

To assess the capability of manipulating objects or to perform Parkinson detection, the Lp-Research “LPMS-B2” IMU is used. Such a device has been chosen due to its small size. Fig. 2.7 shows how the IMU was installed under a glass using customized support.



Fig. 2.7 IMU installed under a glass.

The IMU specifications are the following:

- data transmission rate: up to 400 Hz;
- size: 39×39×8 mm;
- accelerometer: 3 axis, $\pm 2 / \pm 4 / \pm 8 / \pm 16$ g, 16 bits;
- gyroscope: 3 axis, $\pm 125 / \pm 245 / \pm 500 / \pm 1000 / 2000$ dps, 16 bits;

- magnetometer: 3 axis, $\pm 4 / \pm 8 / \pm 12 / \pm 16$ G, 16 bits;
- resolution: $< 0.01^\circ$;
- accuracy: $< 2^\circ$ (dynamic), $< 0.5^\circ$ (static).

2.2.4 Load cell

The “Phidgets” load cell was installed in the stand-lift above the bed (Fig. 2.8). This sensor is useful to assess the force applied by the user during the transition from the laying position to the sitting position in bed. This measurement is important to optimize the loads at the shoulder level to avoid the arising of articular pain. The load cell specifications are the following:

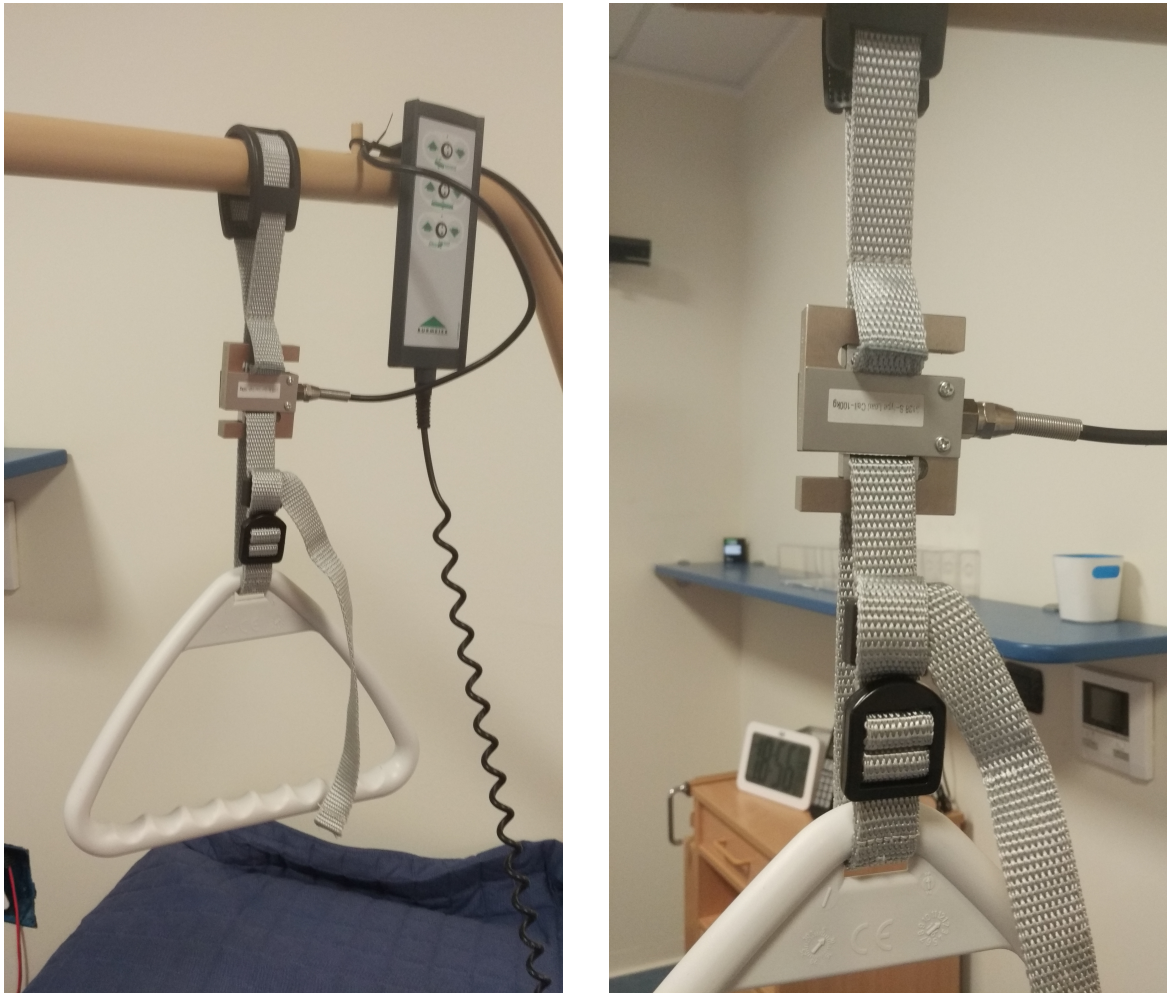


Fig. 2.8 The installed load cell.

- weight capacity max: 100 kg;
- maximum overload: 120 kg;
- compensated temperature min: -10°C ;
- compensated temperature max: 40°C ;
- operating temperature min: -20°C ;
- operating temperature max: 55°C ;

2.2.5 Flow-meter

The flow-meters (Fig. 2.9) were installed to evaluate the correct use of the cold and hot water by the user. This is particularly useful for cognitive disabilities that damage the sense of touch and thus for avoiding burns. The technical details of the flow-meter are the following:



Fig. 2.9 The installed flow-meters.

- working voltage: 5 VDC to 18 VDC;
- max current draw: 15 mA at 5 V;
- working flow rate: 1 L min^{-1} to 30 L min^{-1} ;
- working temperature range: -20°C to 80°C ;
- working humidity range: 35 % to 80 % RH;

- maximum water pressure: 1.75 MPa;
- output duty cycle: 50 % \pm 10 %;
- output rise time: 0.04 μ s;
- output fall time: 0.18 μ s;
- flow rate pulse characteristics: $frequency(\text{Hz}) = 8.1 * flow_rate(\text{Lmin}^{-1}) - 3$;
- pulses per Liter: 485;
- durability: minimum 300,000 cycles.

2.3 Motion capture system

The acquisition system exploited in this project is composed of multiple Microsoft Kinects V2 (Fig. 2.10), low-cost Time of Flight (ToF) cameras. The device provides a 30 Hz data stream of RGB, infrared and depth images plus the skeletonization of subjects moving inside its Field of View (FoV). The device has a maximum uncertainty of about 5 mm at 5 m [112, 176, 150, 29], which is the maximum operative range.



Fig. 2.10 The Kinect V2 camera.

Fig. 2.11 shows where the Kinect cameras have been installed inside the domotic apartment.

As commercial ToF, Kinect V2 presents two main limitations:

- the default driver does not allow the use of multiple devices on the same computer;
- the lack of any trigger or equivalent hardware solution for multiple device synchronization.

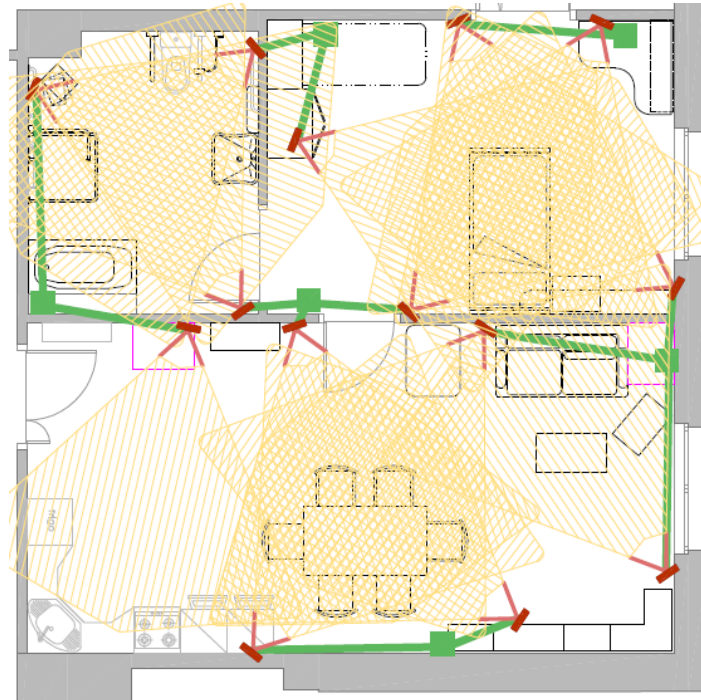


Fig. 2.11 The layout of the domotic apartment showing where the Kinect cameras have been installed and their respective FoV.

Non-proprietary drivers allow the connection of multiple devices on the same PC, like `libfreenect2` [175]. Nevertheless, Microsoft APIs [141] are the ones that offer the skeletonization functionality and present the best performances in terms of stability and usability. The first feature is the most important and is the reason for which Kinect is so much exploited in applications that require an assessment of human kinematic.

Fig. 2.12 shows the typically used setup, in which three Microsoft Kinects V2 cameras were installed. The Kinect positioning was designed to maximize the coverage of the monitored area [96, 15]. The acquisition system was designed to be distributed, using for each sensor a dedicated mini PC connected in a local network. The desired output is the 3D dense point cloud of the subjects in motion.

Since even a shift of 1 frame (33 ms in the time domain) can cause noticeable misalignments in the 3D reconstruction of body parts recorded during daily life activities, a dedicated analysis was performed on the possible methods to synchronize the devices via software.

The acquisition frequency of the Kinect V2 is very stable. From that follows the possible design of a software synchronization responsible for the compensation of time delays higher than the sampling period. Two possible solutions were considered: Network Time Protocol (NTP) synchronization or the use of the internal time information from the device itself.

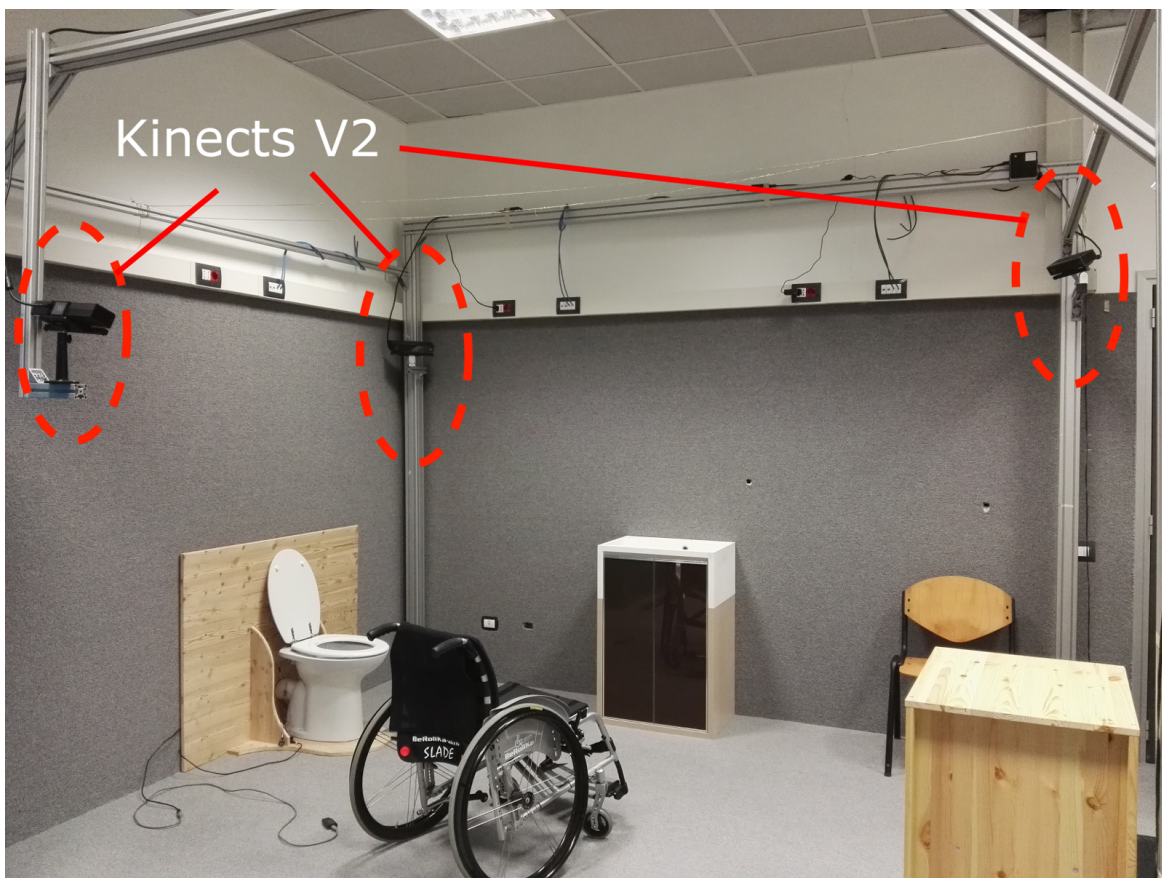


Fig. 2.12 Example of the motion capture setup: three Kinects are placed at a height of 2 m from the floor, distributed and pointing to the centre of the room.

In the NTP synchronization solution, all the PCs are connected over a LAN. A server provides the main clock and keeps synchronized the other devices. Such an organization is functional and provides a level of synchronization in the tens of ms. The uncertainty in synchronization is usually due to latencies in communication over the network. Possible issues are:

- the presence of systematic delays not compensated by the network system;
- the variation of the delay during the acquisitions due to the online synchronization of the clocks.

Quality NTP software solutions minimize and prevent such elements, providing a higher level of time stability and reliability. In the case of a stable network, the NTP synchronization remains reliable also after system shutdown and reboot.

Concerning the possibility to use the internal time information from the device itself, Microsoft Kinect APIs provides information about the time in which the acquisition of data occurs. With a resolution is $0.1\mu s$, this information seems more stable than the time provided by standard calls to the operative system time (also to NTP), Fig. 2.13.

From the testing two important elements were highlighted:

- the time count remains active even if the sensor is powered but not used (or connected);
- the time count resets to zero if the PC resets.

The synchronization of the acquisition system can be achieved in this case by compensating the systematic time-shifts among the activation time instants of each sensor. It is however mandatory not to shut down the PC.

Compared to NTP, the internal time synchronization seems more reliable since it is hardware driven. Considering its usability, it seems more adequate for portable systems, in which a new calibration and synchronization are required at each restart. In the case of fixed devices and long acquisitions, as required in the AUSILIA project, NTP is generally preferable because a system shutdown can be required for appropriate management of power consumption.

Regardless of the choice of time reference, an analysis of the synchronization of the devices is required and advantageous since it can underline unmanaged effects. Once assessed and compensated the delays, by summing or subtracting multiples of periods to the reference clock on each acquisition peripheral, an absolute “shared” time value is available and used to reference each acquired sample.

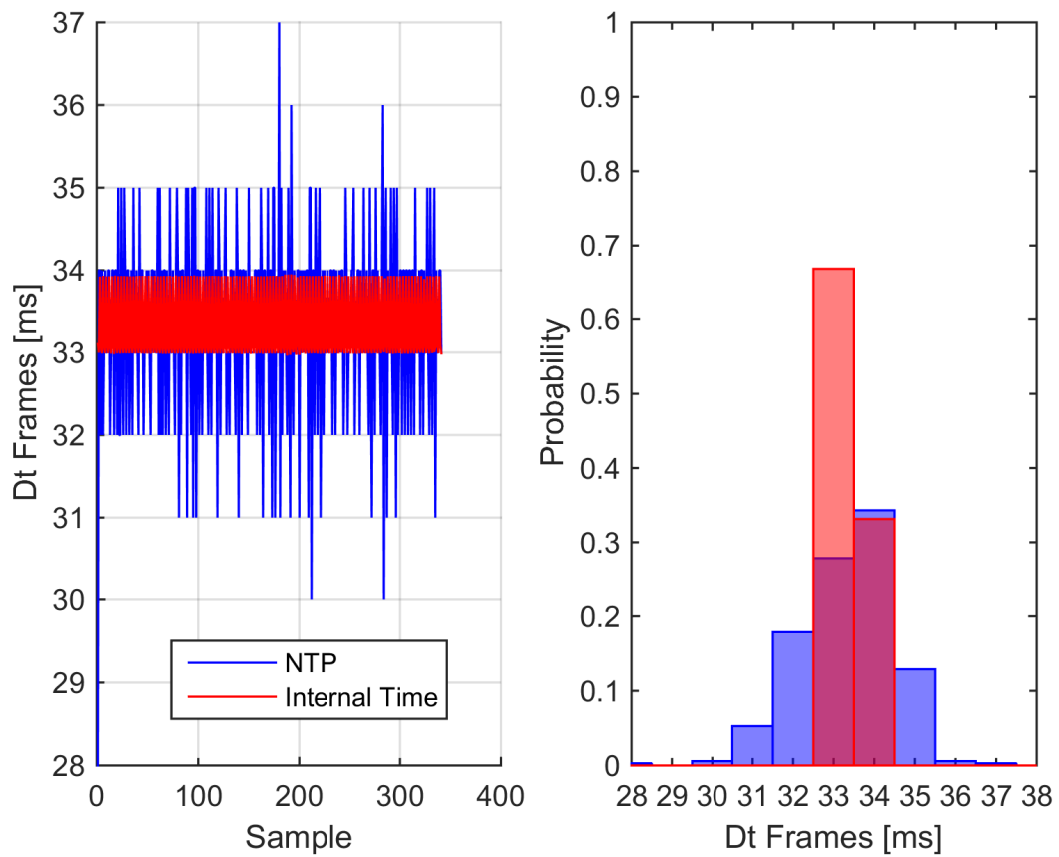


Fig. 2.13 Comparison between inter-frames intervals at a nominal 30 Hz acquisition frame rate: NTP vs. device internal time.

2.3.1 Calibration framework

The proposed spatiotemporal calibration [55] (developed by the MIRo team of the University of Trento) requires a simple and easily reproducible calibration tool, a coloured ball, recorded while being moved by hand inside the monitored area. A requirement is the visibility of the tool from more than one device at a time for most of the calibration sequence. The calibration method is based on the time and spatial matching of the 3D trajectories of the calibration tool and it is organized as presented in Algorithm 1.

The method is designed to be automatic except for the initialization of simple parameters: the radius of a sphere, i.e. of the calibration tool, and the selection of a circular region, an operation performed using three mouse clicks in each initial calibration sample from each device.

The data structure for the calibration is composed of the following elements, all obtainable from Microsoft SDK:

- depth images, 16-bit PNG;
- RGB-D images, RGB images resulting from the projection of the RGB camera over the depth frame, 24-bit PNG;
- time reference used to name each frame (from synchronization).

For each frame, a depth and an RGB-D image are saved and named with the time instant of the acquisition.

To develop a general and usable method, two elements should be considered: 1) the calibration target must be simple and easily reproducible; 2) the amount of information required for the initialization of the calibration must be as few as possible. The choice of the Singular Value Decomposition (SVD) matching has an important advantage: it does not require information on the pose of the target, but only its xyz positions. The simplest and attitude invariant shape was therefore chosen: the sphere. In our case, a simple football ball fixed on a stick was used.

To make the target identification and tracking unsupervised, it is necessary to consider a method for the automatic extraction of the 3D position of the sphere in each frame (if it is inside the FoV). That can be achieved by segmenting either the 2D depth image or the 3D point cloud. The 2D domain is the more convenient choice: the application of 2D masks and filters results simpler and more robust than performing a direct 3D shape matching in the entire point cloud. It follows that it is sufficient to characterize the calibration tool to graphically distinguish it from the environment, to isolate only those pixels that are associated with the tool itself. In the case of devices that have not such a graphic counterpart, the 3D data

Algorithm 1 Calibration method organization

N devices

procedure INITIALIZATION

for $n \leftarrow 1$ to N **do**

Manual initialization of circular ROI

Chromatic selection \rightarrow HSV segmentation

Tool identification and model fitting

if No identification n **then**

Frame skip

end if

Trajectory tracking \rightarrow Position and covariances

end for

end procedure

Selection of the reference device

procedure INTRA-DEVICES SYNC

for $n \leftarrow 1$ to $N - 1$ **do**

Automatic device coupling: reference and n -device

Rough time synchronization

while $Delay > 300$ ms **do**

Principal components analysis

FoV invariant kernel

Cross correlation delay estimation

Apply time compensation

end while

Apply time compensation

SVD based point-to-point matching

end for

end procedure

Automatic generation of the global graph

Graph optimization

return Extrinsic parameters and covariance matrices

analysis remains a valid alternative, however more complex, time-consuming, and potentially less reliable.

Possible choices for the 2D segmentation are shape-detection (Hough Transform) or thresholding segmentation. From the performed tests, shape-based detection fails to achieve a suitable level of reliability for the calibration method. The environment, usually rich in detail, could show very noisy image gradients, resulting in frequently missed identifications.

Thresholding segmentation achieved higher reliability. Two strategies were considered: infrared and colour domain. The infrared camera and depth sensor are coincident. In such a domain, a robust segmentation is quite complex. Retroreflective coatings, like stripes or sprays (Fig. 2.14), provide very good outputs in terms of image saturation. The scattering and reflections of the light emitted by the sensor create blobs in the image with high values in correspondence of the tool. A very simple and robust identification process can be implemented by exploiting such behavior by just thresholding the infrared images. The drawback is the level of reflection, usually too high. This causes the saturation of the IR sensor, influencing the depth measurements and resulting in local deformation of the 3D point cloud. This is not suitable for the accurate localization of the calibration tool.

For the above reasons, the chromatic RGB-HSV domain segmentation is preferable. The segmentation is applied after projecting the RGB information over the depth data (RGB-D data), achievable by using the Kinect APIs and the intrinsic parameters included at firmware level in each device. Fig. 2.15 shows an example of the obtained RGB-D images. The target colour is defined by selecting a circular region, through three mouse clicks, in the first RGB-D image acquired by each device (Fig. 2.16a). Once defined such a region, the algorithm evaluates the mean value and standard deviation ($\pm 2\sigma$) of the HSV channels of the selected pixels (Fig. 2.16b). The choice of the manual initialization rather than automatic processing aims to minimize the influence of light variation among the devices. The main benefit is a more accurate chromatic characterization of the tool in each dataset and thus a more robust segmentation.

The calibration proceeds with the identification of the 3D position of the calibration tool, i.e. the centre of the sphere, in all frames of the calibration sequence.

The chromatic segmentation isolates subsets of 3D points from each frame. However, minor spatial shifts in the chromatic projection over the corresponding depth image can occur for the following reasons: minor internal delays between the RGB camera and the depth sensor, the accuracy of the intrinsic parameters and physical disparity of the RGB and IR sensors. These facts lower the accuracy of the segmentation and so the selection of the 3D points by potentially including outliers in the assessment of the position of the tool. To overcome such issue a RANSAC [52] spherical fitting is used. Parameters used for the fitting

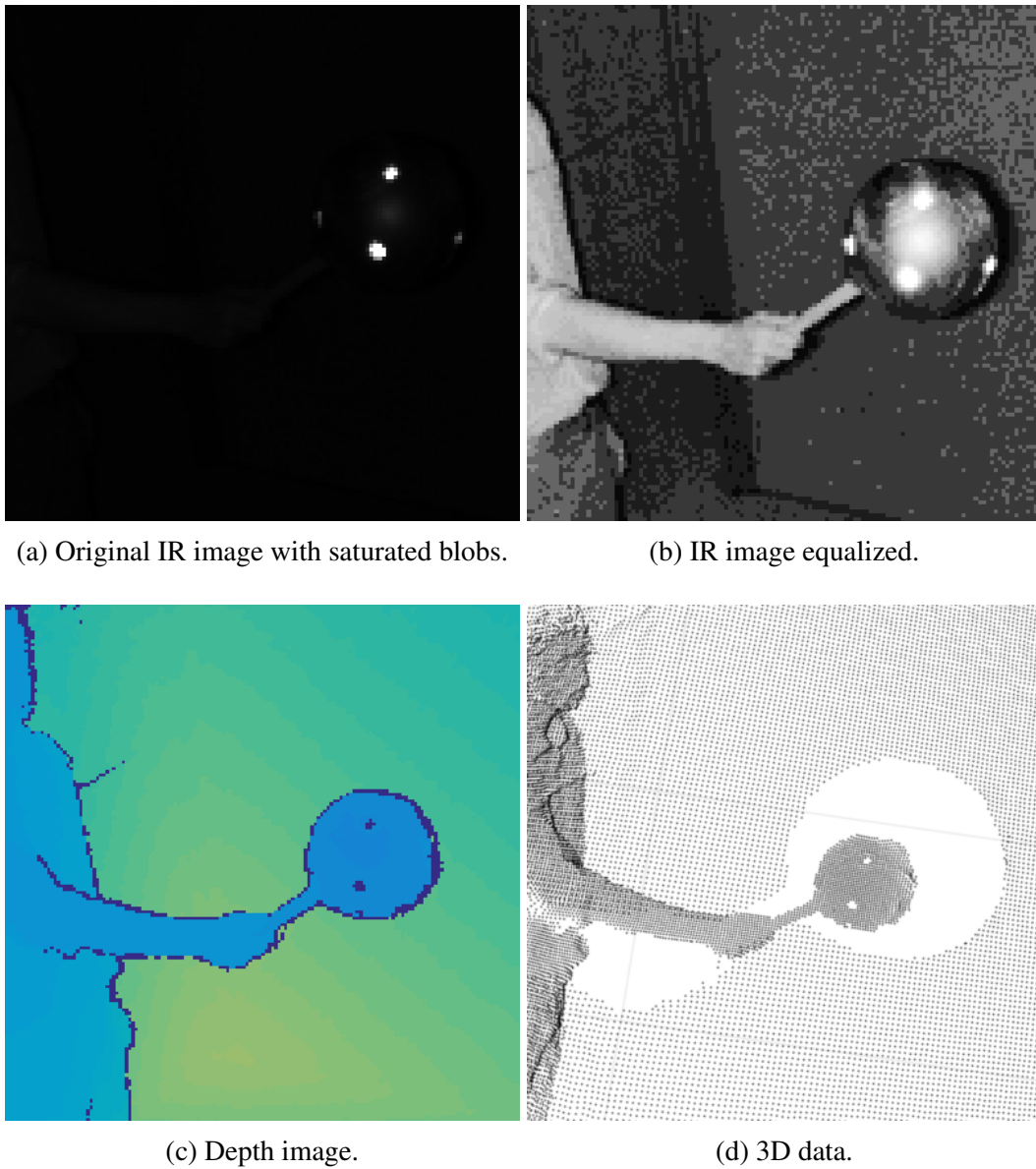
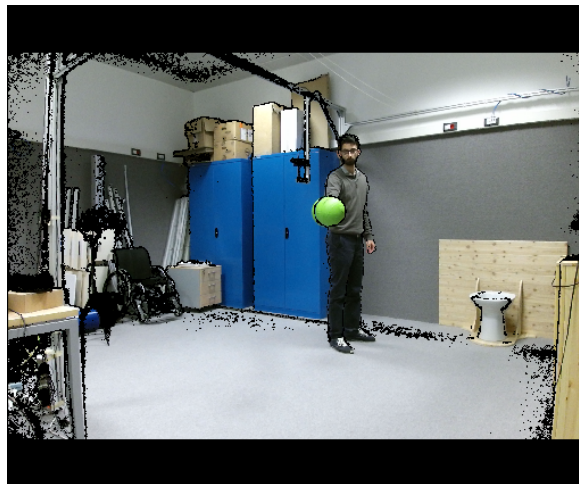


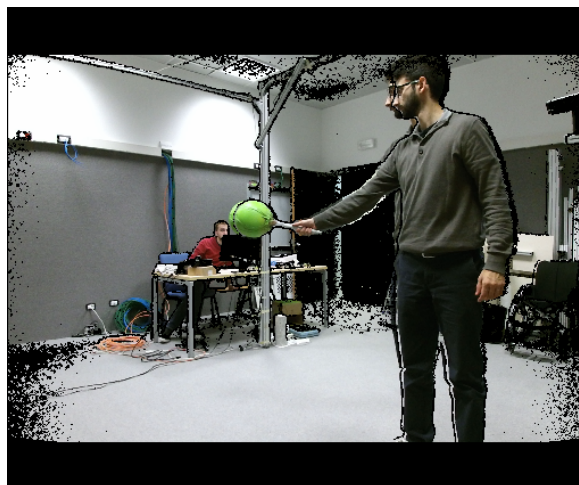
Fig. 2.14 Behaviour of retro-reflective surfaces in the infrared and depth domain. A degradation of the data is noticeable in the proximity of saturated spots both at depth and 3D level.



(a) First Kinect view.

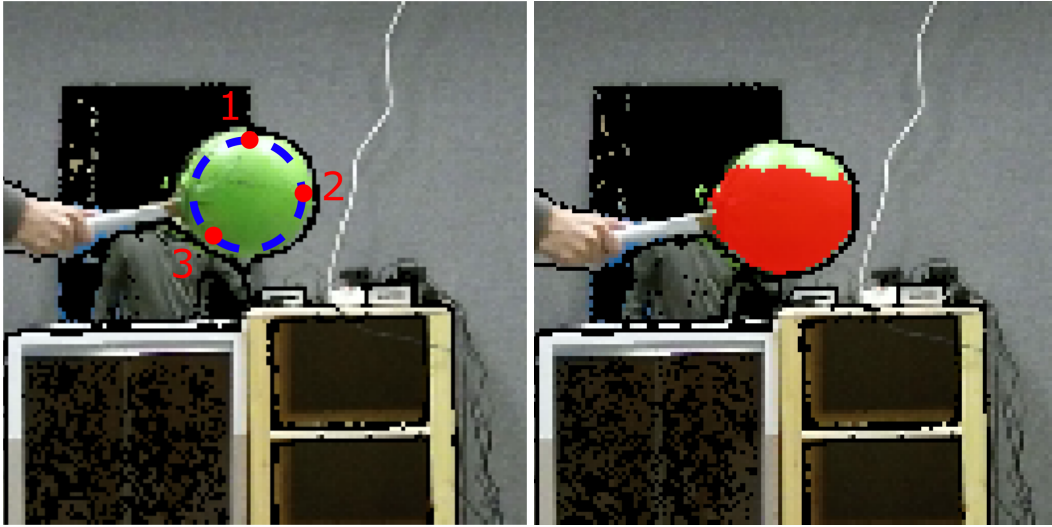


(b) Second Kinect view.



(c) Third Kinect view.

Fig. 2.15 Example of first RGB-D image from each calibration set used for colour initialization.



(a) Manual definition of the circular region for chromatic segmentation by means of three mouse clicks.

(b) Resulting HSV segmentation.

Fig. 2.16 Manual initialization of the circular ROI.

are the nominal radius of the sphere, in this case, 100 mm, and the outlier rejection threshold, 10 mm. In the case of no convergence of the fitting, due to the exit of the tool from the FoV or due to the failure of the algorithm, the frame is automatically skipped.

The 3D position of the calibration tool, $[X_{ct} Y_{ct} Z_{ct}]$, is the result of a minimization process. A closed form notation for the covariance is usually missing in this type of problem because the derivative of the minimization for the measurements is unknown or very complex to be computed. Besides, the minimization condition implies gradients close to zero in correspondence of the identified result, a minimum, preventing the application of standard uncertainty propagation as reported in [78].

For this reason, the associated 3×3 covariance matrix is computed in an approximated form using the formulation reported in [23], a known method amply used in the fields of statistic, computer vision, and robotics. Following this method, the analytic notation for the covariance $\text{Cov}(\hat{\mathbf{x}})$ in case of a minimization process is computed as:

$$\text{Cov}(\hat{\mathbf{x}}) \simeq \left(\frac{\partial^2 J}{\partial \mathbf{x}^2} \right)^{-1} \frac{\partial^2 J}{\partial \mathbf{z} \partial \mathbf{x}} \text{Cov}(\hat{\mathbf{z}}) \frac{\partial^2 J}{\partial \mathbf{z} \partial \mathbf{x}}^T \left(\frac{\partial^2 J}{\partial \mathbf{x}^2} \right)^{-1}. \quad (2.2)$$

Elements of the formulation are: the minimization algorithm A , the error functional J that depends on the set of measurements $\hat{\mathbf{z}}$, the result of the minimization $\hat{\mathbf{x}}$ (the parameter of interest \mathbf{x}) equal to $\hat{\mathbf{x}} = A(\hat{\mathbf{z}}) = \arg \min_{\mathbf{x}} J(\hat{\mathbf{z}}, \mathbf{x})$.

For the considered application, the notation combines the contribution given by the fitting method J , the minimization process A considered in RANSAC and the uncertainties of all 3D measurements used in the process, $\text{Cov}(\mathbf{z})$, i.e. a block diagonal matrix built from the covariance matrices of the p 3D points identified as inlier from the spherical fitting.

Given an inlier point P of coordinates $[x_P, y_P, z_P]$, its covariance matrix C_P is evaluated as:

$$C_P = R^T C^* R + C_S, \quad (2.3)$$

where:

- R is the rotation matrix that aligns the \mathbf{z} versor to the position of the 3D point in space;
- C_S is an additive covariance term that considers the systematic effects that affect the depth readings in relation to the area of the image from which the data is taken.
- C^* is the covariance matrix of a virtual point aligned with the z axis at a depth d :

$$C^* = \begin{bmatrix} (d \cdot \tan(ar_h))^2 & 0 & 0 \\ 0 & (d \cdot \tan(ar_v))^2 & 0 \\ 0 & 0 & \left(\frac{d}{1000}\right)^2 \end{bmatrix}, \quad (2.4)$$

where:

- d is the depth measurement (expressed in mm), coincident with z_P ;
- ar_h is the horizontal angular resolution, 70.6° over 512 pixels;
- ar_v is the vertical angular resolution, 60° over 424 pixels;

For the modelling of the uncertainty, the representation presented in [176] is considered, in which the spatial distribution of the uncertainty over the x and y planes is a function of depth. Such representation is here rearranged: a linear formulation in the direction of the depth measurements (the third element of the diagonal of C^* and a 2D transversal covariance mapping, C_S (3×3 matrix with a null third row and column), also function of depth. The matrix is built starting from the coordinates defined in the reference paper, which were used here to evaluate four continuous functions, semi-lobes, in the FoV of the sensor. Inside these regions a constant uncertainty σ value is considered: 2 mm, 3 mm and 4 mm (from the extreme boundary to infinite).

The reference coordinates of half of each boundary, two on the horizontal plane and two on the vertical plane, are expressed in polar coordinates and then fitted with a polynomial P : $\theta = P_G^{H,V}(r \rightarrow depth)$, where θ is function of radius, coincident with the depth expressed in mm (z

Table 2.2 Coefficients of the semi-lobes.

| | $A \cdot r^2$ | $B \cdot r$ | C |
|--------------------|--------------------------|--------------------------|-------------------------|
| $P_{2\text{mm}}^H$ | 0 | -341.64×10^{-6} | 1.0007 |
| $P_{2\text{mm}}^V$ | -7.95×10^{-9} | -165.42×10^{-6} | 567.90×10^{-3} |
| $P_{3\text{mm}}^H$ | -238.25×10^{-9} | 843.89×10^{-6} | -59.57×10^{-3} |
| $P_{3\text{mm}}^V$ | -157.50×10^{-9} | 536.32×10^{-6} | 59.23×10^{-3} |

axis). A first-order polynomial was found as the best fitting notation for the horizontal 2 mm semi-lobe, second-order polynomials for the others (Fig. 2.17). The identified parameters for the polar representation of the semi-lobes are reported in Tab. 2.2.

Given the horizontal and vertical semi-lobes for a defined uncertainty σ , the representation of the boundary $B_{\sigma}^{xyz}(d^*)$ of the 3D volume is computed using an elliptic formulation. This is a function of the depth d^* and the angular position of the 3D point P_{xyz} , coordinate that has to be verified if internal or external to the boundary itself:

$$P_{xyz} \rightarrow \left[\alpha = \text{atan2} \left(\frac{y}{x} \right); d^* = z \right]$$

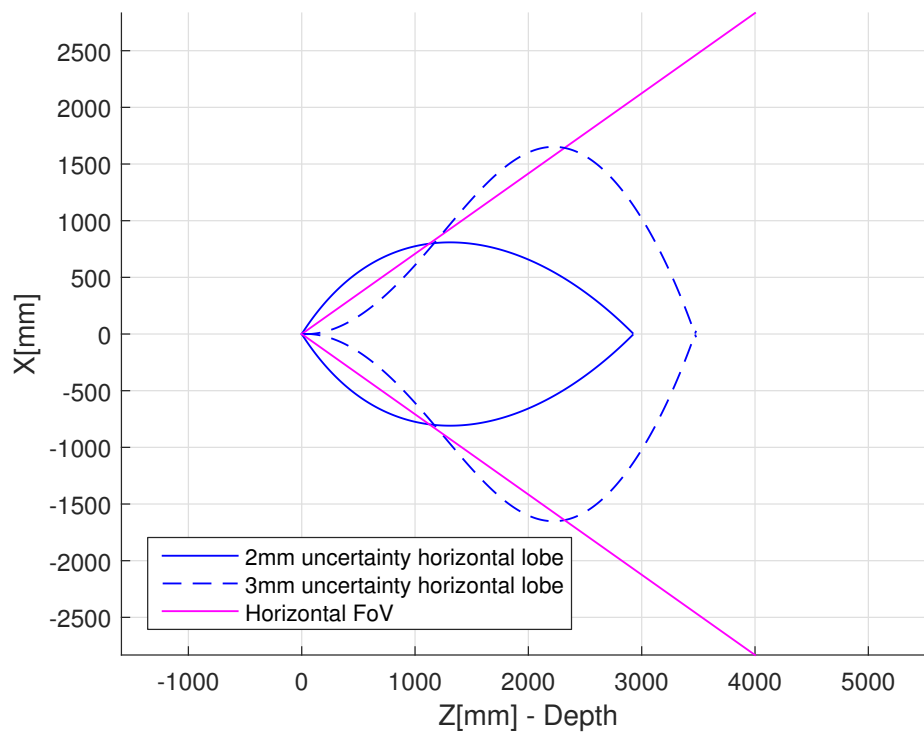
$$B_{\sigma}^{xyz}(d^*) = d^* \cdot \begin{bmatrix} \tan(P_{\sigma}^H(d^*)) \cdot \cos(\alpha) \\ \tan(P_{\sigma}^V(d^*)) \cdot \sin(\alpha) \\ 1 \end{bmatrix} \quad (2.5)$$

If P_{xyz} falls inside $B_{\sigma}^{xyz}(d^*)$, the covariance matrix C_S is populated with the σ uncertainty, otherwise the algorithms tests the successive boundary:

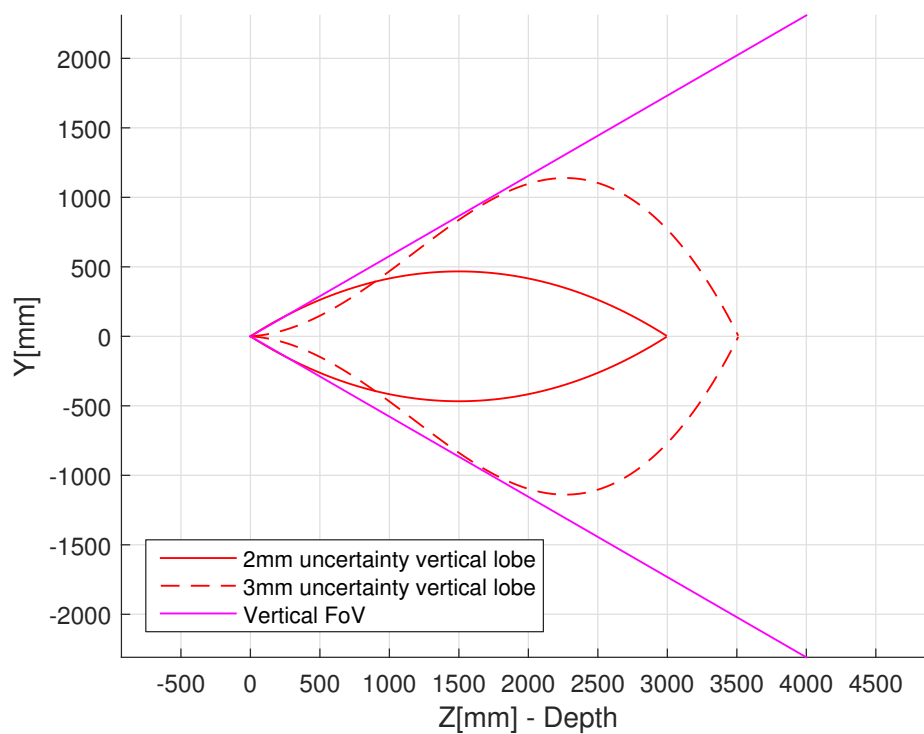
$$\text{if } P_{xyz} \in B_{\sigma}^{xyz}(d^*) \rightarrow C_S = \begin{bmatrix} \sigma^2 & 0 & 0 \\ 0 & \sigma^2 & 0 \\ 0 & 0 & 0 \end{bmatrix} \quad (2.6)$$

C_P is then the result of two contributions: C^* as local uncertainty of the data due to the limits in resolution of the device, C_S as model for the systematic effects, mostly related to the uncertainty in the intrinsic parameters of the sensors with respect to the area of the depth image in which the measurement falls. Fig. 2.18 reports the uncertainty ellipsoids evaluated with the proposed formulation for a set of 3D positions on planes at 1.5 , 2.5 and 3.5 m from the centre of the sensor.

The calibration process computes the positions and the associated covariance matrices for all the frames recorded. In Fig. 2.19, an example of the segmentation and fitting is reported



(a) Horizontal plane.



(b) Vertical plane.

Fig. 2.17 Models used for the definition of spatial uncertainty related to the intrinsic parameters of the device.

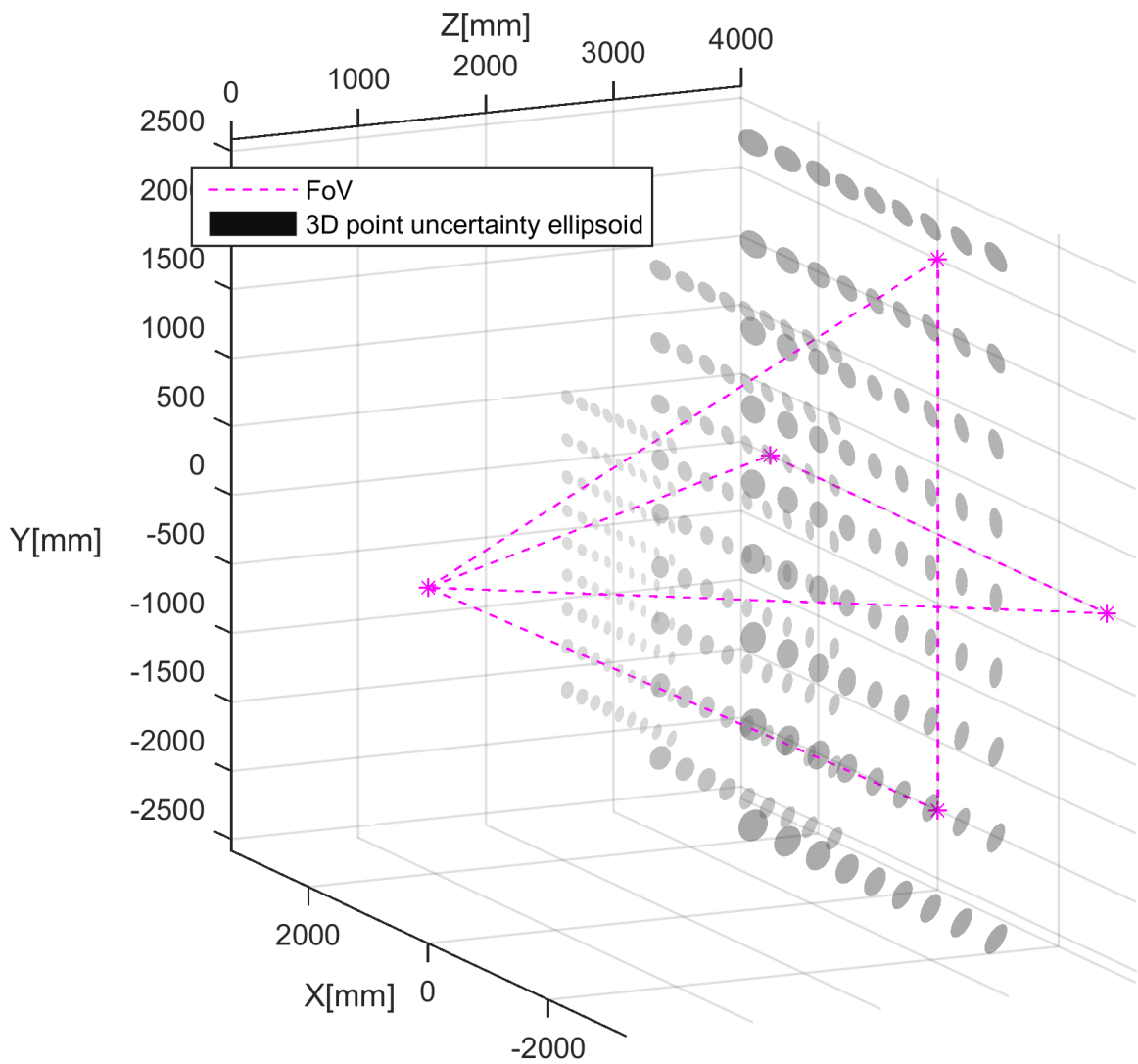


Fig. 2.18 Spatial distribution of the uncertainties, xyz , resulting from the proposed model. Ellipsoids magnified by a factor of 25, ellipsoid 5 times wider.

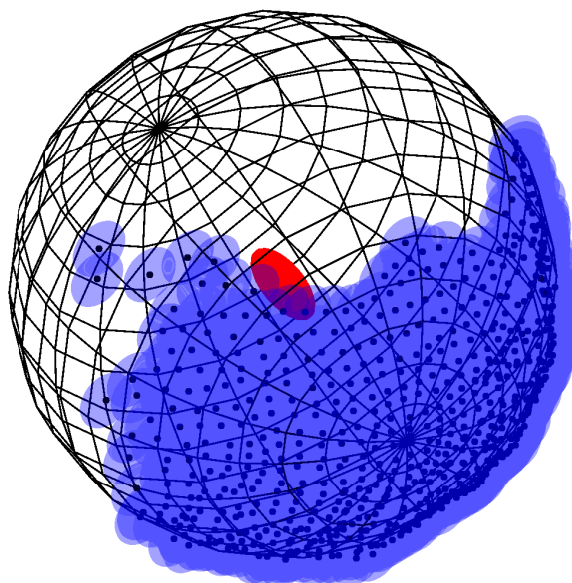


Fig. 2.19 Result of RANSAC fitting, covariances at 95 % ci. The covariance of the centre of the calibration tool is magnified by a factor of 100, ellipsoid 10 times wider.

with 690 inliers and an assessed variance along the Cartesian xyz directions equal to 0.17, 0.23 and 0.75 mm^2 . In the experimental setups, it was found that these values can vary along the trajectories from a minimum of 0.1 to a maximum of 5.8 mm^2 .

After the trajectory extraction, the data are organized in N trajectories, one for each 3D camera. Each trajectory is composed of a sequence of 3D points, their covariances and a time reference (Fig. 2.20). These N datasets must be synchronized to create the geometrical constraints required by the calibration process.

The common approach exploits the idea that points acquired at the same time must share the same position in space. Following such an idea, most of the algorithms identify the points that are close in the time domain, having in practice a low time delay among them, and use such constraint to perform the spatial matching of the data. In the case of acquisition systems made of multiple Kinects, such idea becomes invalid: the points recorded with nominal equal times references could be instead acquired at physically different instants.

The inversion of the paradigm solves the issue: from the spatial matching of the trajectories can be assessed the time delays between the data. The acquisition system records indeed the same motion but seen from different points of view. The method exploits such assumption: an initial analysis of the geometry of the trajectories assesses the time shift

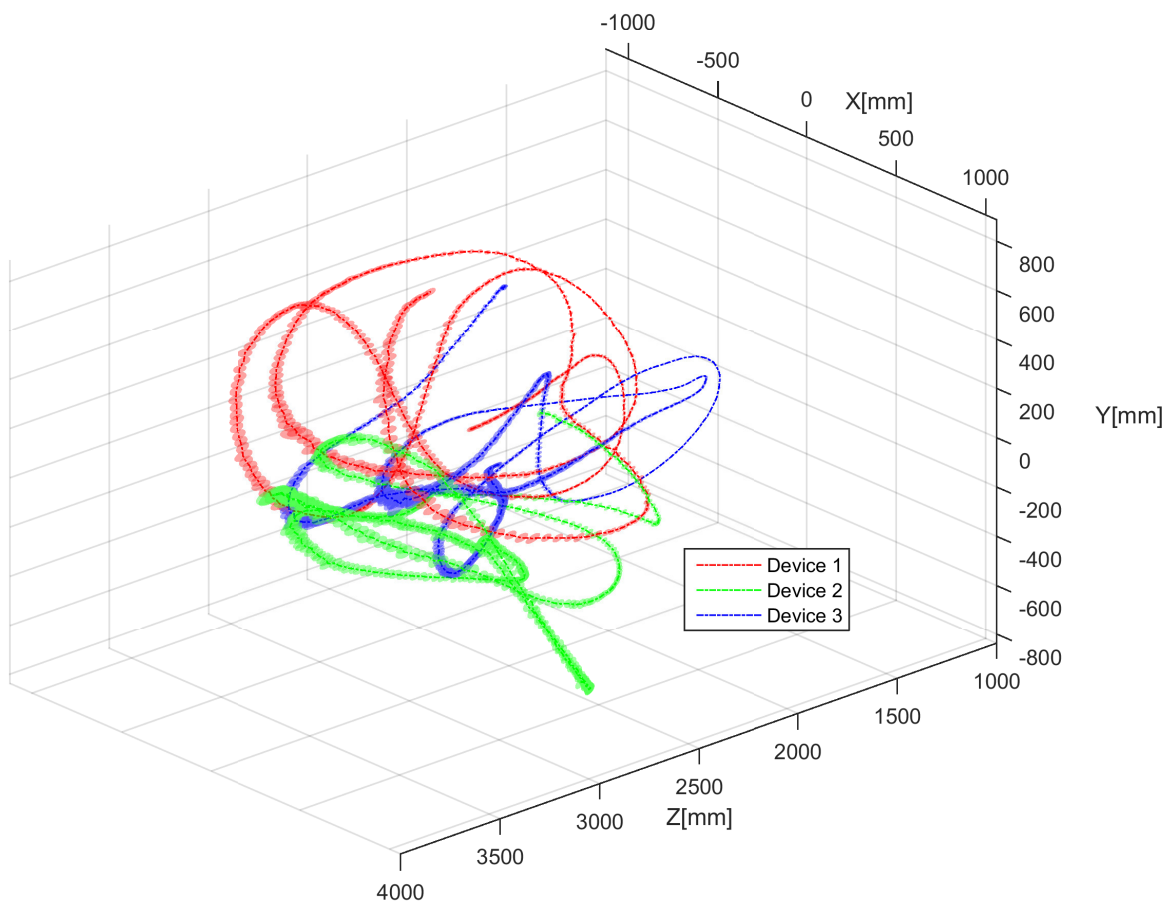


Fig. 2.20 Identified trajectories of the calibration tool and covariances, 95 % ci. The covariances are magnified by a factor of 100, ellipsoids 10 times wider.

between the data; such information is then used to create the spatial constraints for the matching problem.

The assessment of a delay between two signals can be achieved using cross-correlation. The application of such a technique to three-dimensional signals is not trivial and prevents the direct use of the Cartesian coordinates as a spatial reference for the matching. A kernel invariant to the orientation of the sensors to the target is therefore defined to project the 3D data to 2-dimensional space, frame and kernel, in which to perform the synchronization.

The analysis on time delays is organized by selecting one of the trajectories as the reference and performing one-to-one comparisons with the others.

As the first step, a rough sub-sampling of the data is performed using the available time information: given two trajectories at a time, only those points that share a time delay lower than 66 ms, 2 nominal frames, are kept. In the case of multiple matching, the couples with the highest delay are removed. The operation has multiple advantages: (i) it creates two sets of points with the same number of elements; (ii) the removal of points that are seen only by one device at a time; (iii) only the data that are namely synchronous remain in the process (first guess for temporal synchronization). Even if a systematic delay is present, the initial sub-sampling provides as output two sub-trajectories with a similar spatial distribution, equal (apart for the noise components) in the case of zero delays.

The same occurs in the domain of the principal component. The principal bases offer a geometrical representation that is invariant to orientation and relative displacement of data, dependent instead only on spatial distribution. For the application of the cross-correlation analysis, the projection of the trajectories along their first principal vector, associated with the maximum eigenvalue and so to the most reliable among the bases, is used. The result is a 1-dimensional signal expressed in the frame domain (or time) that represents the displacement of the 3D points to the centre of mass of the sub trajectory (from the initial rough sub-sampling) and along the direction with the maximum variance. That defines a FoV invariant kernel, which is applied to all recorded trajectories to obtain a homogeneous representation of the calibration data.

Because of the initial lack of synchronization, the projected signals could result incomplete with mutually missing portions, from the initial and the final parts. That lowers the accuracy of the assessment if the standard cross-correlation is used, as far as the zero paddings of the signal could become not negligible. Customized processing is structured to overcome that issue. An initial cross-correlation is performed to identify which signal is in advance, named “first”, and which is delayed, “second”. A loop is structured. At each iteration, a new cross-correlation is performed after the removal of one sample from each signal: the first one from the “first” and the last one from the “second”. The results of the correlations are

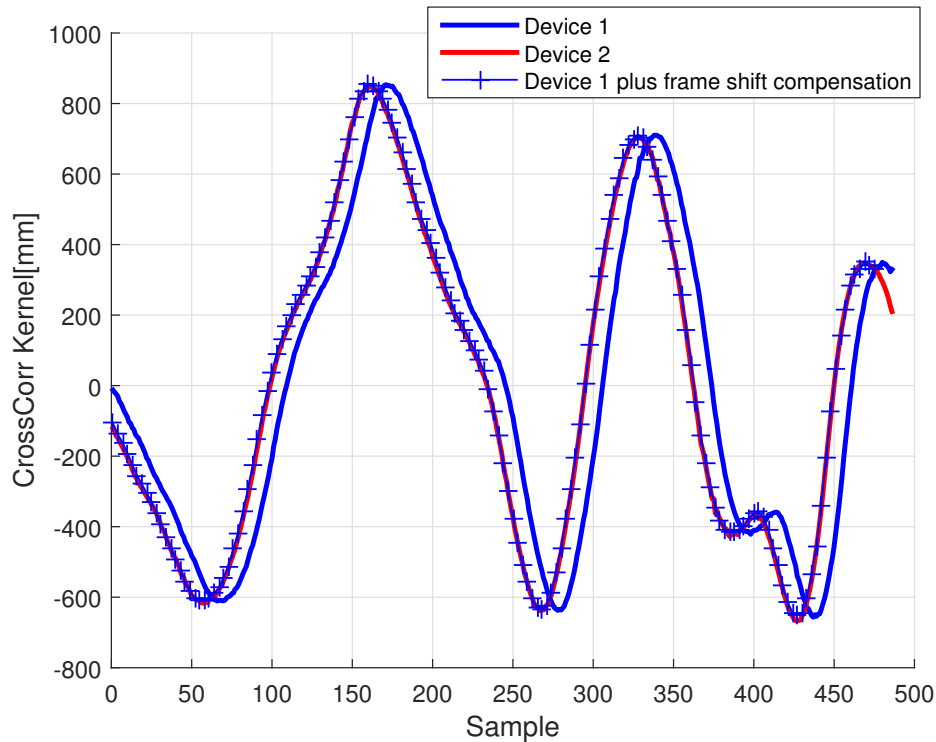


Fig. 2.21 Trajectory projection to FoV invariant kernel and synchronization in frame domain.

recorded in an array. At the end of the loop, the algorithm identifies from this array the first zero crossing and the associated contiguous zeros. The frame delay between the devices is evaluated as the mean value of the indexes associated with the identified zeros. That value multiplied by the mean sampling period represents the time delay between the acquisitions and so the correction factor that minimizes the systematic effects due to a non-synchronous nominal time.

The identified frameshift is used to rearrange the original trajectories to their synchronous sub-parts (Fig. 2.21).

If the delay between the data is high, i.e. more than 300 ms, systematic differences in the geometric distribution and data association can cause relevant discrepancies in the principal decompositions. These differences cause a systematic error in the cross-correlation since the projection of the trajectories takes place along different vectors. The solution to such a problem is the iteration of the proposed algorithm. By performing the first processing it is possible to identify a rough estimation of the delay. That can be applied as the first compensating factor in the time domain, correcting the nominal time reference of the frames. A “more” synchronous subset can now be re-selected from the original trajectories and a further refinement performed. From the performed testing, one iteration is sufficient for standard networks since the NTP can keep the synchronization of the PCs to values lower

than 100 ms. A second interaction is instead suggested for the cases of very high delays or latencies due to limitations of the network.

Once the time delays are identified and compensated, the resulting synchronous subset of trajectories is processed to assess the relative displacement among couples of 3D sensors.

The operation exploits an SVD based processing [156, 5] by spatially matching, point-to-point, the synchronous data. Defined as Tr_1 and Tr_2 the synchronous subset of f frames, $\overline{Tr_1}$ and $\overline{Tr_2}$ the respective centroids, the cross correlation matrix CC_m is computed as:

$$CC_m = [Tr_1 - \overline{Tr_1}] \cdot [Tr_2 - \overline{Tr_2}]^T \quad (2.7)$$

The SVD of CC_m is computed and the searched homogeneous matrix H between Tr_1 and Tr_2 is evaluated as:

$$H = \begin{bmatrix} V \cdot U^T & -(V \cdot U^T) \cdot \overline{Tr_1} + \overline{Tr_2} \\ 0 & 1 \end{bmatrix} \quad (2.8)$$

The above notation is robust since it can compensate for the occurrence of mismatches in the coupling of points and minor deviations in the spatial distributions of the trajectories. $N - 1$ homogeneous matrices are evaluated for the N devices that constitute the acquisition system.

Global optimization is performed to combine all information and to improve the overall accuracy of the extrinsic parameters to the uncertainty content derived from the data acquisition and the processing.

A graph-based approach is used. From the guidelines presented in [35], *GTSAM toolbox*, a dedicated graph is automatically structured. A device is marked as the reference system, for the convenience of the organization the same used for the time synchronization, and placed in the origin.

The nodes of the graph are:

1. the positions of the devices with respect to the reference one ($N - 1$);
2. the positions of the calibration tool seen by each device expressed in the reference system.

Both resulting from the previous SVD matching.

The connections are:

1. among each device and position of the calibration tool (identified by that device). These connections represent the measurements performed by the devices with respect to the calibration tool. The covariance matrices of such measurements are used as uncertainty information.

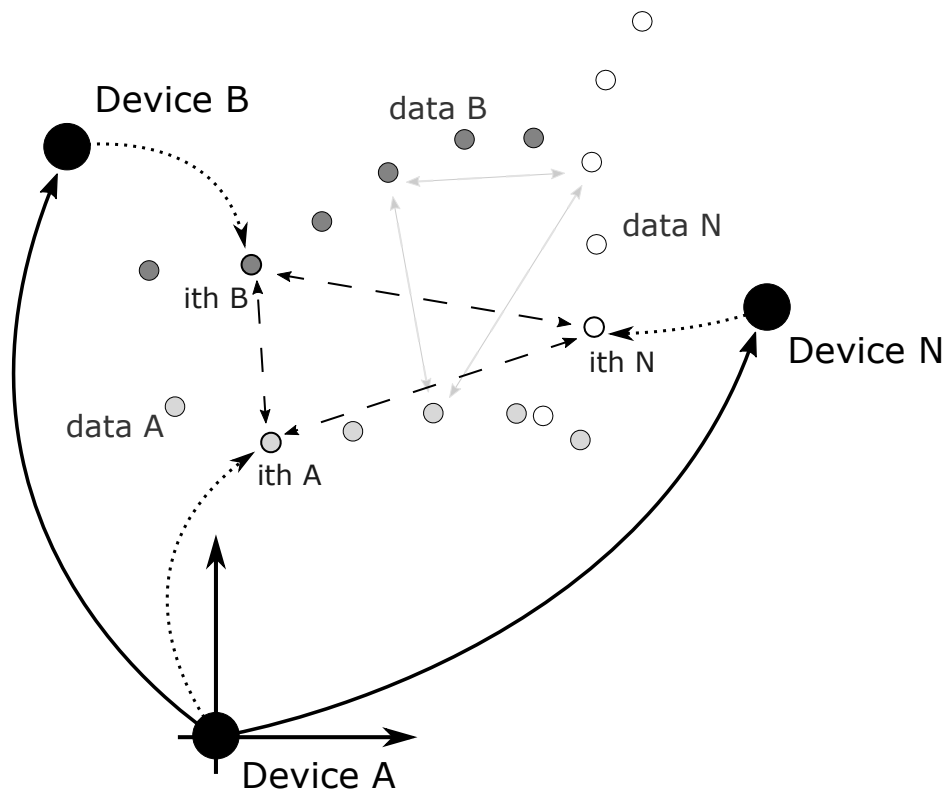


Fig. 2.22 Graph structure for a set of N devices. In the figure are shown the connections among the data that are automatically created before the global optimization.

- among the synchronous positions of the calibration tool, identified at the same time instant by different devices. These connections model the coincidence in the position of synchronous frames. The coupling of the nodes can be performed either considering the corrected time reference or either performing again the spatial FoV invariant synchronization between the $\frac{N!}{2!(N-2)!}$ combinations of devices organized in couples. The number of connections for each node varies according to the identification result, positive or negative (failure or outside FoV). A relaxation parameter is considered: a σ of 2 mm in all directions.

Uncertainties are expressed in the graph in terms of Cartesian coordinates xyz . The angular part is left free because of the invariant behaviour of the shape to such a parameter. For that reason, the σ of the angular values is set to a value of 10π .

The graph is solved using a Levenberg Marquardt optimization, included in the GTSAM library¹. Results of the processing are the extrinsic parameters of the acquisition system and the associated covariance matrices.

¹GTSAM library, <https://borg.cc.gatech.edu/download?destination=node%2F299>

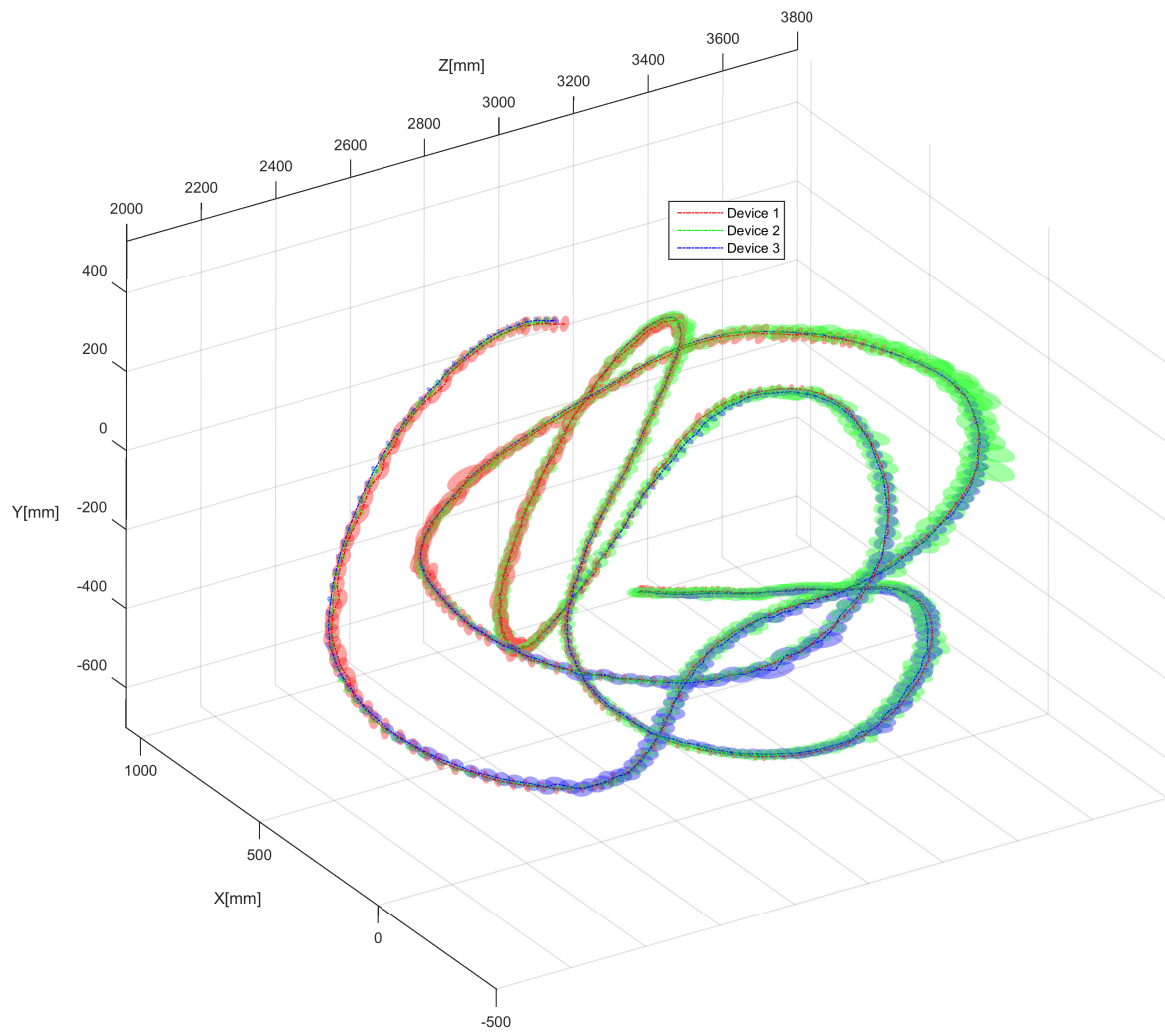


Fig. 2.23 Alignment of the trajectories resulting from graph optimization. The covariances (95 % ci) are magnified by a factor of 100, ellipsoids 10 times wider.

Table 2.3 Identified extrinsic parameters and uncertainties (3σ , 99 % ci).

| | α [rad] | β [rad] | γ [rad] | Tx [mm] | Ty [mm] | Tz [mm] |
|-----|---------------------|----------------------|----------------------|-------------------|------------------|------------------|
| D 1 | 3.0690 ± 0.0024 | -0.9770 ± 0.0015 | -3.1313 ± 0.0024 | -1975.6 ± 3.8 | -181.7 ± 6.0 | 3926.1 ± 0.9 |
| D 3 | 3.0005 ± 0.0021 | 1.3464 ± 0.0015 | 2.9543 ± 0.0024 | 2418.4 ± 3.8 | -175.5 ± 5.2 | 3578.4 ± 0.9 |

For the acquisition system in Fig. 2.12, made of three devices, the standard deviations for the relative displacements resulted in lower than 2 mm, and the relative attitude along the axes lower than 10^{-2} rad (0.6°). An example of the obtained extrinsic parameters is presented in Tab. 2.3, in which the device 2 (D2) is used as reference and origin of the acquisition system.

Completed the calibration process, the identified extrinsic parameters can be used for the reconstruction of the entire shape of subjects moving inside the monitored area. The resulting entire shape is simply the transformation of the data acquired by each device to the reference system. No registration or further optimizations are performed.

Fig. 2.24 shows an example of the results obtained by the presented calibration method for the acquisition of a moving subject.

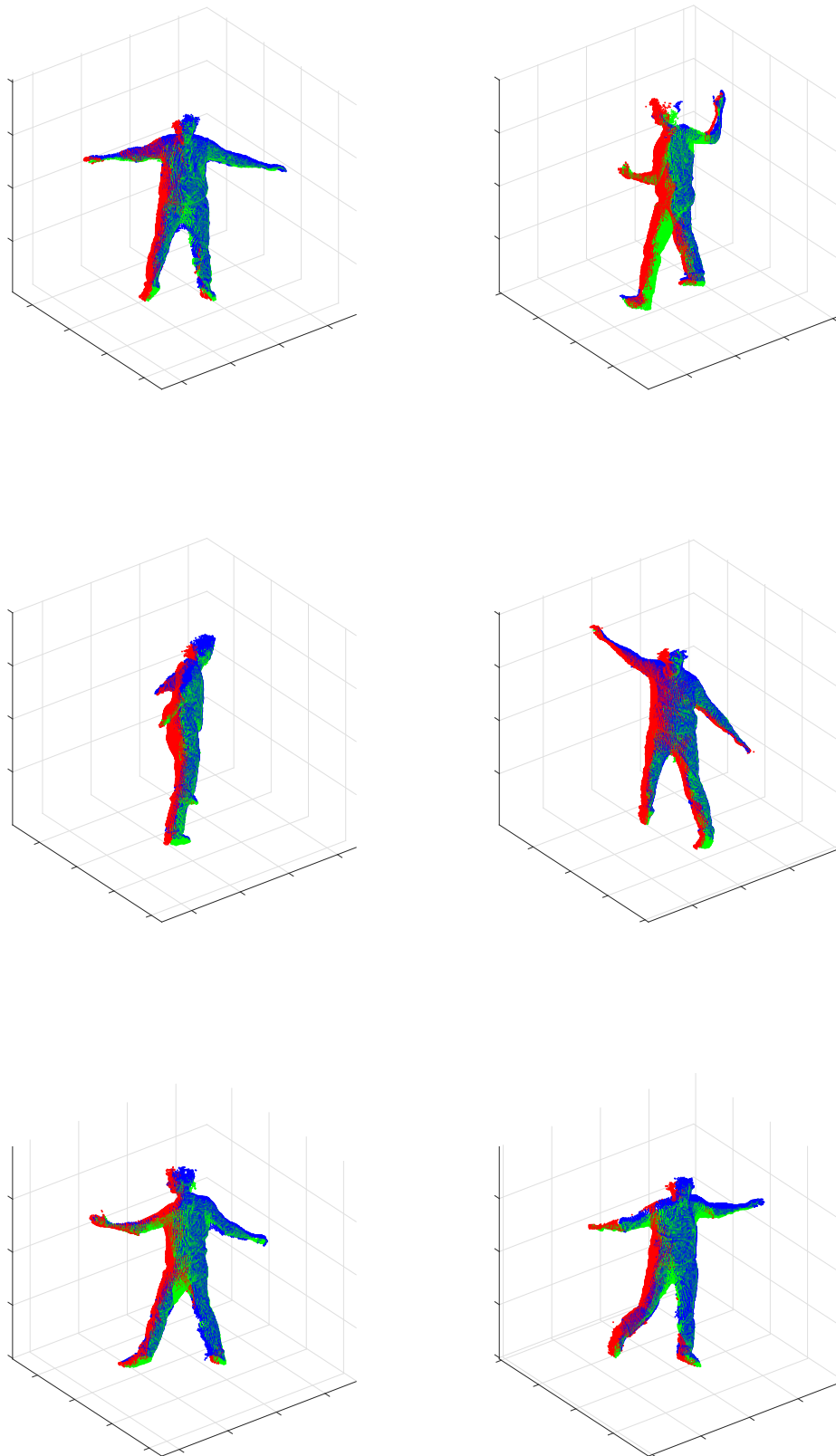


Fig. 2.24 Example of the acquisition sequence of a moving subject. The different colours correspond to the data of the different devices.

Chapter 3

Stress assessment

3.1 The mechanism of stress

The concept of fatigue is related to the effort in carrying out any activity. Human fatigue can be distinguished into three main categories:

- whole body physical fatigue;
- localized muscular fatigue;
- mental fatigue.

Whole body physical fatigue is a condition that affects the whole organism as a deterioration in physical and mental performance. It can arise due to environmental factors, such as noise, illumination, and climate, psychological factors, such as responsibility, worries, conflicts, and condition of health, fitness, and nutrition.

Muscular fatigue affects localized areas of the body. It is the result of sustained or repeated exertions of the body. Symptoms of this kind of fatigue include the increase of the heart and breathing rate, tremor, reduced sensitivity of the muscle to voluntary requests coming from the nerve centres and profuse sweating. The efficiency of muscle work is progressively reduced, also due to psychological factors, such as anxiety, nervousness, and apprehension.

Mental (or cognitive) fatigue is related to cognitive activity. It can be defined as a change in the psycho-physiological state, due to an intense and/or long mental effort. The main symptom is the difficulty in maintaining task performance at an adequate level.

Stress is instead defined as “the non-specific response of the body to any demand for change” [136]. While effort ends together with the activity that generated such effort, stress ends only when danger (real or imagined) is eliminated.

Stress is a key resource that can make the difference between life and death [136]. However, dangerous situations for health can happen, if stress mechanisms activate in a useless manner and for a long time. Indeed, an unhealthy level of stress is a direct cause of diseases and disorders [26, 80] such as sleep disorder, difficulty in concentration and decision, short-term memory loss, altered mood, depression and anxiety, inflammation and cardiovascular problems. Stress is considered one of the most serious social problems in today's society for its high social cost [69]. For the aforementioned reasons, accurate measurements of stress levels are necessary to apply a mechanism for prevention and treatment.

Different areas are interested in mental stress assessment, such as the ones related to cardiovascular risk [159, 40, 31], exercises to reduce stress level [39, 57], work-related stress [83, 138, 182], student stress [166], and environmental stress [149]. Accurate measurement of stress and effort can be also helpful in ambient assisted living [119] scenarios. These kinds of measurements can be helpful for therapists, providing information not directly perceivable by mean of observation.

3.2 Physiological measures for stress detection

Stress detection can be performed acquiring physiological signals. Examples of physiological signals that can be used for stress detection are [140, 146]:

- the cortisol levels, usually measured in saliva. The drawback of this kind of measures is that they are invasive and it is very difficult to obtain continuous monitoring of such levels;
- the cardiovascular system activity usually monitored through ECG, BVP and Arterial Blood Pressure (ABP);
- the respiratory system activity, that is strongly related to cardiovascular system activity;
- EDA, i.e. the electrical conductivity of the skin surface;
- the muscle activity, measured through electromyography (EMG), which measures the level of discharge of the motor nerve fibres that innervate the muscle;
- the brain activity, measured through EEG.

All these signals are in some manner linked to the activity of the autonomic nervous system (Fig. 3.1) that can be subdivided into two parts: the parasympathetic and sympathetic system. Both systems are linked at several organs, such as heart, bronchi, and lungs, skin,

blood vessels, stomach, intestine, and glands. The two systems act on the different organs synergistically to maintain the correct balance in different environmental situations.

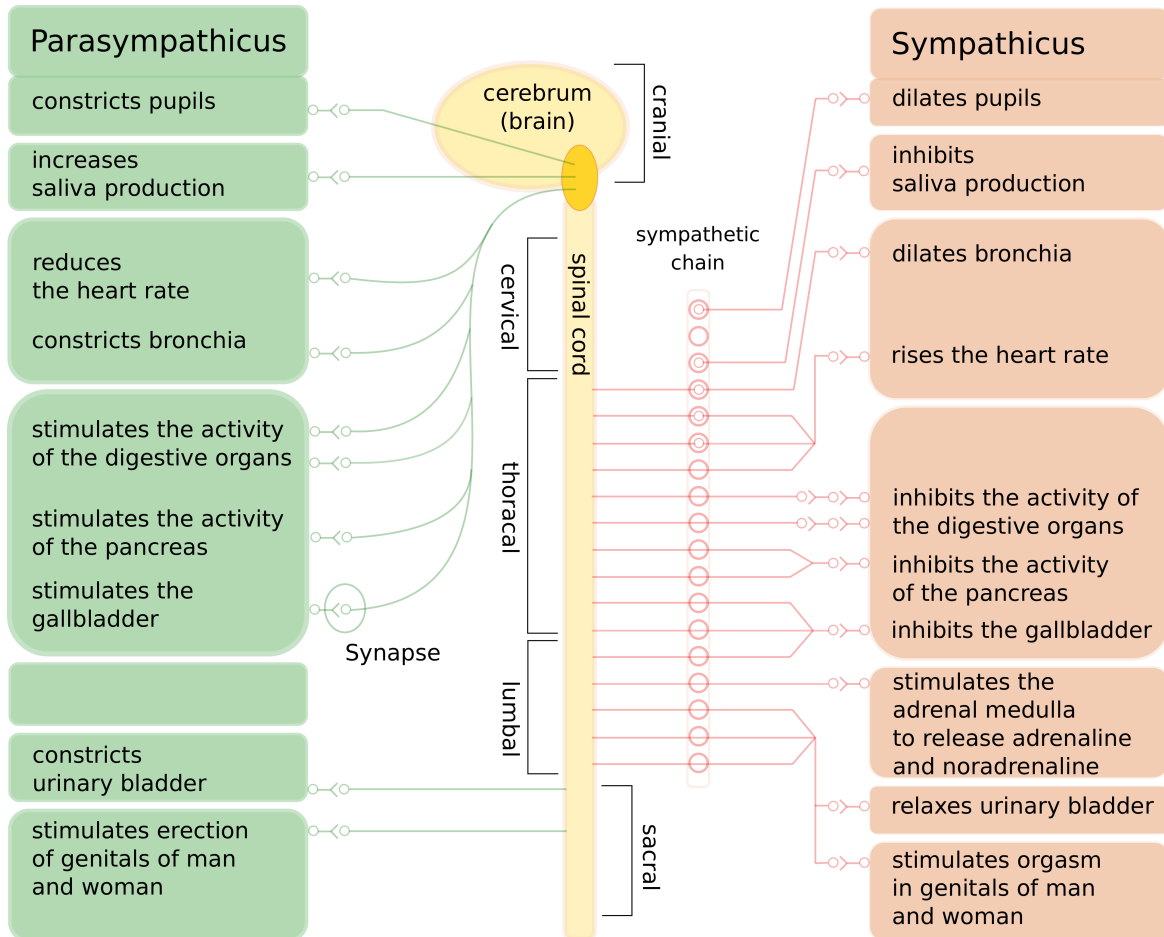


Fig. 3.1 Function of the autonomic nervous system.

The sympathetic system is the component that is linked to the “fight or flight” functions. It prepares the body to face dangerous situations (real or imagined): the heart rate and the blood pressure increase, pupils and bronchi dilate, digestive processes slow down, peripheral blood vessels constrict, while the blood vessels of the appendicular muscles and the coronary system dilate. This component is active during physical activity, during work, or, more generally, during emergencies. The parasympathetic system is instead active in situations such as digestion, rest and energy storage. In this case, the heart rate slows down, the blood pressure decreases, the bronchial muscle tone increases, blood vessels dilate, the respiratory activity slows down and the muscles relax.

Measuring the balance between the sympathetic and the parasympathetic systems can give important information regarding what is happening in the human body. In particular, a

higher activity of the sympathetic system with respect to the parasympathetic system usually indicates that the body is under acute stress. It is, however, important to underline that it is also possible that the parasympathetic system may act in the same as the sympathetic because of the non-linearity of the interaction [153].

3.2.1 Cardiovascular system activity

The cardiovascular system is the set of organs and vessels responsible for the circulation of blood in the organism. The cardiovascular system activity can be measured through BVP and ECG signals. The BVP is related to the change in volume of blood that flows into peripheral vessels and generally is measured through a PPG sensor. The PPG sensor finds the cyclical changes in the pressure tone in the capillaries that represent the heartbeat, illuminating the skin and measuring changes in light absorption [143]. A great advantage of this kind of sensor is that they have low invasiveness, but they are quite sensitive to motion. The ECG instead is the recording of the electrical activity of the cardiac cells on the body surface. The ECG gives a more accurate measure of cardiovascular activity, but the electrodes must be placed in direct contact with the user skin. Therefore, this solution could be less comfortable.

A frequently used measure to study the balance between the sympathetic and parasympathetic nervous system is the heart rate variability (HRV). HRV indicates the variation in the heartbeats within a specific timeframe. The rhythm of the heartbeat indeed has a natural fluctuation caused by the exercised control of the sympathetic and parasympathetic systems. The computation of the HRV depends on what technology is used. Using an ECG, a heartbeat is typically marked by the R peak in the QRS complex (Fig. 3.2). Hence, the intervals between heartbeats are called R-R intervals. Once the exact intervals between the heartbeats are computed, it is possible to draw the so-called tachogram: a diagram that expresses the R-R interval between a heartbeat and the following in function of the heartbeat number (Fig. 3.3).

Standard HRV measures are divided into two broad categories: time domain and frequency domain measures [174]. The analysis in the time domain uses statistical operations applied to the R-R interval. The most frequently used are:

- The standard deviation of normal-to-normal intervals (SDNN) (measured in ms)
- The root mean square of the successive differences (RMSSD) (measured in ms)

RMSSD is a measure of parasympathetic activity, whereas SDNN reflects both sympathetic and parasympathetic modulation of heart rate [174, 94].

The analysis in the frequency domain (spectral analysis) gives instead some value, among which:

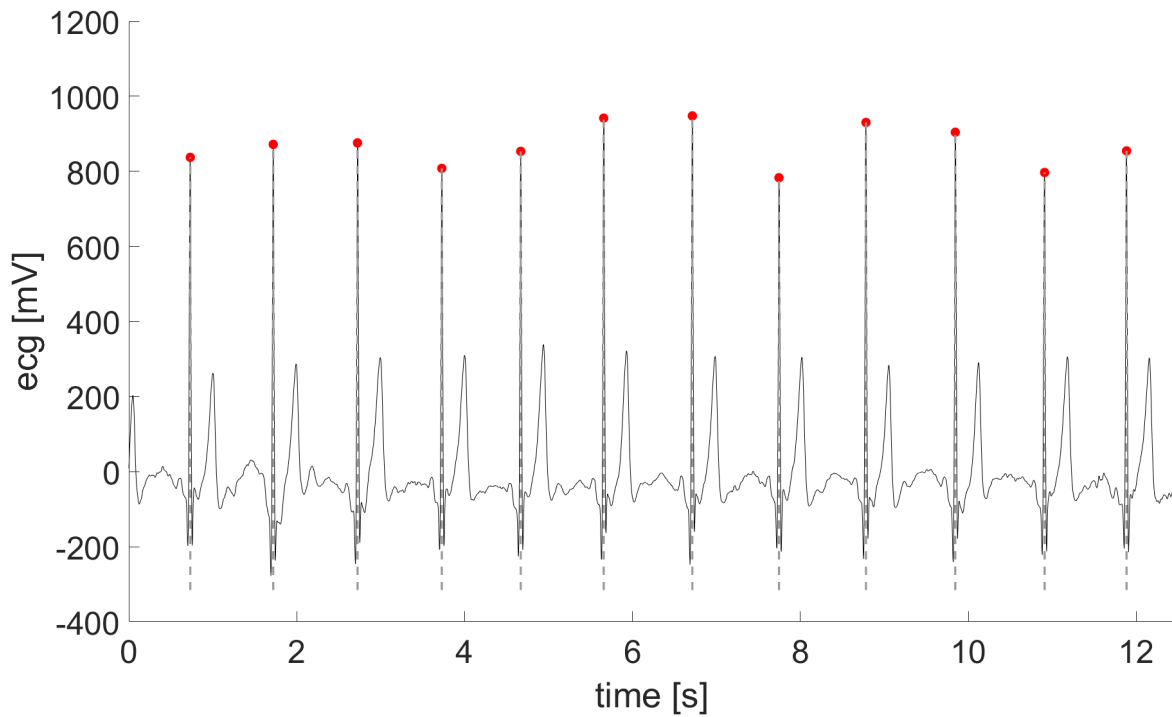


Fig. 3.2 ECG signal. The red dots correspond to the R peak.

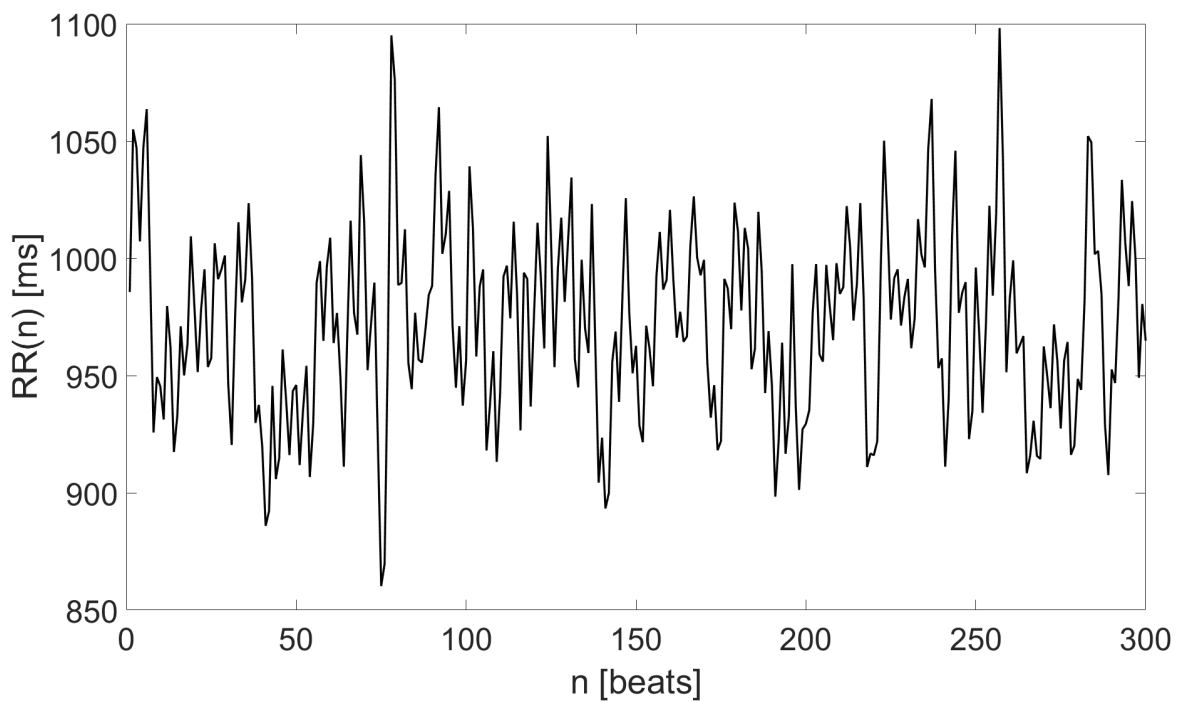


Fig. 3.3 An example of a tachogram. The R-R intervals are plotted over the heartbeat number.

- The low-frequency (LF) power (0.04-0.15 Hz);
- The high-frequency (HF) power (0.15-0.40 Hz);
- The low-frequency high-frequency ratio (LF/HF);

Changes within the LF band are mediated by both cardiac vagal and sympathetic nerves, as well as arterial blood pressure [162, 124]. HF is instead a marker of the parasympathetic tone [174]. The LF/HF ratio is used to investigate the activity of the sympathovagal balance. Reduction of LF/HF ratio appears to be a clear sign of unbalance between sympathetic reflex interactions with a shift toward sympathetic withdrawal, and consequent vagal predominance [174]. Fig. 3.4 shows an example of a Power Spectral Density (PSD) of an RR time series during rest and a mental arithmetic task. It can be noticed how the LF peak increases during the stressful task and consequently the LF/HF ratio increases.

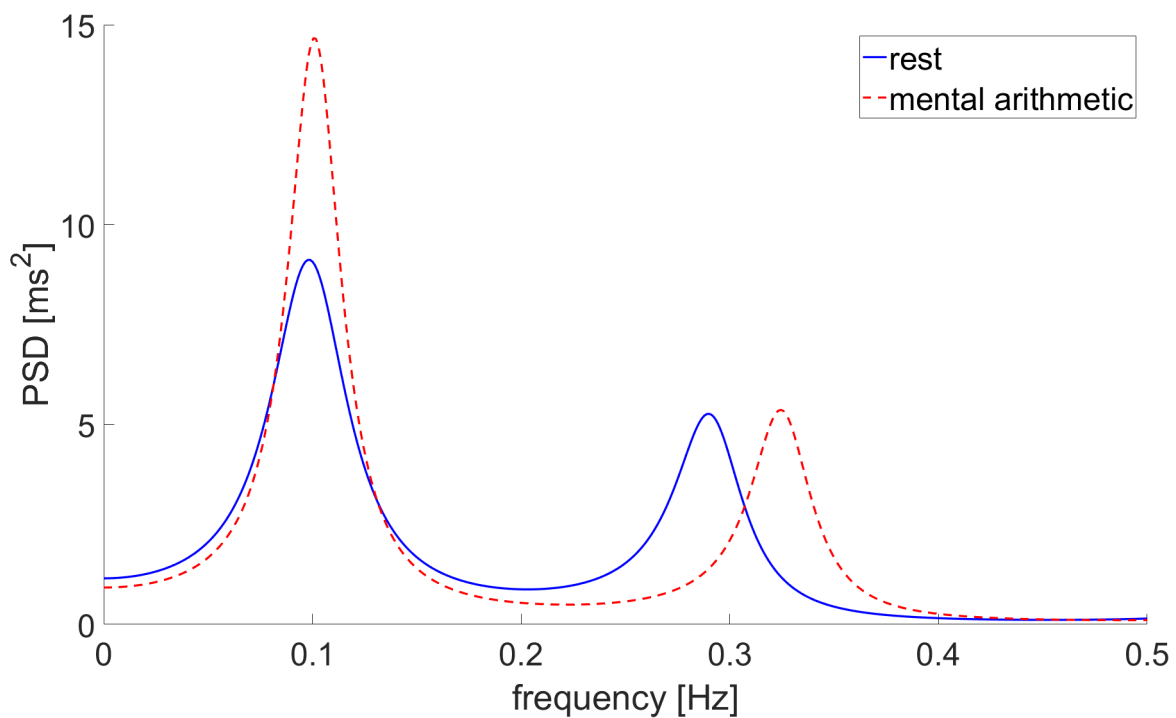


Fig. 3.4 Comparison between a PSD of an RR time series during rest and during mental arithmetic. It can be noticed how the LF/HF ratio increases during the stressful task.

In addition to the standard techniques in the time and frequency domain, there are also nonlinear methods. Such methods try to quantify the structure and complexity of the RR interval time series and are based on chaos theory and nonlinear system theory [59]. Examples are Detrended Fluctuation Analysis (DFA) to investigate the statistical self-affinity

of the HRV, the sample entropy, the fractal dimension, the Lagged Poincaré Plot (LPP), and Recurrence Quantification Analysis (RQA) [1, 63].

Generally, when the body is not under stress conditions, there is a natural variation between an R-R interval and the following. When the activity of the sympathetic system is prevailing, this natural variation is reduced: as soon as the sympathetic activity increases, the parasympathetic effect on the heart rate decreases. This behaviour determines a more stable rhythm. On the contrary, when the parasympathetic activity is very high, an increase in the HRV occurs.

Another parameter used to measure the cardiovascular system activity is the Blood Pressure (BP). BP is defined as the force exerted by blood on the walls of blood vessels as it flows inside them. BP is determined from factors such as force impressed by cardiac thrust, the quantity of pumped blood to each heart contraction and resistance opposed by arteries.

BP is directly correlated to the sympathetic system: during a “fight or flight” response, BP rises due to an increase in heart rate and to contraction of blood vessels.

Researchers have been focused on non-invasive continuous measurements of arterial blood pressure. One of them is the Volume Clamp Method [170]. In this method, BP is measured using a finger cuff with variable pressure. A plethysmograph, installed inside the finger cuff, measures the blood volume changes, which are compared with a set-point value corresponding to a zero transmural pressure, i.e. the condition in which the wall of the blood vessel does not accumulate pressure and the pressure inside the artery is the same as that on the outside. Thus, a pneumatic servo system acts on the pressure exerted by the finger cuff to keep a zero transmural pressure. In this manner, the pressure applied to the finger cuff follows continually the intravascular pressure, giving a non-invasive continuous measurement of BP.

3.2.2 Respiratory system activity

Breathing frequency is an important indicator of stress assessment. In general, anxiety and stress give a faster and shallower breathing [165] and the respiratory rate, i.e. the number of breaths in a minute, increases with the physical or cognitive workload [98]. Moreover, mental stress and sustained attention tasks are proved to reduce respiratory variability [169].

Respiration is also strongly coupled with cardiovascular system activity [49]. The interaction between these two systems can be noticed in the variation in heart rate that occurs during the breathing cycle, the so-called Respiratory Sinus Arrhythmia (RSA). The RSA is a meaningful indicator of the parasympathetic activity of the autonomic nervous system [13].

There are different approaches for respiration monitoring, but generally, they can be distinguished in contact and non-contact measurements [3]. Contact approaches usually

measure parameters such as breathing sounds, airflow, and chest or abdominal movements. In this latter case, the respiratory signal (Fig. 3.5) can be acquired, for example, through a piezoresistive sensor applied on an elastic band or a t-shirt at the chest or abdomen level. Respiratory signals can also be derived from measuring the fluctuations in the ECG [105].

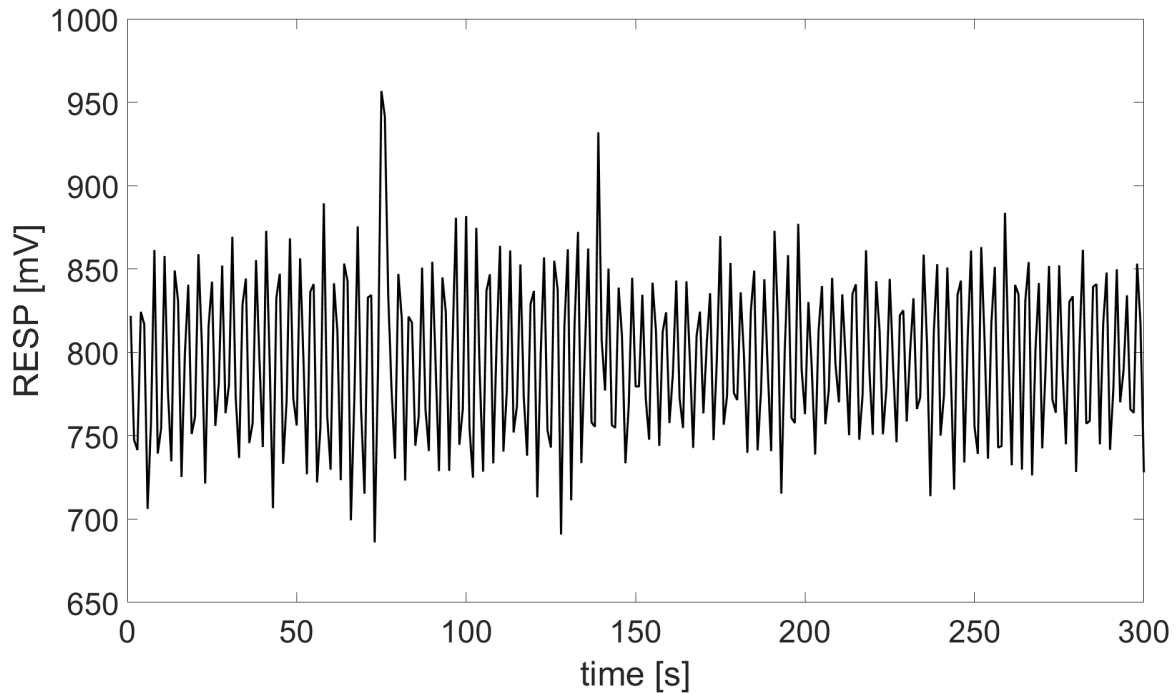


Fig. 3.5 An example of a respiratory signal acquired by a piezoresistive sensor.

Non-contact approaches for respiration monitoring rely instead on cameras [4] or on thermal sensors [74].

3.2.3 Electrodermal activity

EDA, also known as Galvanic Skin Response (GSR), is a measure of the continuous variations in the electrical characteristics of the skin. EDA refers to all the electrical phenomena (active and passive) of the skin. EDA increases when there is a sudden event, an increase in the mental workload and correspondence of both positive and negative emotional states. A common index used to quantify EDA is Skin Conductance (SC). SC varies with skin humidity and it is measured placing two electrodes on the skin, usually on two nearby fingers. The measurement is obtained applying a weak electric current through the electrodes, which generate a voltage from which it is possible to compute the conductance in microSiemens (μS). SC is a good index of “arousal” because the eccrine sweat glands depend exclusively on the sympathetic system [16].

SC can be split in two main components [32]:

- the skin conductance level (SCL), which is the tonic level, i.e. the basic level in absence of external stimuli. It is an index of the general state of activation of the nervous system. The more the individual is keyed up and nervous, the more is the skin sweating and consequently, the conductance rises;
- the skin conductance response (SCR), i.e. rapid phasic components. SCR changes in the function of emotional, sensorial or ideational events and acts in a short period.

Fig. 3.6 shows an example of a raw SC signal decomposed in its phasic and tonic components, using the cvxEDA algorithm [65]. It can be noticed how the SCR components are significantly higher and how the SCL rises during the mental arithmetic task with respect to the rest condition.

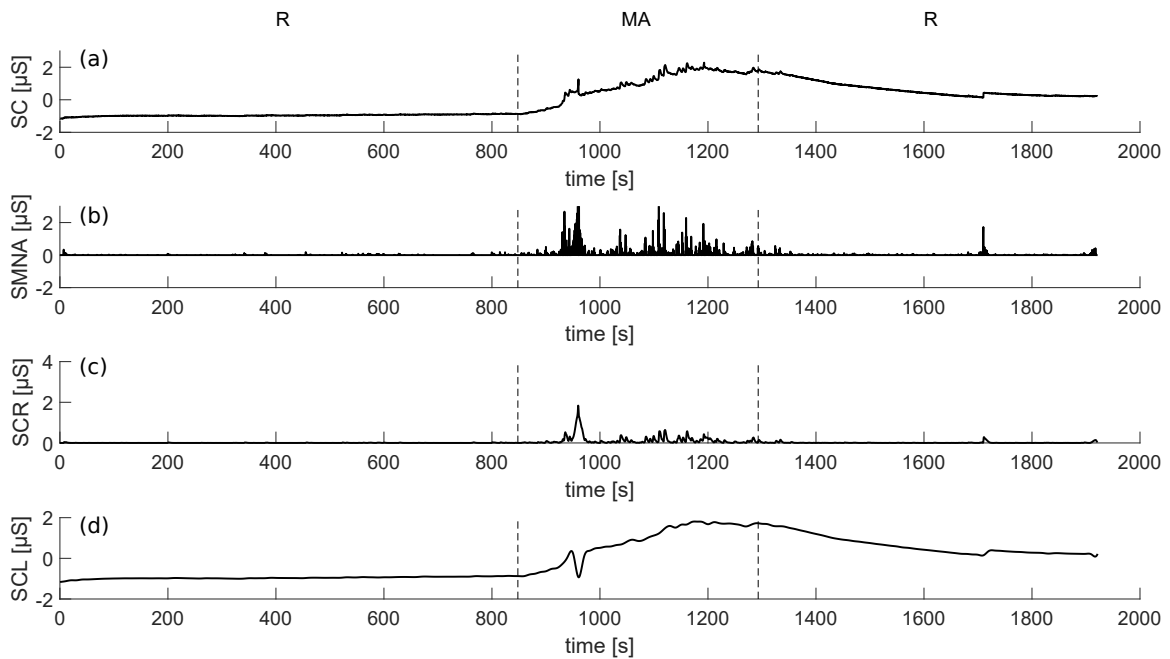


Fig. 3.6 Application of the cvxEDA decomposition procedure [65] to the SC signal recorded for a representative subject during rest (R), mental arithmetic (MA) and rest again. (a) Raw SC signal. (b) Sparse sudomotor nerve activity (SMNA) driver of phasic component. (c) Estimated phasic component. (d) Estimated tonic component.

3.2.4 Muscle activity

The electrical activity produced by skeletal muscles can be measured using an electromyograph, which measures the level of discharge of the motor nerve fibres that innervate the

muscle. The EMG signals provide information concerning muscle tone. The most frequently monitored muscles are the trapezius and the forearm muscles because these muscles reflect more than others the overall degree of tension in the organism.

Typical used features are the mean and the Root Mean Square (RMS) of the EMG, together with features concerning the frequency content of the EMG [145, 172].

Under acute stress, EMG signals show higher amplitudes, in particular in the upper trapezius muscle groups [139]. Moreover, in the frequency domain analysis, significant increases of the lower frequency contents are observed during stress in the EMG signals [172].

Also, facial muscle activity can provide useful information regarding the emotional status, because emotions are usually related to facial expression. In this case, one of the main problems is related to the uncomfortableness that can be experienced wearing the electrodes on the face.

3.2.5 Cerebral activity

The use of EEG for stress detection is an emerging field. The development of wireless and dry EEG systems makes possible to use this technology to study human brain activity in a generic environment without mechanical restrictions. The main problem in the use of this technology for stress detection is that an exploratory phase is required to identify the recording sites, frequencies and frequency pairs. Moreover, some problems are related to motion artefacts that can corrupt the signals.

In EEG-based stress assessment algorithms, power features are the most commonly used [73]. EEG power spectrum can be subdivided essentially into 5 bands:

- delta (δ): 0.5-4 Hz
- theta (θ): 4-8 Hz
- alpha (α): 8-12 Hz
- beta (β): 12-30 Hz
- gamma (γ): 32-100 Hz

δ waves have the greatest amplitude and are related to deep sleep. They are very common in infants and younger children. These waves are mainly related to involuntary bodily activities, such as heart rate or digestion. The rhythm of θ waves is dominant in newborns. θ waves are usually associated with drowsiness in adults and teens and with states of emotional tension and hypnosis. α waves predominantly originate from the occipital lobe and they are

dominant during relaxation with closed eyes. α waves are characteristic of waking conditions and mental rest. β waves are dominant in open-eyed subjects who are engaged in brain activities. Therefore they are usually present during active concentration or anxious thinking. In particular, regarding stress measurements, a stressful situation usually coincides with the suppression of α waves and boost of β waves [155]. γ waves are instead linked to emotions and cognition [64, 154].

3.3 The Network Physiology paradigm

Physiological systems react individually and interact among them in different manners during different physiological, cognitive and pathological states [25]. As a result, the physiological quantities constituting the output variables of the different physiological systems display a rich oscillatory activity, which is typically investigated through the acquisition of physiological signals obtained via low invasive instrumentation. These signals are elaborated to extract time series of interest, which are then analysed using proper signal processing methods to reveal the underlying physiological mechanisms. The traditional approach consists of studying the function of the single system in isolation to prove the evidence of a relationship between a particular property of a time series and a given physiological state. Some examples were reported in Sec. 3.2.

Another approach is the so-called multivariate approach, whereby multiple physiological signals are analysed at the same time to extract information of interest from the dynamics of each signal or the interaction between different signals. This approach is the basis of research fields investigating the distributed dynamical activity of individual organ systems, such as brain connectivity [72] and cardiac mapping [113], or the joint dynamical activity of anatomically connected systems, such as cardiovascular variability [135]. From an engineering point of view, this kind of approach is often used to extract features to train classifiers for the detection of particular physiological/mental states. Examples are studies concerning emotional recognition [95, 163] or stress detection [76, 147, 130].

The multivariate approach to the study of physiological dynamics has moved a step forward with the recent introduction of the concept of Network Physiology [10, 9]. With this perspective, the various physiological systems that compose the human organism are considered as nodes of a complex network (Fig. 3.7). Accordingly, each system has its internal regulatory mechanisms but also continuously interacts with the other systems to ensure correct responses to the various stimuli to achieve the proper functioning of the whole organism. This new paradigm requires that not only are quantities relevant to the dynamics of a single system studied, but also the interaction between different network

nodes must be assessed to provide a thorough characterization of the human organism as a whole. To accomplish such an exhaustive description of the dynamical activity of the human physiological network, methods are needed which can deal with the diversity of the network nodes and the complexity of the resulting dynamics. Different nodes of the human physiological network produce information at different rates, and the information produced can be preserved to a different extent for different nodes, or exchanged between nodes following multiple interaction pathways. In this case, since traditional analysis in time or frequency domains may not suffice, alternative approaches coming from the information domain can be proposed to investigate multiple aspects of the dynamics of physiological networks. In particular, the framework of Information Dynamics has been recently introduced to quantify, from multivariate time series representing the dynamical activity of multiple systems, the amounts of information produced by each system, stored in the system, transferred to it from the other connected systems, and modified as a consequence of the interaction between source systems sending information to a target system [47, 50]. Measurements taken from this framework have been used recently to study physiological brain-heart interactions during sleep [46, 43] and during visual emotional elicitation [164], and to assess cardiovascular and cardiorespiratory interactions during postural stress and mental stress [47, 161].

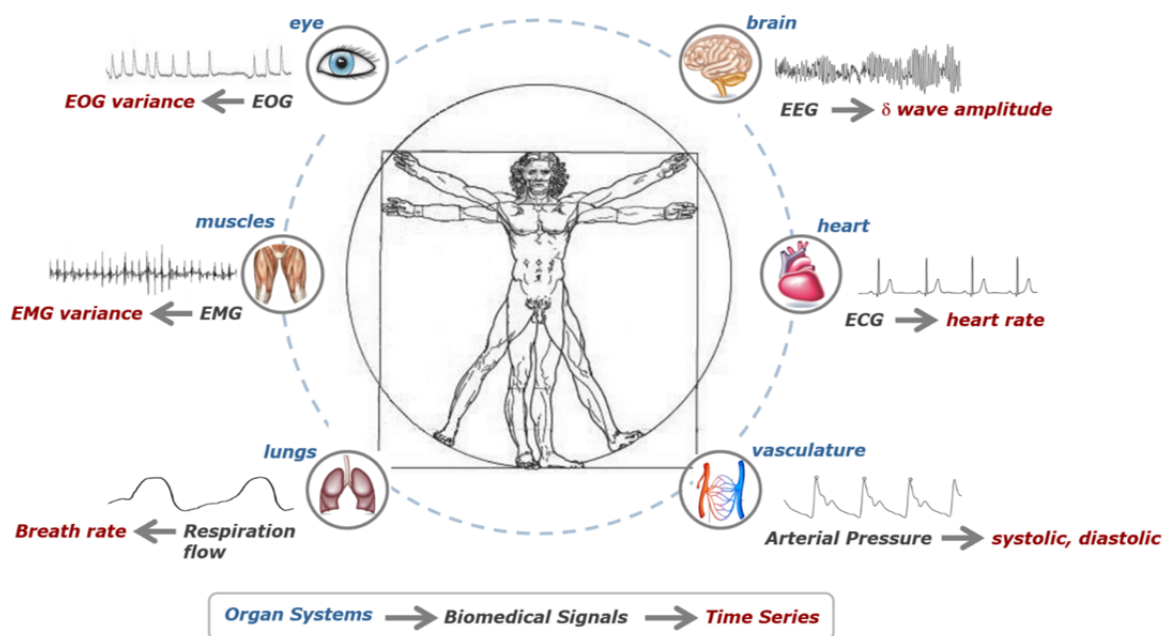


Fig. 3.7 The network physiology perspective: acquisition of simultaneous recording of biomedical signals from different body areas and extraction of time series to evaluate the interaction among the different signals.

3.4 Data acquisition

To develop and test algorithms for stress assessment, a database was recorded. Eighteen young healthy volunteers (age: 20–30 years; gender: 5 females, 13 males) participated in this project. The acquired physiological signals were the ECG, the respiratory signals, the BVP, the EEG, and the EDA. The wearable sensors described in Sec 2.1.1 were used.

Concerning the physiological signals described in Sec. 3.2, the EMG signal was not considered for the work presented in this thesis. This choice was mainly due to difficulties in finding wearable and low invasive sensors. Moreover, the experimental model would have been more complex. The EDA signal, processed using the *cvxEDA* algorithm, was only used for comparison among different classifiers and features (see Sec. 3.7). Indeed, with respect to the other signals, EDA has a much slower dynamic. For such a reason, the information decomposition analysis that will be presented in Sec. 3.6 does not take into account EDA.

The recording sessions were performed between 10:30 a.m. and 12.00 a.m. to avoid differences due to day time. No caffeine had to be assumed by the participants at least three hours before the recording session. The participants were seated in front of a PC in a comfortable room at constant illumination. They were instructed to not speak, limit their movements during the recording session, sit comfortably without changing posture, and to try to relax before the experiment. Three different mental stress levels were induced to the participants collecting signals during specific experimental conditions. The first was a resting condition, induced by watching a relaxing video. The second was a stressful task obtained through mental arithmetic: the participants had to perform the maximum number of 3-digit additions and subtractions in a fixed amount of time and write the solution in a text-box using the keyboard; no pen and paper were allowed as well as finger counting. The third condition was a sustained attention task induced by playing a serious game, which consisted of following a point moving on the screen using the mouse and trying to avoid some obstacles. This experimental design was devised following previous works in which varying levels of mental engagement and stress were evoked by means of non-stressful attention tasks or by stressful mental load tasks [168, 171, 179]. Here, the made assumptions are that playing serious games elicits a condition of sustained attention characterized by mental involvement and low stress while performing a mental calculus is a more stressful task characterized by a higher workload.

For every participant, two different recording sessions were performed (one for the mental arithmetic and one for the serious game), using the same schema (Figure 3.8):

- rest (12 min);
- mental arithmetic/serious game (7 min);

- recovery (12 min).

The two recording sessions were performed with a pause of at least 15 min between the two. All subjects have submitted all tests.

All participants provided written informed consent. The experiment was approved by the Ethics Committees of the University of Trento. The study was in accordance with the Declaration of Helsinki.

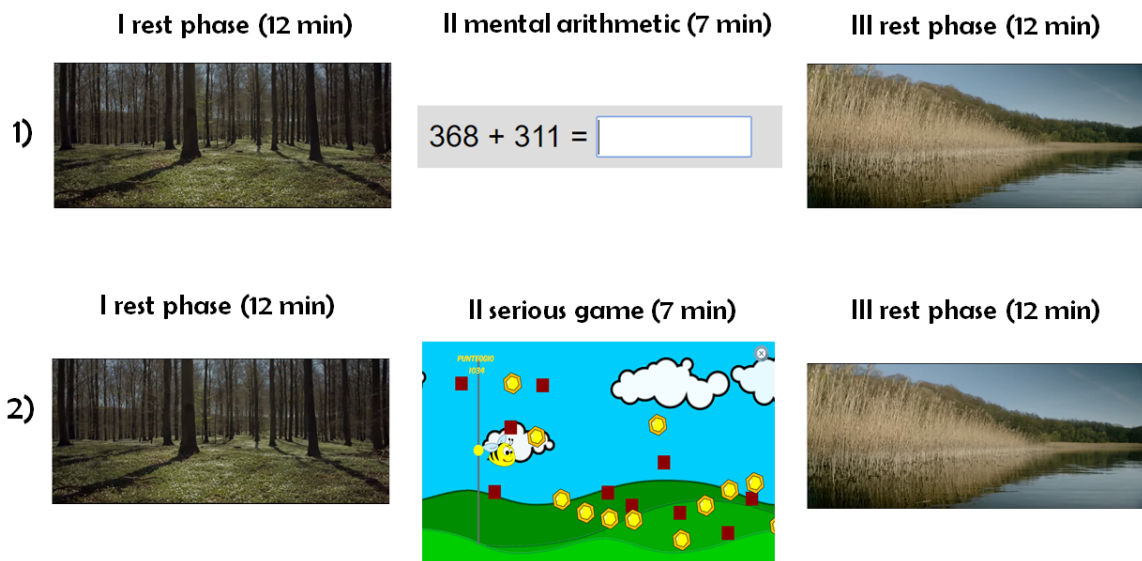


Fig. 3.8 Schematic representation of the experimental protocol adopted.

In this study, three phases of the whole protocol were considered for the analysis for each participant: the first rest phase before mental arithmetic (REST), the mental arithmetic phase (MA), and the serious game phase (SG). Only the first rest phase was used, leaving for further studies the analysis of the recovery rest phases, to make sure that the epoch analysed in the resting relaxed condition is free from possible habituation phenomena that could still be present after completion of the mental arithmetic stressful task.

3.5 Time series extraction

After simultaneous collection of the physiological signals, data were analysed offline using MATLAB R2016b (MathWorks, Natick, MA, USA). Fig. 3.9 shows schematically the analysis performed on the acquired signals.

The baseline wander of the ECG was removed using a high-pass filter with a half-power frequency of 1 Hz. High-frequency noise was removed using a low-pass filter with a half-power frequency of 20 Hz. Then, the tachogram (i.e., the sequence of the consecutive

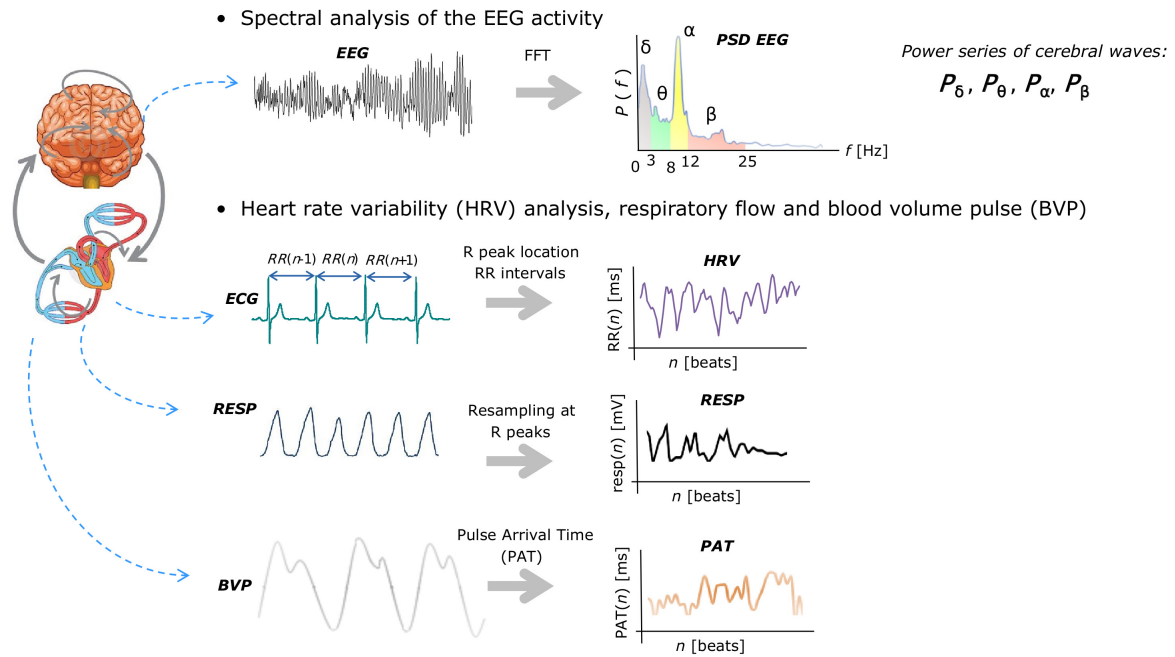


Fig. 3.9 Time series extraction procedure from the acquired physiological signals.

durations of the cardiac period, RR interval) was obtained detecting the R peaks in the ECG using a template matching algorithm [148, 111, 36], and then taking the difference between the occurrence times of consecutively detected R peaks. R peak detection is based on finding the local maxima of the cross-correlation between a template of the QRS complex and the ECG, applying a threshold on the cross-correlation, and finally locating the time of the R peak at the time of the maximum value of the aligned template [111, 36]. The detected R peaks were visually inspected for the insertion of missing beats and the correction of ectopic beats. Corrections were made by hand. From the respiration signal, a respiratory time series synchronous with the tachogram was obtained sampling the signal in correspondence of the detected R peaks [49]. The time series representative of the cardiovascular dynamics was obtained from the ECG and BVP signals calculating the sequence of the consecutive pulse arrival times (PATs); each PAT was computed as the time elapsed from the occurrence of the R peak in the ECG to the corresponding point of maximum derivative in the BVP signal, which denotes the arrival of the blood pulse at the level of the wrist [178, 99, 110]. Figure 3.10 shows schematically the detection of the points of interest for the reconstruction of the time series of RR, the respiratory signal, and PAT.

The three physiological time series of RR intervals, values of the respiratory signal, and PATs were then synchronously resampled at 1 Hz using spline interpolation. An example of the three resulting time series is reported in Figure 3.11.

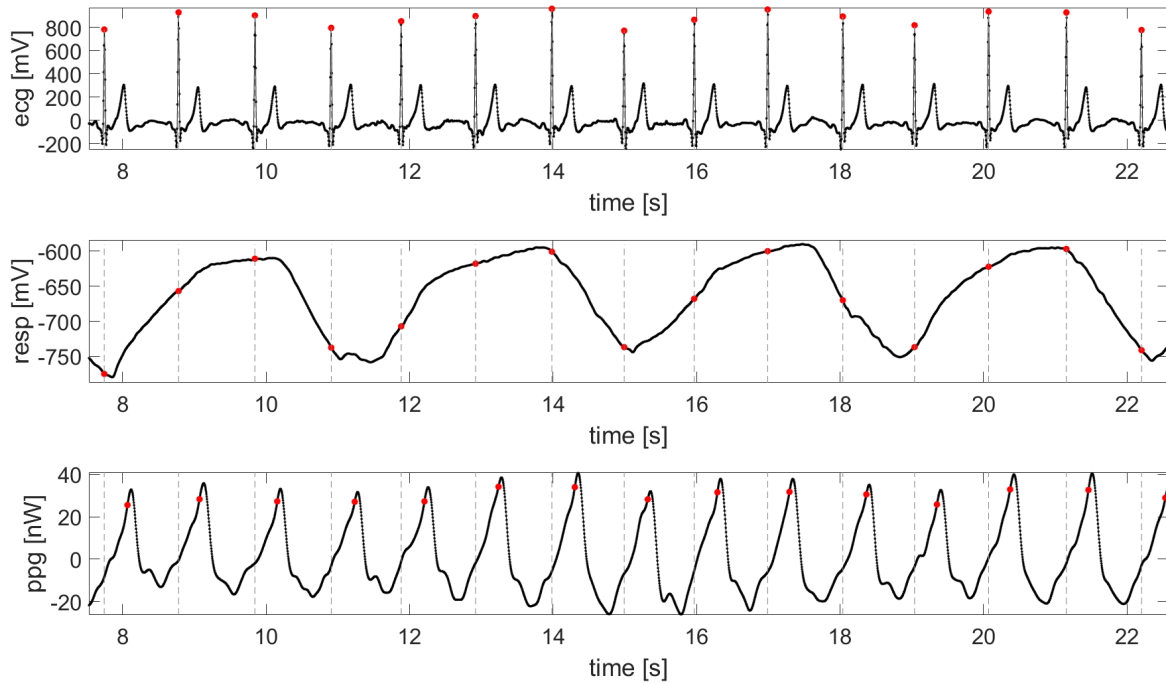


Fig. 3.10 ECG, respiratory signal and BVP acquired from the wearable sensors. The red dots indicate what concerns the ECG, the detection of the R picks; for the respiratory signal, the corresponding value; and for the BVP the point of the maximum derivative.

In order to obtain time series representing the variations in time of the amplitude of the various EEG rhythms, the PSD was computed on the recorded EEG signals using the periodogram method and quantifying the total power content of the δ (0.5–3 Hz), θ (3–8 Hz), α (8–12 Hz) and β (12–25 Hz) frequency bands. The γ band (32–100 Hz) was not extracted due to limitations of the hardware at our disposal. Indeed, the Emotiv EPOC+ has a bandwidth of 0.2–45 Hz. Moreover, the γ band overlaps entirely with the spectral bandwidth of muscle activity [107]. For this reason, special techniques must be used to remove such artifacts.

An example of the four-time series obtained, for a single subject in the three analysed conditions, computing the spectral power content of the EEG inside a specific band (δ , θ , α or β) is reported in Figure 3.12. PSD was computed for EEG epochs lasting two seconds, with 50 % overlap, to obtain one value for each band-power at each second. The four brain time series obtained in this way, which resulted in being sampled at 1 Hz, were synchronous with those obtained resampling the three cardiovascular time series at 1 Hz. This uniformity of the final sampling rate, together with the synchronization of the signals acquired from the different devices, ensures to obtain synchronous time series for the different body districts. The described procedure, used to obtain synchronous and meaningful information about the

dynamics of different physiological systems, adheres to those proposed in previous studies in the field of network physiology [10, 9].

With the pre-processing described above, 59 synchronous time series, representative of the cardiac, cardiovascular, respiratory and brain wave amplitude dynamics (14 electrodes per 4 bands), were obtained with a sampling period of one second for each subject and experimental condition. Then, windows corresponding to a duration of five minutes (300 samples) were selected in each experimental condition. To reduce transient behaviours, window selection was performed after at least three minutes from the beginning of data collection in the rest periods. As regards the mental arithmetic and serious game tasks, the extraction of the windows to be analysed was performed starting from one up to two minutes after the transition from the rest phase. This choice was because, in this case, the phenomenon of habituation can occur and therefore the earlier during the task (except the first one minute of the state change) this happens, the higher (usually) the response will be. After extracting time series of 300 points for each condition (Figures 3.11 and 3.12), a restricted form of weak sense stationarity was tested using the method proposed in [120], which checks the steadiness of mean and variance across randomly selected subwindows. All the extracted time series passed the test with a $p > 0.95$ both for mean and variance.

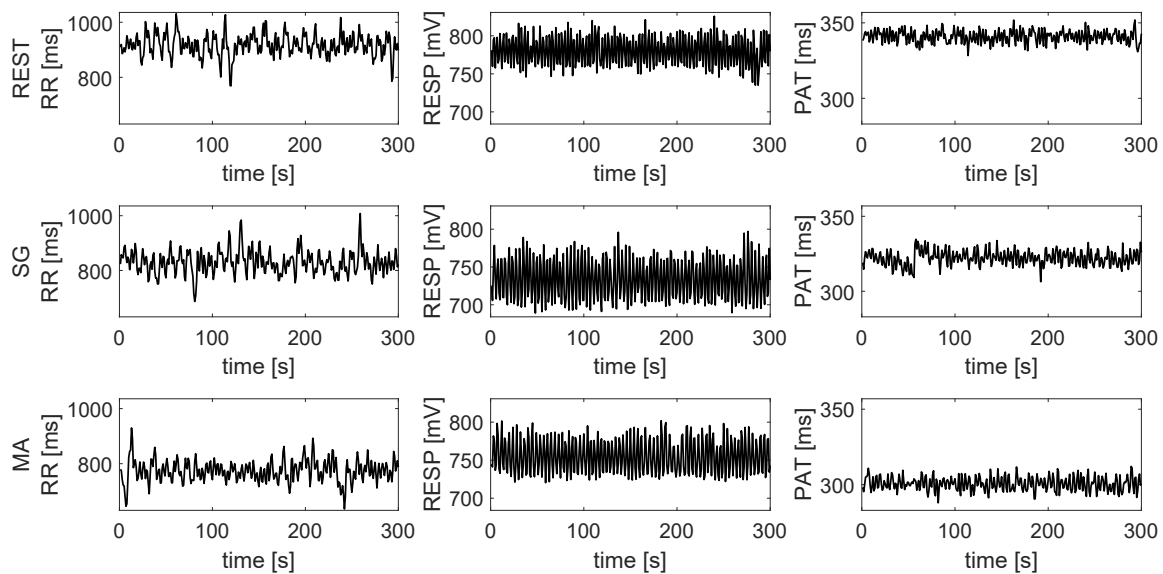


Fig. 3.11 RR interval, respiratory and PAT time series measured for a representative subject and resampled at 1 Hz during the resting phase (REST), the serious game test (SG) and the mental arithmetic test (MA).

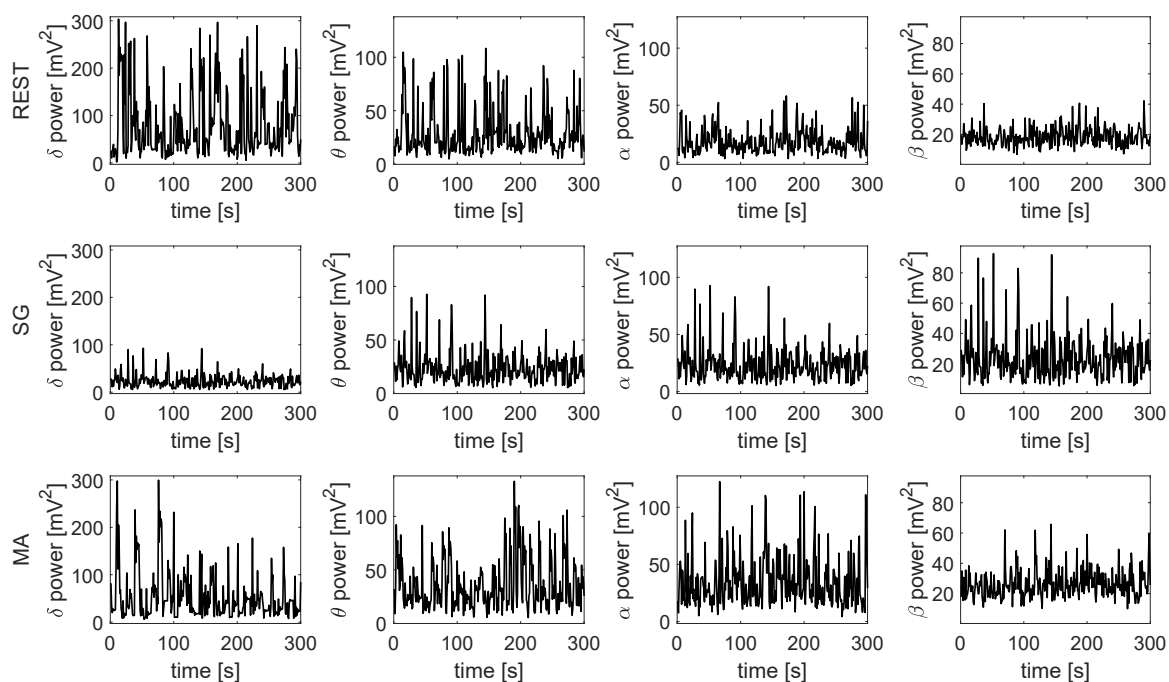


Fig. 3.12 Brain wave amplitude (PSD of a sliding window of 2 s of duration with 50% overlap) time series measured for a representative subject as the time course of the δ , θ , α , β EEG power (electrode F3) during the resting phase (REST), the serious game test (SG) and the mental arithmetic test (MA).

3.6 Information Dynamics during different levels of mental stress

The work presented in this section aims at combining the paradigm of Network Physiology with the algorithmic flexibility of Information Dynamics to assess the dynamical properties of the network of brain, cardiovascular and respiratory interactions during different levels of mental stress [180]. This combined approach may help to shed light on the physiological mechanisms underlying the dynamical regulation of different organ systems during altered mental states and may help to provide indexes with physiological meaning that can find interesting applications in contexts such as ambient assisted living scenarios.

Previous attempts of studying stress mechanisms and their influence on the regulation of multiple physiological systems include the analysis of the complexity of short-term cardiovascular and respiratory signals during orthostatic and mental stress [161], the analysis of cardiorespiratory dynamics during mental arithmetic and sustained attention through bivariate entropy measures [171], and the analysis of short-term multivariate complexity of cardiovascular and respiratory dynamics under physiological stress [160]. Here, the experimental protocol was extended considering different levels of mental stress, increase the number of physiological systems analysed simultaneously considering the cardiac, cardiovascular and respiratory systems as well as different brain subsystems, and extend the methodological approach considering univariate measures together with measures of directed coupling obtained following a fully multivariate perspective. In particular, an investigation was carried out on how the information is stored in each node and exchanged between different nodes of the network, analysing also the topology of such a network. Moreover, the use of wearable sensors connected wirelessly favours the application of the developed framework also in practical areas of use where stress needs to be assessed in real-life scenarios.

3.6.1 Information decomposition

The theory described in this section is partially taken from [50, 47]. The analysis framework presented in this study is implemented in the MATLAB ITS Toolbox, available for download at the link www.lucafaes.net/its.html. The various physiological systems are considered as dynamic systems whose dynamical activity is described using stochastic processes. Specifically, a network $\mathcal{X} = \{\mathcal{X}_i\}$ comprising the dynamic systems $\mathcal{X}_1, \dots, \mathcal{X}_M$ was considered, where M is the number of nodes of the network. The activity of such network is described by the vector stochastic process $\mathbf{X} = \{\mathbf{X}_n\}$, where $\mathbf{X}_n = [X_{1,n} \dots X_{M,n}]^T$ quantifies the state of the overall system at the n -th time step in probabilistic terms.

A realization of the stochastic process \mathbf{X} is the multivariate time series $\mathbf{x} = [\mathbf{x}_1, \mathbf{x}_2, \dots, \mathbf{x}_N]$, containing the values measured over N consecutive samples that take the form of an $M \times N$ data matrix. Each row of this data matrix is a scalar time series $x_i = [x_{i,1}, x_{i,2}, \dots, x_{i,N}]$, representing a realization of the process X_i which describes the activity of the individual dynamic system \mathcal{X}_i . Moreover let us consider, for example, X_j as the “target” process in our network and the remaining processes \mathbf{X}_s , with $s = \{1, \dots, M\} \setminus j$, as “source” processes. Assuming that \mathbf{X} is a Markov process of order m , its whole past history \mathbf{X}_n^- can be truncated using m lags, i.e. $\mathbf{X}_n^- \cong \mathbf{X}_n^m = [\mathbf{X}_{n-1}^T \dots \mathbf{X}_{n-m}^T]^T$; in a similar way, the past of the i -th scalar process can be written $X_{i,n}^m = [X_{i,n-1}, \dots, X_{i,n-m}]^T$.

A straightforward measure of the amount of information contained in the target process X_j at time n is given by the entropy of the variable $X_{j,n}$:

$$H_j = H(X_{j,n}), \quad (3.1)$$

where dependence on the time index n can be omitted assuming stationarity of the process X_j . Then, considering the source processes, the target information can be decomposed as:

$$H_j = S_j + T_j + N_j, \quad (3.2)$$

where S_j , T_j and N_j represent respectively the information stored in the j -th process, the information transferred to it from all source processes, and the new information generated about its present state when the past states of the whole network are known. Specifically, the information storage is defined in terms of the so-called self entropy as:

$$S_j = I(X_{j,n}; X_{j,n}^m) = H(X_{j,n}) - H(X_{j,n} | X_{j,n}^m), \quad (3.3)$$

where $I(\cdot; \cdot)$ denotes mutual information and $H(\cdot | \cdot)$ denotes conditional entropy. The self entropy is a measure of the amount of information contained in the present state of the target process that can be predicted by its own past states. The total information transfer is defined in terms of the *joint transfer entropy* as:

$$T_j = I(X_{j,n}; \mathbf{X}_{s,n}^m | X_{j,n}^m) = H(X_{j,n} | X_{j,n}^m) - H(X_{j,n} | \mathbf{X}_n^m), \quad (3.4)$$

where $I(\cdot; \cdot | \cdot)$ denotes conditional mutual information. The joint transfer entropy is a measure of the amount of information contained in the present state of the target process that can be predicted by the past states of all source processes, above and beyond the information that is predicted already by the past states of the target itself. Note that the sum of the self-entropy and the joint transfer entropy of a target process quantifies the so-called prediction entropy,

which is a measure of the total amount of predictive information contained in the process interpreted as a node of the considered network. The new information is defined in terms of the newly generated entropy as:

$$N_j = H(X_{j,n} | \mathbf{X}_n^m), \quad (3.5)$$

measuring the residual amount of information contained in the present state of the target process when the past states of the whole network are known. As such, the new entropy of X_j reflects the information newly produced by the network that appears in the target process after the transition from the past states to the present state.

The measures defined above quantify the processing of information for an assigned target of the observed network of multiple interacting processes. In addition to the information received by the target from all source processes defined in Eq. (3.4), it is possible to consider the information that the target receives referring exclusively to an individual source process. Specifically, the information transfer from the source process X_i to the target process X_j when the remaining source processes \mathbf{X}_k , $\mathbf{k} = \mathbf{s} \setminus i = \{1, \dots, M\} \setminus \{i, j\}$, are assigned, is defined in terms of the conditional transfer entropy as:

$$T_{i \rightarrow j | \mathbf{k}} = I(X_{j,n}; X_{i,n}^m | \mathbf{X}_{\mathbf{k},n}^m, X_{j,n}^m) = H(X_{j,n} | \mathbf{X}_{\mathbf{k},n}^m, X_{j,n}^m) - H(X_{j,n} | \mathbf{X}_n^m). \quad (3.6)$$

The conditional transfer entropy is a measure of the amount of information contained in the present state of the target process that can be predicted by the past states of a specific source process, above and beyond the information that is predicted already by the past states of the target and of the other source processes. This measure reflects the information transferred between two specific processes in the network and, as such, is useful to identify the topology of the network itself.

The measures defined above were computed exploiting the linear method described in [49, 50]. Under the assumption that the observed dynamical network \mathcal{X} produces a jointly Gaussian vector stochastic process \mathbf{X} , exact formulations can be provided as follows for the information measures defined above. The entropy of the target process X_j is computed as [30]:

$$H_j = \ln(\sigma_j \sqrt{2\pi e}), \quad (3.7)$$

where $\sigma_j^2 = \mathbb{E}[X_{j,n}^2]$ is the variance of X_j . The new information N_j can be instead computed as [7]:

$$N_j = \ln(\sigma_{j|j,s} \sqrt{2\pi e}), \quad (3.8)$$

where $\sigma_{j|j,s}^2$ is the partial variance of the target process given the past of all processes in the network, quantified as the variance of the prediction error of a linear regression of $X_{j,n}$ on \mathbf{X}_n^m . In a similar way, the conditional entropy of the present of the target given its own past can be derived using linear regression as $H(X_{j,n}|X_{j,n}^m) = \ln(\sigma_{j|j}\sqrt{2\pi e})$, where $\sigma_{j|j}^2$ is the variance of the prediction error of a linear regression of $X_{j,n}$ on $X_{j,n}^m$; this term, together with the information computed as in Eq. (3.7), can be plugged in Eq. (3.3) to compute the information storage of X_j as:

$$S_j = \ln \frac{\sigma_j}{\sigma_{j|j}}, \quad (3.9)$$

Following the same reasoning, the total information transferred to the process X_j from all sources can be computed relating the partial variance of the linear regression of $X_{j,n}$ on $X_{j,n}^m$ with the partial variance of the linear regression of $X_{j,n}$ on \mathbf{X}_n^m :

$$T_j = \ln \frac{\sigma_{j|j}}{\sigma_{j|j,s}}, \quad (3.10)$$

and the conditional information transferred from the process X_i to the process X_j given \mathbf{X}_k can be computed relating the partial variance of the linear regression of $X_{j,n}$ on $(\mathbf{X}_{k,n}^m, X_{j,n}^m)$ with the partial variance of the linear regression of $X_{j,n}$ on \mathbf{X}_n^m :

$$T_{i \rightarrow j|\mathbf{k}} = \ln \frac{\sigma_{j|j,\mathbf{k}}}{\sigma_{j|j,s}}. \quad (3.11)$$

The variance of the target process and all the partial variances that are needed for the computation of the information measures according to Eqs. (3.7), (3.8), (3.9), (3.10), (3.11) were derived using the theory of state space models as described in [8, 44]. The approach is based on describing the observed network process as a vector autoregressive process, which is in turn represented as a state space model. Then, sub-models are obtained from the state space model for which the state equation is obtained and the observation equation is reduced removing one or more processes. Finally, the partial variance is obtained as the variance of the prediction errors obtained regressing the present of the target process on the past of the processes which have not been removed (e.g., when the assigned source process X_i is removed from \mathbf{X} in the observation equation, the estimated partial variance is $\sigma_{j|j,\mathbf{k}}$). More details about state space modelling and computation of the partial variances are given in [8, 44].

The time series obtained from each subject and time window (see Sec. 3.5) were interpreted as realizations of a vector autoregressive process, and the parameters of such process were estimated using the standard least squares method. The order of the underlying Markov

model was identified using the Akaike Information Criterion (AIC) [92]. All the series were reduced to zero mean and unit variance.

For what concerns the time series derived by the EEG signals, it was chosen to process only the ones of the F3 electrode. This choice was because, in the literature, prefrontal electrodes are typically considered for the analysis of brain signals concerned with the detection of stress conditions [60, 102, 128]. Then, considering each time series as the target x_j ($i = 1, \dots, 7$), the information storage S_j , the new information N_j and the total transfer T_j were computed according to the methodology described in this section. Moreover, the conditional information transfer from the source x_i to the target x_j given the remaining sources $x_{\mathbf{k}}$, $T_{i \rightarrow j|\mathbf{k}}$ was computed for each source x_i ($i = 1, \dots, 7, i \neq j$).

Tab. 3.1 summarizes all variables and indices that will be analysed.

Table 3.1 Time series and information dynamic indices analysed.

| time series | Information dynamic indices |
|------------------------------|---|
| cardiac period (RR interval) | Information Storage (S_j) |
| respiration (RESP) | New Information (N_j) |
| pulse arrival time (PAT) | Information Transfer (T_j) |
| EEG δ_{F3} power | Conditional Information Transfer ($T_{i \rightarrow j \mathbf{k}}$) |
| EEG θ_{F3} power | |
| EEG α_{F3} power | |
| EEG β_{F3} power | |
| | |

3.6.2 Statistical analysis

Statistical analysis was performed through the nonparametric Friedman's test assuming the mental state (REST, SG, MA) and the network node process (RR, RESP, PAT, δ , θ , α , β , corresponding to $j = 1, \dots, 7$) as categorical independent variables, and one of the information measures (S_j , T_j , N_j) as continuous dependent variable. The test was aimed at detecting statistically significant differences among the different physiological systems (network nodes) in (a) an assigned mental state, and (b) among the different mental states with respect to an assigned physiological system. Post hoc analysis with Wilcoxon signed-rank tests was conducted with a Bonferroni correction applied, resulting in a significance level set at $p < 0.007$ for (a) and at $p < 0.017$ for (b). The aim of this statistical analysis, performed at a group level, is to investigate the significance of the median differences across conditions and network nodes of each measure of information dynamics, i.e., S_j , T_j , N_j , computed for all subjects.

Moreover, the statistical significance of the measure of total information transfer T_j , and of the measure of conditional information transfer $T_{i \rightarrow j|k}$, computed for each source system, was assessed using a Fisher F -test that compares the prediction error variances of two nested linear regression models. This analysis was performed individually for each subject, for each experimental condition and target system. The conditional information transfer was considered as statistically significant, and a directed link was detected from the node i to the node j of the network when the F -test returned a $p < 0.05$.

The difference in the number of links in the three different mental states was statistically analysed using a χ^2 test.

3.6.3 Results

Figure 3.13 displays the information storage of the considered time series, reported as the distribution across subjects of the index S_j computed in the three considered mental states, i.e., rest (REST), mental arithmetic (MA), and serious game (SG). The information stored in the cardiovascular and respiratory systems is significantly higher with respect to that stored in the four brain subsystems. Moreover, the information storage is higher for RR than for RESP, and for RESP than for PAT, the differences being statistically significant during REST and MA, and less evident during SG. Considering the transitions across the different mental states, S_{RR} , S_{RESP} and S_{PAT} show a similar trend, with a lower value of information storage in MA and in SG with respect to REST. The decrease of the information storage moving from REST to MA is documented by the statistical significance of the Wilcoxon signed-rank test for S_{RESP} ($p = 0.001$), and by the fact that the index becomes comparable with the information storage of the EEG time series for S_{PAT} .

For what concerns the information storage in the EEG power time series, values of the information storage are rather low in all the three mental states, with no statistically significant differences detected among REST, MA, and SG. Moreover, no statistically significant differences are present among the different EEG power series when considering the information storage evaluated in the same mental state.

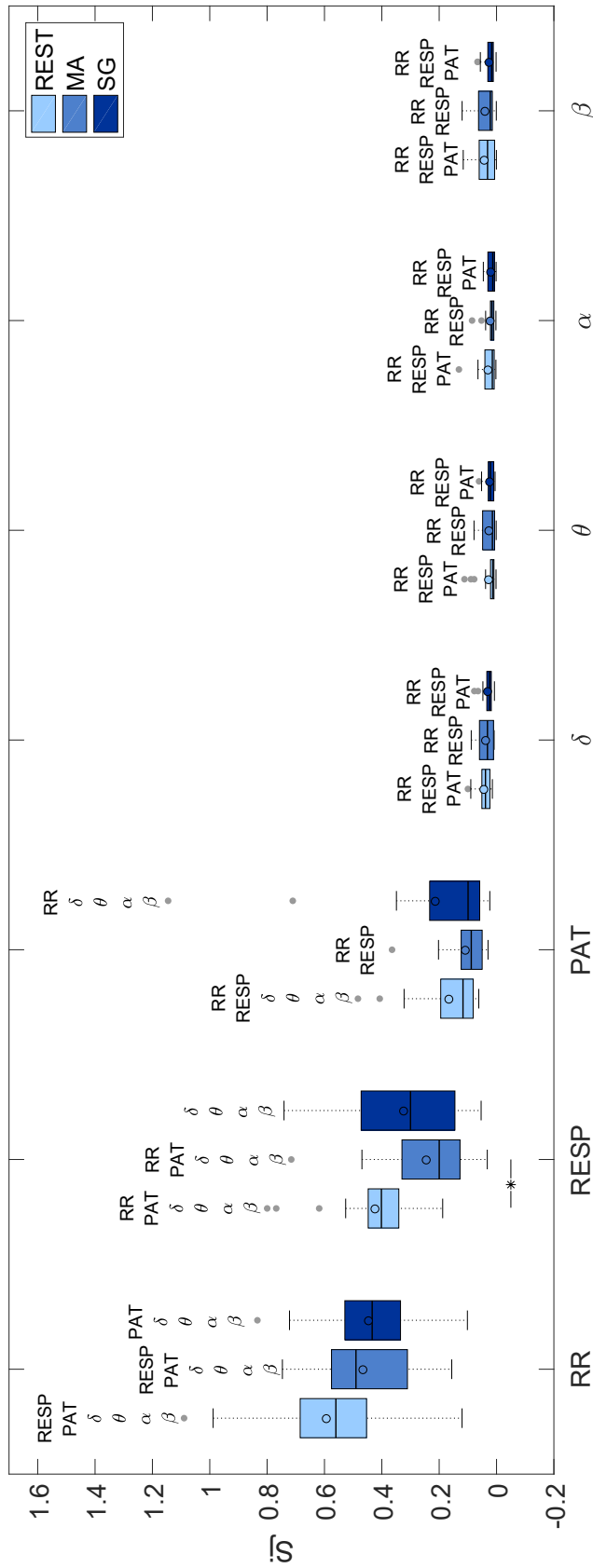


Fig. 3.13 Boxplots of the information storage S_j for the seven time series under consideration during rest (REST), mental arithmetic (MA), and serious game (SG). The lines under the boxplots indicate significant differences between the linked mental states as determined by the Wilcoxon signed-rank test ($p < 0.017$); moreover, the names of the time series that are significantly different from the one under consideration for any assigned mental state, listed above each boxplot ($p < 0.007$).

Table 3.2 lists the median values of S_j for every node in every state condition.

Table 3.2 Median values of S_j for the seven time series under consideration during rest (REST), mental arithmetic (MA), and serious game (SG).

| | RR | RESP | PAT | δ | θ | α | β |
|-------------|-----------|-------------|------------|----------------------------|----------------------------|----------------------------|---------------------------|
| REST | 0.560 | 0.401 | 0.117 | 0.039 | 0.013 | 0.015 | 0.031 |
| MA | 0.490 | 0.200 | 0.088 | 0.032 | 0.014 | 0.016 | 0.022 |
| SG | 0.434 | 0.300 | 0.099 | 0.024 | 0.022 | 0.013 | 0.017 |

Fig. 3.14 shows the distributions across subjects of the new information N_j computed for each time series in the three mental states and Tab. 3.3 shows the corresponding median values. In general, the values of this quantity are complementary to those of the information storage S_j : the same average values and trends noticed in Figure 3.13 are here present in the opposite way. Indeed, the EEG power time series show a high amount of content of new information, while the PAT, RESP, and RR generate progressively lower amounts of new information. These trends are associated with higher complexity (lower predictability) of the brain time series, and progressively lower complexity of cardiovascular, respiratory and cardiac time series. Also, in this case, no differences can be noticed among the different mental states for what concerns the EEG time series.

Table 3.3 Median values of N_j for the seven time series under consideration during rest (REST), mental arithmetic (MA), and serious game (SG).

| | RR | RESP | PAT | δ | θ | α | β |
|-------------|-----------|-------------|------------|----------------------------|----------------------------|----------------------------|---------------------------|
| REST | 0.674 | 0.951 | 1.155 | 1.347 | 1.357 | 1.365 | 1.362 |
| MA | 0.772 | 1.117 | 1.222 | 1.333 | 1.369 | 1.364 | 1.342 |
| SG | 0.777 | 0.965 | 1.178 | 1.349 | 1.351 | 1.357 | 1.343 |

Figure 3.15 displays the distributions of the values of total information transferred to each node of the network from all other nodes, while Table 3.4 lists the median values of T_j for every node in every state condition. All nodes of the network receive a significant amount of information, as documented by the F -test conducted on the values of T_j for every physiological signal and state. Indeed, the test returned a p -value < 0.05 in at least 15 out of 18 subjects for all target time series and in each experimental condition, documenting the existence of predictable dynamics also for the time course of the amplitude of the different EEG waves, which present a lower regularity. Figure 3.15 shows that the information transfer T_j is higher for the cardiovascular and respiratory districts than for the subsystems of the brain district, with a difference that is statistically significant for the RR series in all states, for the RESP series during SG, and for the PAT series during REST and SG. For what concerns the peripheral districts (RR, RESP, PAT), the values of T_{RR} , T_{RESP} , and T_{PAT} are comparable among each other during REST and MA, while, during SG, higher values of T_{RR} are observed, such that the network transfers significantly higher amounts of information to RR than to RESP and PAT. No statistically significant differences were detected among the different mental states. As regards the brain time series, the total information transfer does not differ significantly across subsystems.

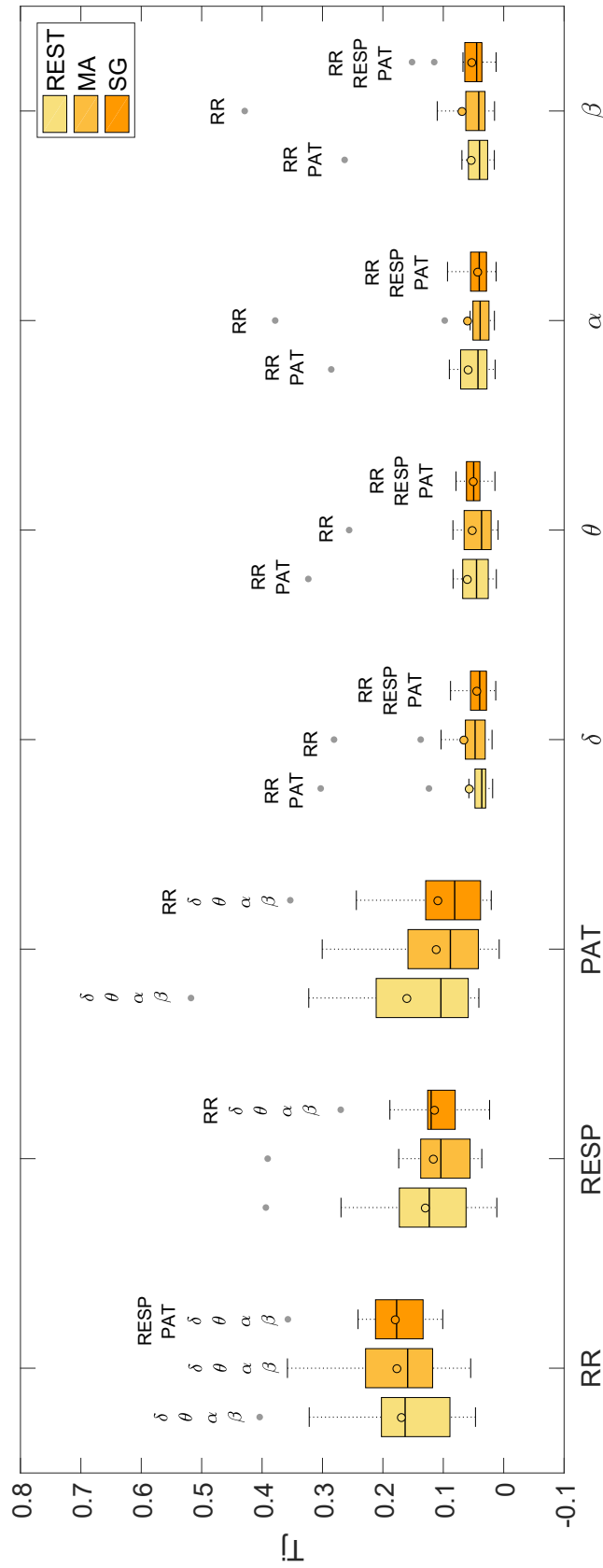


Fig. 3.15 Boxplots of the total information transfer T_j for the seven time series under consideration during rest (REST), mental arithmetic (MA), and serious game (SG). The lines under the boxplots indicate significant differences between the linked mental states as determined by the Wilcoxon signed-rank test ($p < 0.017$); moreover, the names of the time series that are significantly different from the one under consideration for any assigned mental state, listed above each boxplot ($p < 0.007$).

Table 3.4 Median values of T_j for the seven time series under consideration during rest (REST), mental arithmetic (MA), and serious game (SG).

| | RR | RESP | PAT | δ | θ | α | β |
|-------------|-----------|-------------|------------|----------------------------|----------------------------|----------------------------|---------------------------|
| REST | 0.163 | 0.123 | 0.104 | 0.036 | 0.045 | 0.043 | 0.040 |
| MA | 0.159 | 0.104 | 0.088 | 0.047 | 0.037 | 0.039 | 0.041 |
| SG | 0.177 | 0.120 | 0.081 | 0.040 | 0.050 | 0.040 | 0.045 |

The total transfer T_j provides incomplete information on how the different systems are connected because it refers, for every system under consideration, only to the information that the system receives from all other systems when they are considered together. Hence, to investigate the topology of the network regarding pairwise directed interactions, an analysis of the conditional information transfer $T_{i \rightarrow j|k}$ was performed, computing the statistical significance of the estimated values of $T_{i \rightarrow j|k}$ along all possible directions, according to the analysis presented in Section 3.6.2. A causal link exists from one time series to another if the past of the first series helps in predicting the present of the second above and beyond the past of any other time series forming the observed network. This concept is formalized by the measure of conditional information transfer defined in Eq. 3.6 and computed as in Eq. 3.11. The results of such analysis are displayed in Fig. 3.16, which shows, in each of the three mental states, the total information transferred to each node (colour-coded values of the mean T_j across subjects) and the most active connections among systems (arrows present when at least 7 subjects show significant $T_{i \rightarrow j|k}$, and thicker arrows when more than 12 subjects show significant $T_{i \rightarrow j|k}$). The absence of an arrow linking two nodes in Figure 3.16 suggests that the causal connection is weak or not consistent, rather than absent. A χ^2 -test was performed on the number of links among physiological systems. This test aimed to verify if the difference in the number of links in the three different mental states is statistically significant. The test returned a $\chi^2 = 6.47$ corresponding to a $p = 0.039$.

Analysing the topology of the resulting network of the brain and peripheral interactions, we can notice an evident variation in the number and location of the active connections during the different mental states. The subnetwork containing the cardiovascular and respiratory time series receives the highest amounts of information, and the active network links show that such information is transferred mostly within the nodes of this subnetwork according to a consistent topology. In particular, there is a strong bidirectional coupling between RR and RESP, a unidirectional influence from RR to PAT, and a connection between PAT and RESP. The topology of the peripheral subnetwork is the same during REST and MA, while a dominant link from RESP to PAT emerges during SG.

On the other hand, the topology of the brain subnetwork is less stable, showing bidirectional interactions between the θ and β brain wave amplitudes at REST, the emergence of $\alpha - \beta$ interactions and of multiple links directed towards the θ subsystem during MA, and a residual connectivity involving the α waves during SG. Overall, the number of connections is higher during MA than during rest, and lower during SG than during MA.

The analysis of the links connecting the nodes of the brain and peripheral subnetworks reveals important properties featuring the topology of brain-cardiovascular interactions. At REST, the high information transfer towards RR can be partly explained by the δ and β brain activities that, also interacting with each other, send information to the heart both directly acting toward RR and indirectly acting toward RESP. During MA, the connection between the cardiorespiratory network and the $\delta - \beta$ brain subnetwork is clearly emphasized through the presence of bidirectional interactions between δ and both RR and RESP, and the emergence of links directed from RR and RESP towards the β node. Finally, only a residual activity of brain-heart interactions is present during SG, characterized by the connections of the pathway $\alpha \rightarrow RR \rightarrow \theta$.

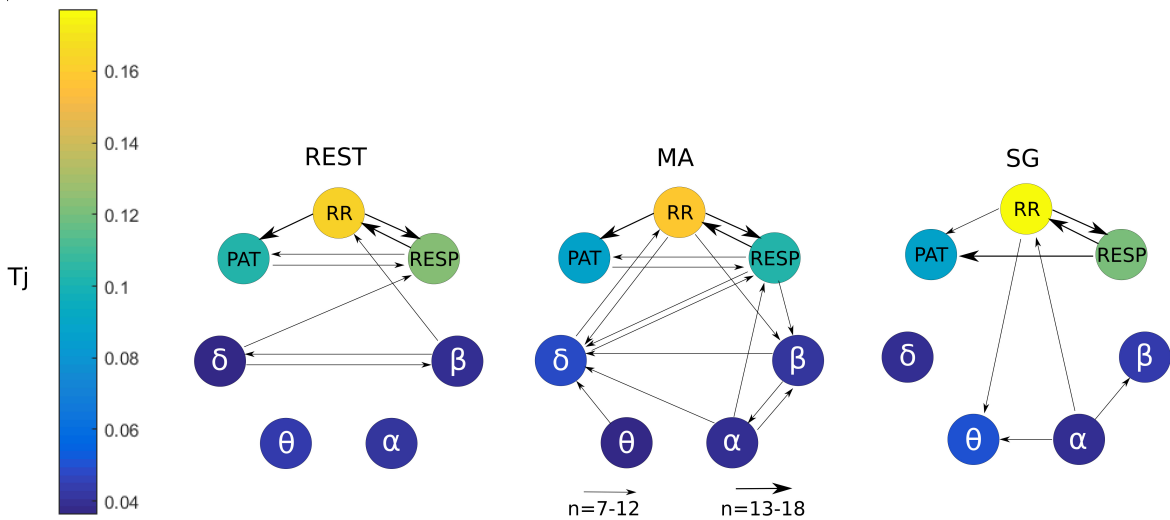


Fig. 3.16 Information transfer for the cardiorespiratory-brain network using the conditional information transfer $T_{i \rightarrow j|k}$. The arrows thickness is proportional to the number of subjects for which that link is statistically significant ($p < 0.05$) using an F -test. The magnitude of T_j for each node is coded accordingly to the colour bar on the left.

3.6.4 Information produced and stored in the nodes of the human physiological network

The framework of information dynamics allows for quantifying, from the analysis of the multivariate time series describing the activity of an observed physiological network, the amounts of information produced at each moment in time at the j -th node of the network, and the amount of information dynamically stored in the node. These two amounts, which are quantified by the measures of new information N_j and of information storage S_j , reflect respectively the complexity of the node dynamics (related to the unpredictability of the present state of the target when the past network states are known) and the regularity of these dynamics (related to the predictability of the present state of the target when its own past states are known) [47]. The results show that, in the analysed network of the brain and peripheral interactions during different stress levels, the amounts of new information and information storage are always complementary to each other (when one is higher, the other is lower), both in their variations across conditions and in their variations across network nodes. Methodologically, this behaviour indicates that variations of the information content of a node (measured by the entropy H_j) and of the information transferred to it (measured by the total transfer T_j) contribute essentially to the same extent to the dynamics (see Eq. 3.2: $N_j + S_j = H_j - T_j$). This behaviour leads us to observe an invariance across physiological systems and physiological states of the capability of the network to produce and store information: if a node generates more new information, either between conditions or in comparison to another node, the information stored in it roughly decreases the same amount.

The analysis of the cardiovascular and respiratory time series reveals a decrease in regularity during the stressful cognitive tasks, reflected by the lower values of S_j and the higher values of N_j measured moving from REST to MA. The increased respiratory and cardiovascular complexity induced by mental stress, documented by the lower S_j and higher N_j during MA, is in agreement with the increase of the vascular and respiratory complexity previously found as a result of mental stress [161]. On the other hand, if considered for the cardiac system, this result is in disagreement with previous studies, which have shown that the regularity of the RR series increases significantly as a consequence of activation of the sympathetic nervous system induced by postural stress [167, 21, 47]. However, the type of sympathetic activation which takes place in the case of mental stress can be related to different mechanisms than that induced by postural stress. In particular, it is likely that sympathetic activation is driven mainly by the cardiac baroreflex during postural stress, and by central commands originating in the central autonomic network during mental stress [34].

The behaviour of the brain subnetwork, studied in terms of new information and information storage of the EEG power time series, seems to be less informative in terms of the involved mechanisms. Indeed, we can see, regardless of the analysed brain subsystem and mental state, high values of N_j and low values of S_j which are indicative of low predictability of the time course of the various brain wave amplitudes with respect to the cardiovascular and respiratory time series. On the other hand, the information transferred to the brain subnetwork, though remaining lower than that transferred to the peripheral subnetwork, was statistically significant. This suggests that the dynamical properties of the brain wave activity can be better understood in terms of connectivity than single node activity.

3.6.5 Information transfer across the nodes of the human physiological network

Using a fully multivariate approach, we can study how the information is transferred among the systems constituting the physiological network under consideration. In particular, the analysis of the total information transfer T_j allows us to establish the overall amount of information received by each network node (Figure 3.16), while the analysis of the conditional information transfer leads to inferring the topological structure through which information flows across nodes (Figure 3.15). In the following, a discussion is made about findings relevant to the analysis of information transferred within the network, distinguishing the description of the peripheral subnetwork, the brain subnetwork, and the subnetwork of brain-peripheral interactions.

The topology of the cardiovascular and respiratory subnetwork is quite consistent across conditions, showing significant cardiorespiratory and cardiovascular interactions in the three analysed mental states. In particular, the high amounts of information transferred to the RR time series reflect a strong coupling between the HRV and respiration, which is very likely due to well-established mechanisms such as the respiratory sinus arrhythmia [13] and cardiorespiratory synchronization [133]. The influences observed from RR to PAT reflect the well-known effect of the heart rate on stroke volume and arterial pressure, which in turn determine variations in the PAT [132, 38]. In addition, the effects of respiration on the PAT variability are expected, since they should reflect breathing influences on the intra-thoracic pressure, cardiac output, blood pressure, and ultimately blood flow velocity [38]. As a new finding, we observe that, while almost all mechanisms are stable across conditions, respiratory effects on PAT seem more elicited during the mild stress condition (SG).

Compared to the peripheral subnetwork, the brain subnetwork shows less consistent links (found in 7-12 subjects out of the 18) and more variable in topology across the different

mental states. An apparent result is that the brain subnetwork is more connected during the stressful condition elicited by MA as compared to REST and SG. This result, which can be useful to distinguish stress states using EEG power dynamics, is consistent with studies regarding the role played by the different brain waves during rest and stressful tasks [137] and is particularly in agreement with previous reports suggesting that increased brain connectivity is expected during stressful tasks [151]. The correlation between α and β found in MA and SG is also somewhat expected, as studies in the literature report a decrease of the α power band and an increase in the θ power band during stressful and sustained attention tasks [144, 109]. Moreover, the link found during MA between α and δ , which can be explained with a correlation between the two, is supported by previous findings where during mental tasks, an increase in δ and a decrease in α power was concomitantly observed [51]. Thus, the results of the present research support the hypothesis of a higher degree of connectivity within the brain network during high levels of mental stress evoked by MA. It should also be noted that participants could be more accustomed to playing video games due to their young age (from 20 to 30 years), and this may limit the capability of the designed protocol to elicit sustained attention during the SG condition. This observation could partly explain the presence of limited connectivity within the brain subnetwork during SG, and in general, the higher difficulty in differentiating REST from SG observed for some of the measures considered. In this respect, the design of new experimental protocols able to elicit higher mental workloads than the SG task would be appropriate to test the hypothesis that increasing mental levels relate to higher degrees of connectivity within the brain and physiological networks.

Finally, the possibility to explore brain-peripheral interactions enables us to make insightful inferences about how brain dynamics driven by the central nervous system are related to autonomic effects manifested in the cardiovascular and respiratory dynamics. In this perspective, the main result is the emergence during the mental stress of a higher number of network connections linking the brain dynamics (in particular, δ and β dynamics) with the cardiorespiratory subnetwork (RR and RESP nodes). This fact strengthens the hypothesis described above of a central role played by the central autonomic network during mental stress in the regulatory mechanisms. The correlation of δ and β waves with HRV was studied in several previous works, mainly related to sleep analysis. In [2, 17], a correlation was found between δ EEG power and HRV, supposing an influence on the sympathetic nervous activities, while, in [87], a relationship was found between β power and the autonomic activation. In [46], the β node was the main one for the exchange of information between the cardio and brain subnetworks during the different sleep phases. The results of the present research suggest that similar mechanisms could play a role in the increased

brain–heart connectivity observed in the transition from rest to stress, possibly in analogy with the modifications observed in the transition across different sleep states. In addition, we note that the network changes substantially moving from MA to SG, with the emergence of brain-heart interaction underlined by links from α to RR and from RR to θ . The role of α and θ dynamics during sustained attention was highlighted in [11], who hypothesized that the cerebral neuronal systems producing α and θ oscillations are crucial for this task. Moreover, a correlation between cardiac autonomic activities and the θ rhythm was also found in [85] during an attention demanding meditation procedure. These results are consistent with the re-modulation of the network of brain-heart interactions that are observed moving from MA to SG, possibly suggesting that different brain rhythms contribute in a different way to the link between central and autonomic activities depending on the mental state.

The presence of isolated nodes in the network represents weak or inconsistent causal relations involving these specific network nodes. In such a case, it is possible to hypothesize that the dynamics of the corresponding time series, like θ and α power during REST and δ power during SG, are independent of the dynamics of the other time series. Some of these behaviours are observed likely for the first time, given that the topic of our work is little explored in the literature. Taken together, the different behaviours of connectivity across brain rhythms observed in the different states contribute to characterizing the topology of the brain subnetwork in these specific states.

3.7 Stress classification

Using the same database presented in Sec. 3.4, some classifiers were implemented to distinguish among the three different mental states, i.e. rest, mental arithmetic and serious game.

For what concerns the use of physiological parameters for the detection of mental stress, large differences arise in the literature. These differences are mainly due to aspects such as different protocols and equipment for signal monitoring, in addition to the data analysis performed [147]. [152] considered features extracted from a professional 128 channel EEG to distinguish among 4 different levels of stress. The reached accuracy was 83.4%. In [73] the authors reached an accuracy of 67.1%, 75.2%, and 85.7% in distinguishing respectively among 4, 3, and 2 different levels of stress. They used features extracted from EEG signals obtained from a wireless headset to train a Support Vector Machine (SVM) classifier. In [147], an analysis of different classification algorithms was performed to distinguish between stressful and non-stressful situations. The acquired physiological signals were ECG, respiration, EDA, and temperature. The acquisition of such signals was performed

using wireless devices, even if quite invasive since the recording of the ECG was performed applying electrodes on the skin. A similar setup was used in [76], where unsupervised learning was used to distinguish between relax or stress phases. The authors obtained an accuracy of 84.6 % using personalized dynamic Bayesian networks and an accuracy of 82.7 % using generalized SVMs. [130] used wearable devices to monitor EDA and PPG signals to detect stressful situations in five participants. The maximum accuracy was 83.08 % using an SVM algorithm. In [104], the authors used ECG and Thoracic Electrical Bioimpedance (TEB) signals provided by wearable devices to distinguish between low mental load and mental overload, reaching an accuracy of 67.7 %.

The proposed method in this thesis exploits information-theoretic measures starting from the 59 time series computed as reported in Sec. 3.5. In particular, the selected features were the self-entropy, already explained in Sec. 3.6.1 and the mutual information $I(X;Y)$, and the conditional mutual information $I(X;Y|Z)$ [50, 48].

Considering two distinct dynamic processes X and Y , the mutual information $I(X_n;Y_n)$ measures the amount of information that can be obtained about the present value of a random variable observing another one, and it is defined as:

$$\begin{aligned} I(X_n;Y_n) &= H(X_n) - H(X_n|Y_n) \\ &= H(Y_n) - H(Y_n|X_n) \\ &= H(X_n) + H(Y_n) - H(X_n, Y_n), \end{aligned} \tag{3.12}$$

where $H(X_n)$ and $H(Y_n)$ are the marginal entropies, $H(X_n|Y_n)$ and $H(Y_n|X_n)$ are the conditional entropies, and $H(X_n, Y_n)$ the joint entropy.

The conditional mutual information $I(X_n;Y_n|Z_n)$ is instead defined as:

$$\begin{aligned} I(X_n;Y_n|Z_n) &= I(X_n;Y_n, Z_n) - I(X_n;Z_n) \\ &= I(Y_n;X_n, Z_n) - I(Y_n;Z_n). \end{aligned} \tag{3.13}$$

where $I(X_n;Y_n|Z_n)$ is the expected value of the mutual information between X_n and Y_n , given the value of a third variable Z_n , measuring the fraction of the information shared between X_n and Y_n that is not shared with Z_n .

For the practical computation of the above quantities, under the hypothesis of Gaussian distribution of y , it is possible to apply the formulas described in [7, 121].

Given the covariance Σ and precision Σ^{-1} matrices of X and Y :

$$\Sigma = \begin{bmatrix} \sigma_X^2 & \sigma_{XY}^2 \\ \sigma_{XY}^2 & \sigma_Y^2 \end{bmatrix} \quad (3.14)$$

$$\Sigma^{-1} = \begin{bmatrix} \gamma_X^2 & \gamma_{XY}^2 \\ \gamma_{XY}^2 & \gamma_Y^2 \end{bmatrix}, \quad (3.15)$$

$I(X_n; Y_n)$ and $I(X_n; Y_n | Z_n)$ can be computed as [58]:

$$I(X_n; Y_n) = -\frac{1}{2} \log \left(1 - \frac{\sigma_{XY}^2}{\sigma_X^2 \sigma_Y^2} \right) \quad (3.16)$$

$$I(X_n; Y_n | Z_n) = -\frac{1}{2} \log \left(1 - \frac{\gamma_{XY}^2}{\gamma_X^2 \gamma_Y^2} \right), \quad (3.17)$$

where Z_n contains all the variables except X_n and Y_n .

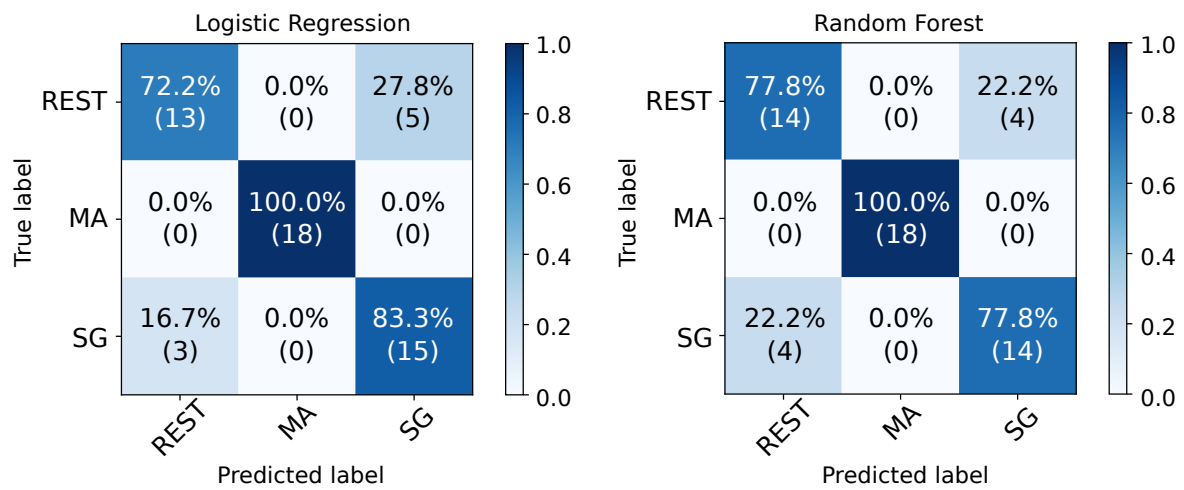
The experimental testing protocol produced 3 time series from the cardio-respiratory part and 56 (14×4) from the EEG, for a total of 59. These were processed for every possible combination, obtaining 3481 features: 59 from the computation of the self-entropy, 1711 from the mutual information and 1711 from the conditional mutual information. To compare the time series among different participants, all extracted features were initially normalized with respect to the REST session, supposing it as the baseline condition. Given the three mental states, i.e. REST, MA, and SG and the feature f_i , for $i = 1, 2, 3, \dots, 3481$, the normalized feature $f_i^{j,*}$, where $j = \{REST, MA, SG\}$, was computed as follows:

$$f_i^{j,*} = \frac{f_i^j}{f_i^{REST}}. \quad (3.18)$$

3.7.1 Results

Different classification algorithms were tested for the classification of the stress status: (i) Support Vector Classification (SVC), (ii) Random Forest (RF), and (iii) Logistic Regression (LR). The hyper-parameters for each classifier were optimized by a grid search: C, γ , and kernel for SVC, depth and the number of estimators for RF, and C and penalty for LR [19]. Leave-One-Person-Out cross-validation was applied to test the accuracy of the considered classification algorithms.

LR and RF achieved the best classification accuracy, equal to 85.2 % and 85.2 % respectively. Fig. 3.17 reports the confusion matrices.



(a) Logistic Regression (C: 1.0, penalty: L2).

(b) Random Forest (depth: 4, estimators: 8).

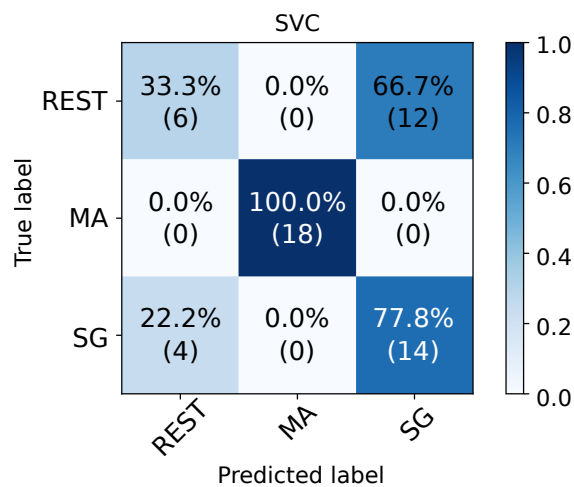
(c) SVC (C: 1.0, γ : 0.0001, kernel: RBF).

Fig. 3.17 Classification results for different classifiers. The best result was obtained by LR and RF classifiers, with an accuracy of 85.2%.

Table 3.5 Top 10 feature importance of Random Forest classifier.

| | feature | importance (%) | | feature | importance (%) |
|---|-------------------------------|----------------|----|------------------------------|----------------|
| 1 | $S-\delta_{FC6}$ | 7.024 | 6 | $MI-\alpha_{F8}-\beta_{AF4}$ | 6.068 |
| 2 | $MI-\delta_{F3}-\delta_{O1}$ | 7.015 | 7 | $MI-\beta_{AF3}-\beta_{P8}$ | 5.872 |
| 3 | $S-\theta_{T7}$ | 6.937 | 8 | $MI-\beta_{F3}-\beta_{P8}$ | 5.672 |
| 4 | $MI-\alpha_{FC5}-\alpha_{P8}$ | 6.648 | 9 | $MI-\delta_{F4}-\alpha_{F8}$ | 4.188 |
| 5 | $MI-\alpha_{P7}-\alpha_{O2}$ | 6.189 | 10 | $MI-\beta_{F7}-\theta_{T8}$ | 3.677 |

The most remarkable result concerns the classification of MA status: all classifiers correctly classified this task for 100 % of the cases, and at the same time other tasks were never misclassified with it. It follows that the feature values for MA strongly characterize the task, making it well distinguishable from others. The outcome is that a heavy mental stress status can be reliably be recognized by the proposed method.

As for the remaining classes, these present some misclassified results, proof that the considered feature base presents some similarities in these two stress states. However, since the logistic classifier and random forest classifier have correctly recognized about 80 % RESTs and SGs, this represents a sub-optimal but anyhow sufficiently accurate classification outcome for the applicability of the method.

The SVC with the low classification accuracy wrongly recognized many RESTs as SGs. The soft-margin SVM with RBF kernel allows some examples placed on the wrong side to be ignored based on the C parameter, on fitting. Since the classifier with a low C parameter like this classifier ignores many examples placed on the wrong side, it is considered that the classifier was built so that many REST placed on the SG side were ignored, in this result. However, the overall classification accuracy decreased by using a higher C parameter; therefore, it can be concluded that the SVM algorithm is not suitable for this dataset.

RF algorithm builds a set of decision trees based on feature importance. This can be exploited to investigate what feature is important for classification. Tab. 3.5 reports the values, as the normalized percentage, of the ten most important features identified by the RF model. Such features count for the 59.3 % of the overall feature importance score. The most important features are the ones relative to EEG signals. In particular, 4 features out of 10 are relative to the mutual information shared between pairs of electrodes in which one is positioned in the frontal part and the other in the occipital part of the head. Among the most important features, there are also the self-entropies of the electrodes FC6 and T7.

Since the Emotive EPOC+ is a quite invasive device for a real-life scenario, the accuracy of the classification algorithms was tested using the features provided only from the cardio-respiratory series. Moreover, in a real-life scenario, it is very difficult to use EEG signals because of artifacts derived from movement. Since, in this case, there would be only 9

Table 3.6 Feature importance of Random Forest classifier without Emotive EPOC features.

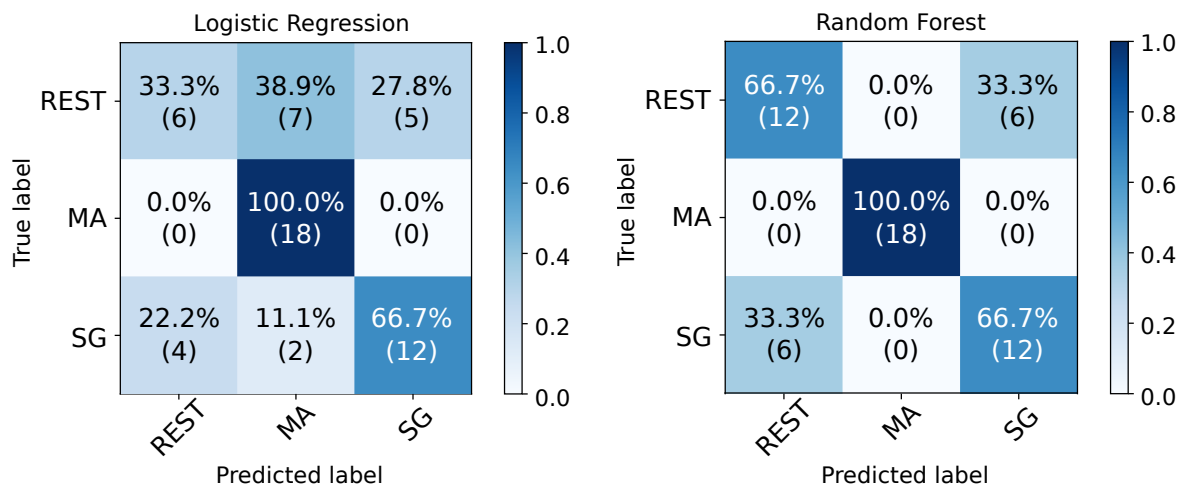
| | feature | importance (%) | | feature | importance (%) |
|---|-------------|----------------|----|----------------|----------------|
| 1 | mean-RR | 24.033 | 6 | mean-phasicEDA | 5.918 |
| 2 | std-RR | 16.624 | 7 | S-RESP | 5.487 |
| 3 | S-RR | 8.998 | 8 | MI-RR-RESP | 5.123 |
| 4 | S-PAT | 7.369 | 9 | RESPfreq | 4.378 |
| 5 | CMI-RESP-RR | 6.971 | 10 | CMI-PAT-RESP | 3.547 |

features, more traditional features for stress measurement were added, i.e. the LF/HF ratio, the mean and the standard deviation of the RR series, the respiratory frequency and the mean of the phasic component [65] of the EDA signal, which is provided by the Empatica E4 wristband. In this case the best obtained accuracy was of 77.8 % using the RF classifier (Fig. 3.18).

All classifiers could correctly recognize MA even without the Emotive EPOC+ features. However, the LR classifier and SVC have recognized some RESTs and SGs as MA. Especially, the LR classifier wrongly recognized about 70 % of REST as others and the classification accuracy decreased by around 20 % with respect to the LR classifier with the Emotive EPOC+ features. The SVC recognized several RESTs and SGs as MA, but it has correctly recognized a greater number of RESTs than the SVC with the Emotive EPOC+ features and the classification accuracy was increased by almost 4 %. Therefore, it can be concluded that the dataset without the Emotive EPOC+ is suitable for SVC, and is not for LR. RF classifier has increased a few numbers of incorrect classification between REST and MA; therefore, the classification accuracy decreased by around 7 % than the classifier with the Emotive EPOC+ features. However, the RF classifier has no REST and SG recognized as MA, unlike the other classifiers, and has kept enough high classification accuracy even without the Emotive EPOC+ features. In both datasets, RF has been the best classifier. Therefore, it can be concluded that it is suitable for the presented recognition.

Tab. 3.6 shows the feature importance of the random forest classifier. In this case, the most important features are relative to the ECG signal; i.e. the mean and the standard deviation of the RR series and its self-entropy.

Tab. 3.7 shows the comparison of the obtained results with respect to others found in the literature and analysed in Sec. 3.7. The framework proposed in this paper falls among the best results. For such a reason, it is possible to claim that the Network Physiology paradigm can be a good framework to detect stressful situations, even among different subjects.



(a) Logistic Regression (C: 10.0, penalty: L2).

(b) Random Forest (depth: 6, estimators: 32).

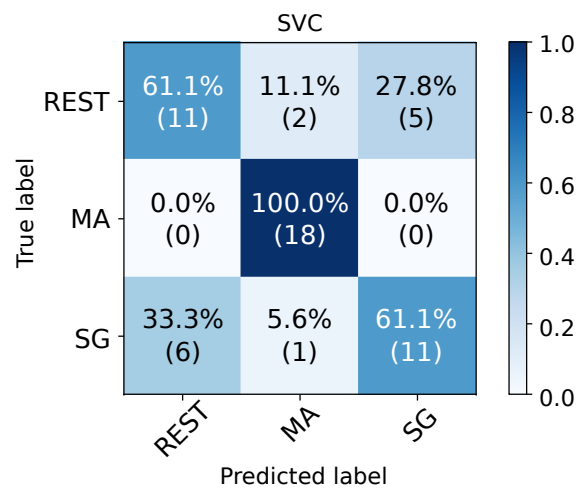
(c) SVC (C: 10.0, γ : 0.1, kernel: RBF).

Fig. 3.18 Classification results for different classifiers without EEG. The best result was obtained by RF classifiers, with an accuracy of 77.8 %.

Table 3.7 Comparison of the obtained results with respect to similar works in the literature.

| study | acquired signals | mental states | accuracy (%) |
|-----------------|-----------------------------|---------------|--------------|
| proposed | ECG, Resp., BVP, EEG | 3 | 85.2 |
| [147] | ECG, Resp., EDA, Temp. | 2 | 84.6 |
| [152] | EEG | 4 | 83.4 |
| [130] | EDA, PPG | 2 | 83.1 |
| [76] | ECG, EDA | 2 | 79.0 |
| [104] | ECG, TEB | 2 | 67.7 |
| [73] | EEG | 4 | 67.1 |

Chapter 4

Virtual Reality interface

4.1 Reality-virtuality continuum

The last decade was characterized by the so-called Augmented Reality (AR) and Virtual Reality (VR) revolution [89]. The emergence of these new technologies enabled the mix-up of reality with virtual worlds to create new environments (Fig. 4.1). In particular, if the virtual is superimposed to the current reality we speak of AR, if real data are imported and shown in the virtual context we speak of AV.

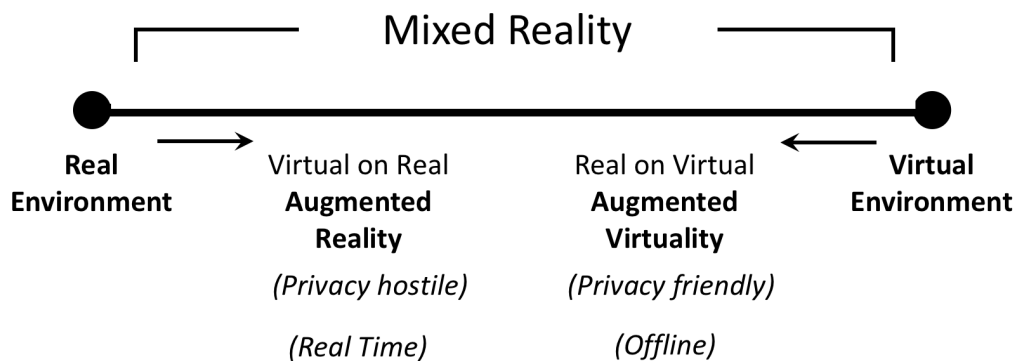


Fig. 4.1 Reality-virtuality continuum.

In AR, virtual cues and real data are superimposed to the real view of the scene via different technologies that span from smartphones, tablets, glasses, and projectors. In AV, real cues are superimposed to the virtual world via similar technologies to AR with the only difference to be more immersive. As an example, AR glasses allow us to see through, AV glasses are usually blind showing only the virtual environment. Considering clinical applications privacy can be an important requisite. In AR, it is more difficult to keep private

information while in AV real (sensible) data can be easily anonymized. AR must be played in real time. For this reason, information coming from real data acquired via distributed sensor networks shall be quickly elaborated and presented with low latency to the user. AV can be instead played offline: information coming from real data acquired via distributed sensor networks can be elaborated with complex algorithms and presented in a different time to the user.

4.2 Mixed Reality in healthcare systems

Mixed Reality (MR) has many applications that span from gaming, military, space, marketing, journalism, tourism, education and training, location-based services for mobile devices, to the service of industrial maintenance for parts analysis, simulation and/or staff support.

VR, which completely immerses the person in a simulated environment [122], has also a long use in the field of mental health, psychotherapy [61], to treat acrophobia [70] and the fear of flying [71, 126]. In rehabilitation it has been applied during the assessment of upper extremities mobility [18] and cognitive deficits [81, 79]. In addition, VR has been used in cognitive and physical rehabilitation using video games [66, 90, 131, 27, 28] and for gait training [77, 101, 82], as well as during the retraining of activities of daily living [88]. Furthermore, it has been used in combination with robotics [129], treadmill training [177], during driving assessments for people with head injuries [91], and to optimize driving interfaces and learning, for example with individuals who use wheelchairs [100].

The impact of MR on healthcare affects different areas such as surgery, doctors, physicians and nurses training, patient education and treatment, and diagnostic tools.

For example, AR is already applied in executing surgical operations. In the operative phase, surgeons can see radiographic superimposed to the surgical site with the overlaid simulated route [142]. AV can instead empower surgeons in pre-visualizing anatomy and thus plan the route of intervention.

A better understanding of registration and ergonomics will help the widespread of MR in this field. As an example, one of the difficulties in using head-mounted displays (HMDs) is the requirement for a common optical focal plane for both the real world scene and the computer-generated image. To increase the clinical acceptance, they have adapted for AR a miniature, cost-effective, head-mounted binocular [14].

Innovations in VR and AR have also the potential to significantly enhance the training-education stage of surgery [117].

Other applications involve pathology residents performing an autopsy wearing HoloLens while remotely instructing them with real-time diagrams, annotations, and voice instructions.

Telepathology allowed users to remotely access a pathologist for guidance and to annotate areas of interest on specimens in real-time [67].

4.3 Possible means to provide VR for occupational therapy

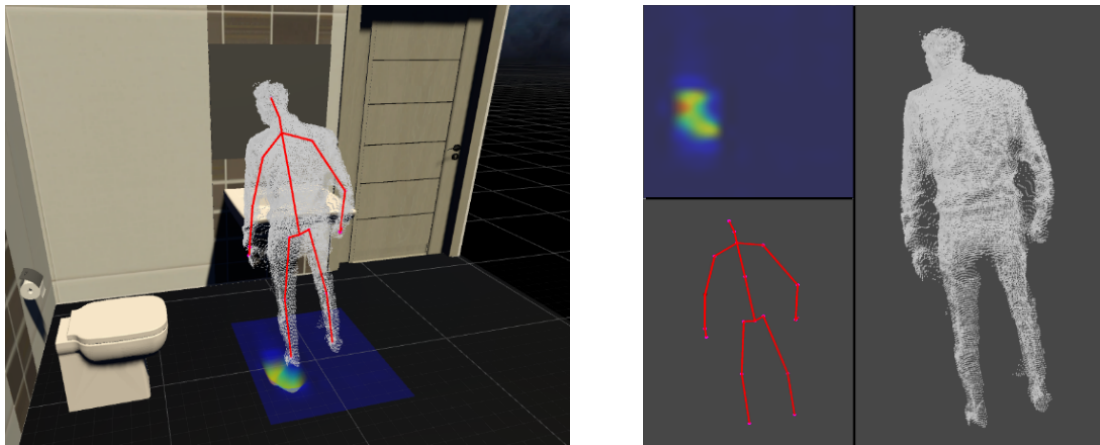
In rehabilitation medicine and occupational therapy, the assessment tool is essentially the human eye observing the person performing activities of daily living to evaluate his/her level of independence, efficacy, effort, and safety, to design an individualized treatment program. Thanks to MR technologies, it is now possible to provide, in addition to the evidence provided by the human eye, a large amount of data for therapists. Examples are data describing the person's motion in 3D, the interaction with the environment, such as forces, contact pressure maps and motion parameters related to the manipulation of objects, and the "internal" parameters, such as heart rate, respiratory rate, and sweating. This amount of information can be fed back to the clinician in an animation representing all the above parameters using MR methodologies. The main benefit of this new interaction methodology is twofold: the observed scenarios depicted in animations contain all the relevant parameters simultaneously and the related data are well defined and contextualized. This new methodology is a revolution in rehabilitative evaluation methods that allow on one hand to increase the objectivity and effectiveness of clinical observation, and on the other hand to re-define more reliable assessment scales and more effective rehabilitation programs, more user-centred.

Fig. 4.2 shows a visual comparison between the traditional interaction methodology and the VR one. The main benefit of VR is twofold: the observed scenario contains all the relevant parameters simultaneously and the related data are well defined and contextualized (Fig. 4.2a) for proper use by a clinician. On the other hand, the more traditional way to display data singularly has the advantage to allow a deeper analysis of each time series (Fig. 4.2b).

There are different possibilities to provide proper feedback to the clinician to enhance his/her point of view while observing an individual that uses different technological solutions in a domotic scenario. It is possible to define as VR-on-2D the VR achieved in a two-dimensional domain and VR-on-3D the one in a three-dimensional one. A further element to consider is the choice of the most suitable hardware support for the data and VR: immersive interfaces and standard flat displays.

Considering VR-on-2D or VR-on-3D, it is possible to consider the following:

- in the 3D domain, it is possible to link the information with the corresponding object. As an example it is possible to explore the mixed environment, find a specific object,



(a) Data reported in a virtual context (model) of the environment.

(b) Traditional way to display data.

Fig. 4.2 Domotic scenario with the following relevant data acquired: patient shape, motion (estimated via skeletonization), pressure on the floor.

select it and then display different kinds of information directly linked to the specific object;

- in 2D it is possible to choose the time instant and in some sense navigate in “time”, in 3D it is possible both to navigate in time and “space” by choosing the best viewpoint (Fig. 4.3);
- in 2D domain traditional cameras are used, in the 3D one, it is possible to employ both traditional and 3D ToF cameras. The main advantage of 2D technology is its higher resolution and chromatic rendering. The main advantage of 3D is its “direct” three-dimensional representation even though, currently, the technology suffers from a lower resolution;
- in 3D it is possible to estimate directly the 3D shape. In 2D it is also possible to estimate the shape of objects or human subjects at the expense of much more elaborated algorithms. For example, Shape-From-Silhouette (SFS) methods can recover the Visual Hull (VH) from silhouette images and thus a 3D shape estimate. One of the limitations of SFS, however, is that the approximated shape can be very coarse when there are only a few cameras. To solve this limitation it is possible to fuse different silhouettes captured across time [24] with the constraint of a rigid body (thus barely applicable to human motion) or there is the need to fuse texture and silhouette information [41]. Methods that rely on texture can be very effective in some cases but require a proper texture suitable to extract features and complex procedures not perfectly suited for

real-time applications. The same applies to the problem of object detection with the only current limit of ToF camera resolution that could make traditional 2D technologies more suitable for some applications;

- from the 3D shape it is possible to improve/enable the skeleton estimation via modelling and fitting a human mannequin on the 3D data [181, 75], or estimating skeleton accuracy by comparing the skeleton and the 3D data and then fusing the result [116, 106];
- in 3D it is possible to exploit modern animation frameworks to animate virtual and real objects as a function of the distributed augmentative measurements. This enables to create proper links between cause and effect that best suits the human brain representation of the specific context (see Sec. 4.4.1), thus improving the feedback to the user in terms of intuitiveness and thus “readability”;
- in 3D dimensional perception and thus shape measurement display are much more effective;
- 3D ToF data are much more privacy-friendly: it is indeed possible to blur, by smoothing, the 3D shape of the subject while keeping intact its overall physiognomy, still useful for motion and action analysis. The same kind of operation on standard 2D vision-based technologies causes a higher loss of information.

Differences between the immersive interface and 2D display are the following:

- with the 2D display based solution it is possible to use the traditional display technology that is certainly of lower cost both in terms of the display itself and the required computing/graphics resources. With this solution it is possible to display both the 2D and the 3D data;
- with the immersive solution it is possible to navigate within the environment with natural gestures (e.g. looking around, moving, turning the head, etc.) so that observation through navigation results much more effective in terms of speed and truthfulness;
- with the immersive solution there is the possibility to use 3D joysticks over which it is possible to link several variables of interest (such as physiological wearable data as in the project described in this thesis). Those data can appear or disappear just raising or dropping the hand. Further possibilities are haptic feedback driven by the 3D interaction between the joysticks and the objects displayed in the “virtual” environment and more friendly but also effective manipulation or selection of the data, such as a 3D lasso or a 3D laser pointer operating directly inside the scene.



(a) Traditional camera view.



(b) ToF 3D camera view.



(c) The “best” viewpoint.

Fig. 4.3 Different viewpoints available in 3D with respect to a traditional camera view.

4.4 Integration of body and environmental data

The sensing environment includes multiple 3D cameras, several environmental sensors and wearable devices as explained in Ch. 2. The design was optimized to measure the parameters of interest for the analysis and understanding of the most relevant actions related to the quality of life of disabled subjects. The 3D infrastructure was calibrated using the procedure described in Sec. 2.3.1, achieving as output a dense 3D point cloud as dynamic scansion of the room. A static scansion was initially used as a reference base to match the measured geometry with a Virtual Environment (VE), cad-based. Custom design graphical elements were successively included in the VE for each sensor to provide an effective and intuitive visual feedback of the data, contextualizing the measured quantities with the area in which these were collected. On top of that, a plot-like graphic was included in proximity to each device to display the data as time series.

The objective of the sensing infrastructure and visualization interface is the record and cyber reproduction of actions to remove from the clinical observation practice the presence of the therapist nearby the monitored subject (Fig. 4.4). In the proposed research, such element is tackled by recording a wide pool of data, amount and types, in a more complete way than a standard video-based solution. The structure includes 3D geometries of the subjects, physiological measurements, and a wide set of physical quantities useful in the reproduction and visualization of the interactions of the monitored subject with the environment.

The development of the VR interface is a team work of the MIRo lab of the University of Trento.

The idea is that the VE (data acquisition, stream, and display) must be self-sufficient, allowing the therapist both to understand and monitor the actions performed by the subject, both to assess his/her emotional/cognitive and physical status, supported by more objective information. The avoidance of the therapist to be side by side to the patients potentially has various benefits. First, the independence of the subject during the actions. It is indeed known that the presence of an external observer influences the behaviour of the observed subject. To avoid such distracting/influencing element, the monitoring system must grant the same amount and quality of information that the therapist usually assess from the physical observation. In this preliminary exploitation, no relevant loss of information was reported by the therapists, who were able to properly understand and analyse the actions of the subject in a way comparable to the standard observation practice. Important improvement regards the privacy of the subject. Despite the recording, necessary for the observation and analysis, the privacy is granted because the data collected are always filtered by an automatic process before the transfer to the server, blurring the shape of the subject while keeping intact the global volume (useful for the analysis of actions). That allows the usage of the system in



(a) The standard approach based on the presence of the therapist side by side to the patient.



(b) The proposed AR structure in which the patient is independent and the therapists can assess his/her state from an augmented view.

Fig. 4.4 Comparison of occupational therapy support/interaction [33].

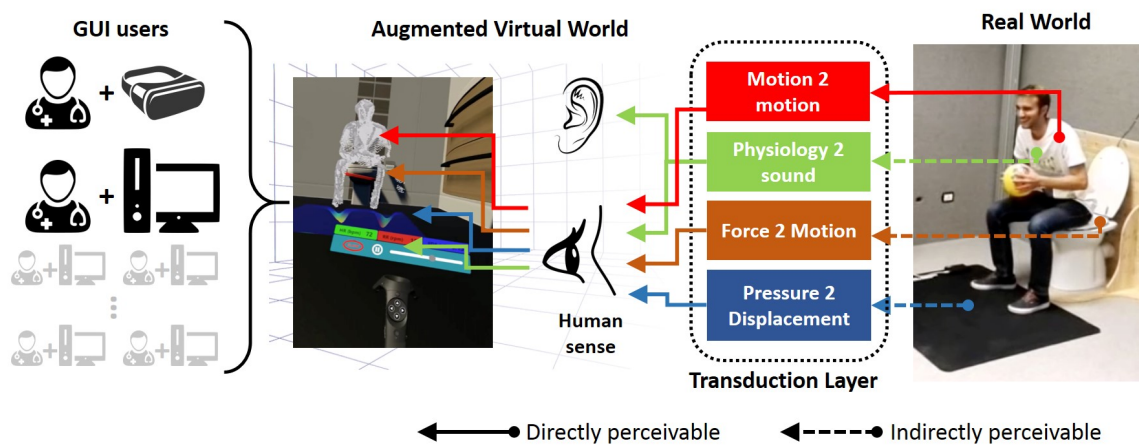
areas in which it is not possible to apply the direct observation unless in a “simulated” form, as in the bathroom. A further element is an augmentation of reality, which allows the natural integration of parameters and measurements from different realms in a unique, contextual and meaningful representation. In our case, one of the most significant examples was the aggregation of the heartbeat and breath (as sounds) synchronous with the 3D shape and motion of the subject. The two inputs, visual and auditory, suggested to the therapists a natural correlation of the two quantities with respect to the status of the subject, assessing in this way stress, fatigue, and pain.

The system was designed to store those data on a local server, and a custom client service to get the data stream back into the main GUI. According to data of interest, bandwidth, computation power, and available VR technologies, this can be displayed either by multiple digital supports, either from different locations. Two solutions were considered: VR headset (local) and a standard PC monitor (local or remote), as shown in Fig. 4.5. Such structure enables a collaborative working environment, in which multiple therapists can take a look at the data in a parallel and/or concurrent ways. The main benefit is the opening of the analysis of recorded data to a broader pool of experts, with the possibility of watching them repeatedly, optimizing the workflow.

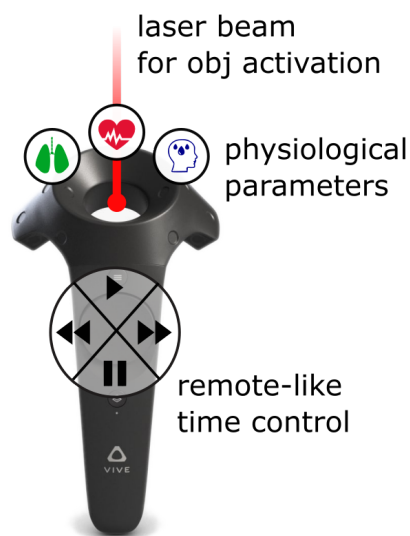
To be effective, the visualization interface must be intuitive, easy to use and provide a clear and meaningful representation of the data as if those were directly perceived by the user. That is a critical point: from it derives the capability of the therapist to focus on the actions under analysis rather than on the GUI itself or its usage.

The developed sensing infrastructure represents, however, a complex environment, in which several sensors provide measurements of both directly perceivable parameters both indirect ones. In the first category, the natural and intuitive perception of the quantity enables the definition of simple and established graphical solutions and visualization modalities: i.e. a 3D point cloud displaying the shape of the user, visible in Fig. 4.6. As for the latter, these require specially designed interfaces properly defined concerning the nature and physical domain of the indirect perceivable quantity.

As already explained in Sec. 2.2, several environmental sensors measure the force exchanged by the subject with objects and/or items of furniture during his/her interaction with them. Currently, four patients tested the AUSILIA infrastructure in the domotic apartment. For each subject, the acquired physiological signals were the ECG, the respiratory signal and the EDA. Each patient performed recording sessions of about half an hour. During the time spent in the domotic apartment, there was always an occupational therapist with the patient. It is important to underline that, at the time of the writing of this thesis, we are still in a preliminary stage for what concerns the tests with patients. During these recording sessions,



(a) A schematic representation of the sensing, and visualization system. The 3D point cloud was blurred and presented without colour for privacy sake.



(b) The VR controller augmented with physiological parameter and control interfaces for the time flow.

Fig. 4.5 The general scheme of the transduction from the sensing infrastructure to the augmented virtualized observation and control of the data in the developed GUI.

the therapists concentrated mainly on two specific activities: the transfer from a wheelchair to the toilet seat, and the transition from the laying to the sitting position in bed. For both, the flow of the forces applied by the subject is a parameter of extreme interest for the therapist: the most of the loss of autonomy or simply articular pain and fatigue suffered by disabled subjects are often caused by wrong motion patterns.

The implemented sensing systems for these cases were (see Sec. 2.2 for further details):

- **Toilet seat:** 4 pressure sensors embedded in the seat. Two main quantities were computed: the average pressure, as the percentage of the total body weight, and its point of application, from the differential analysis of the measurement points. These provide the required amount of information to assess the balance and thus the stability of a subject in the transfer from and to the wheelchair so as the correctness of the seat.
- **Patient lift:** a load cell was included in a stand-lift. This measures the amount of force applied by the subject during the transition from the laying position to the sitting position in bed. The optimization of the loads at shoulder level resulting from the motion is here critical to prevent the rise of articular pain.

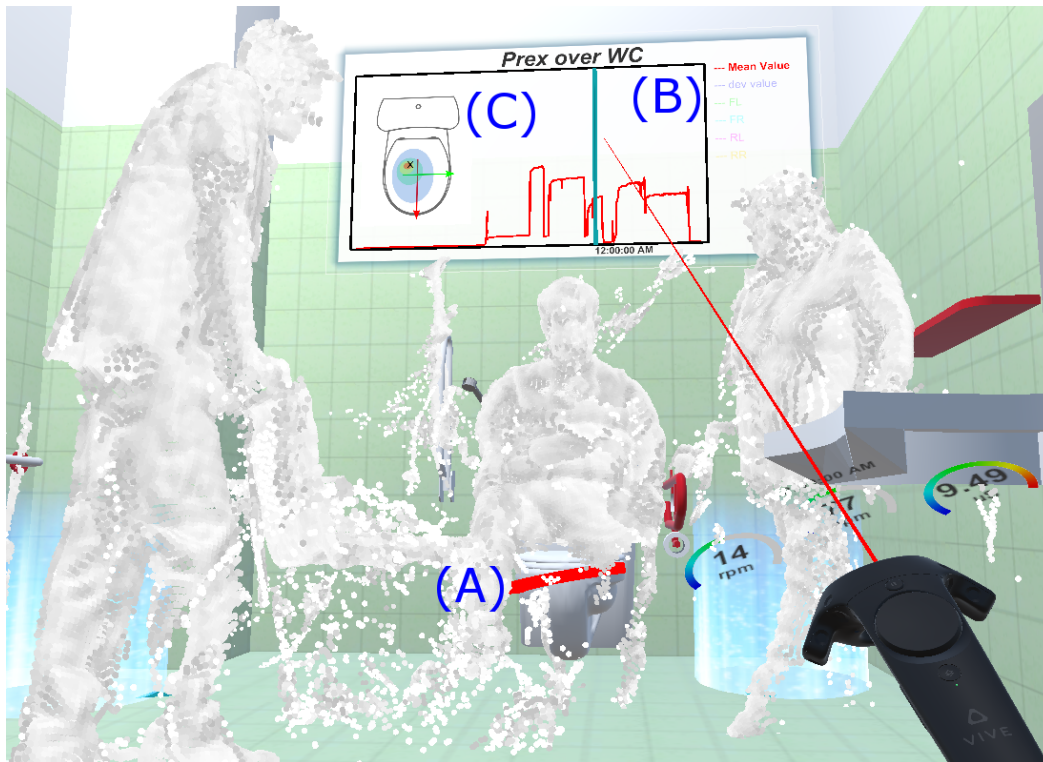
The visualization of these quantities was organized as a three-level representation: magnification, direct time management, and average trend [54].

These are activated by pointing and clicking with a laser beam generated by a virtual controller the object/sensor of interest. The graphics of the controller, shown in Fig. 4.5b, were customized starting from the default one (from HTC Vive) and augmented with physiological parameters acquired from the monitored subject, i.e. the respiratory rate, the heart rate and SC (Fig. 4.6a). The interface was meant to provide clinicians a continuous and synthesized overview of the hidden internal state of the subject, which represents another kind of indirectly perceivable quantity, useful in the assessment of stress or fatigue. Fig. 4.6 reports a detailed view of the GUI and the implemented solutions.

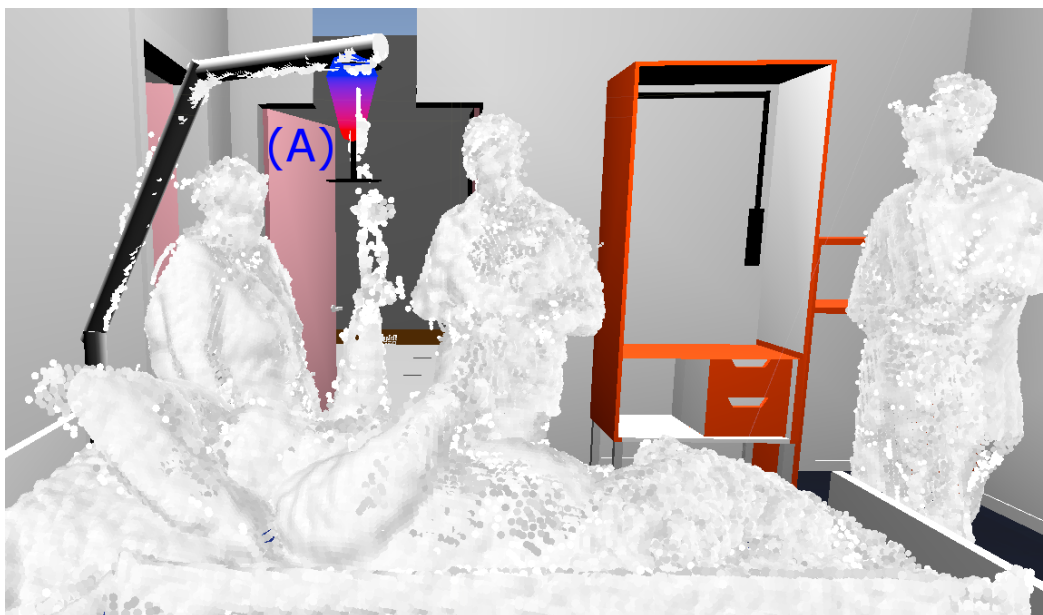
4.4.1 Magnification

The magnification of a physical quantity represents the most intuitive form of data visualization: a virtual object was included in the environment and transformed or deformed accordingly to the measured trend.

In the case of the toilet, a 3D model of the seat is moved upward or downward accordingly to the total pressure, and rotated along the frontal and transversal direction with respect to the differential pressure on the sides on the seat, as Fig. 4.6a shows. As for the lift, a cone was placed at the top of the holder: the height of the solid was set to zero and increased



(a) Bathroom, toilet seat. On the controller, the respiratory rate, the heart rate and SC are shown.



(b) Bedroom, bed lift.

Fig. 4.6 Examples of GUI in action for the augmented virtualized visualization of hidden physical variables: (A) magnification, (B) direct time management, and (C) average trend.

accordingly to the applied force, so as for its colour which changes from blue to red, shown in Fig. 4.6b. The total body weight of the subject was used as the normalization factor. In both these examples, the pressure was transduced into motion or size deformation as far as these resulted in the most intuitive effects that we perceive from a force acting on a surface.

From the therapists' feedbacks, this representation resulted to be adequately intuitive and effective for a quick understanding of the loads, especially under the postural point of view. On the other side, the simplified nature of the representation resulted to be not sufficiently informative and objective: the density of the 3D point cloud was perceived as not sufficiently dense in some areas of the environment, with a loss in details for the reconstruction of the hand and fingers.

4.4.2 Direct time management

A more traditional visualization included in the GUI was a plot-like panel. This was dynamically generated on the walls of the VE accordingly to the sensor position in the real environment. Such graphic reports one or more temporal trends of the collected data, also providing derived quantities from the processing of the measurement, i.e. the coordinates of the barycentric pressure point. The user can interact with that using the same laser pointer used for the activation of the visualization. Three modalities were defined: (i) the selection/activation of the trends, (ii) the selection of a time window, and (iii) a temporal sliding.

The last modality, the most interesting from the therapists' point of view, enables a fast forward or backward of the AR data stream in the interface by simply moving the laser point on the plot. By using such functionality, the therapists were able to easily identify from the plot anomalous behaviours and quickly reach the associated temporal instant. Thanks to the magnification of the plot, the same strategy can be applied to analyse the recorded actions in slow motion, which represents a visualization modality not available in a direct, real world, observation.

4.4.3 Average trend

For a better understanding of some measurements, the average of the results represents a better option than the punctual data, as time instant. This was the case of the toilet seat, in which neither of the two aforementioned visualization modalities was able to provide to the therapists an intuitive and effective representation of what happened in the recorded actions.

The outcome of the design was then depicted by an average representation of the trends, computed within a period selected directly from the plot-like graphics. In the case of the seat,

this was represented as its top view plus a heat map generated by the percentage of the time spent by the pressure barycentre position in an area of the seat.

In the proposed GUI, each sensor (and the associated interfaces) constitutes a temporal gate useful in the analysis and examination of actions that took place at different times. In this new domain, the user has the full control of the time flow, with also the possibility of combining, synchronously, all kinds of data and physical quantities of interest to better enhance his/her comprehension of the state of the monitored subject. The GUI results then in an augmentation of the reality not only under the spatial/geometrical point of view but also from the multi-physical and temporal ones.

4.4.4 Potential of the proposed solution

The proposed system will certainly enable a great innovation in occupational therapy as far as it enables:

- a better perceptual inference of relationships between the subject behaviour, the environment and his/her interaction with it;
- the data are aggregated and thus simultaneously shown;
- the monitoring of a large number of potential events (i.e. specific user actions such as opening doors, transporting on the toilet table, cooking, etc.);
- a medium that, unlike static diagrams, enables the exploration of a space of inhomogeneous parameters where each of them can represent a trigger for the contextualization of the full set.

The whole constitutes an interface able to empower a physician or an occupational therapist to optimize the best technological aid in a home scenario for the personalized restoring of autonomous functions.

Chapter 5

Conclusion and future developments

The present thesis presented a novel framework for supporting domiciliary care treatments and prevention, to delay the cognitive impairment of disabled and old people and facilitate their recovery. The framework relies on an ecosystem of wearable devices, environmental and motion capture sensors aimed at providing an infrastructure to continuously monitor and assist users in a non-invasive manner. The main aim is to assess the proposed aid technologies with respect to their impact and acceptability by users and relatives-caregivers.

The therapists can evaluate the performances of users during their daily activities without the need to stay with them and thus without influencing their natural behaviour while performing daily routine actions fundamental to restore their autonomy. The innovative developed VR interface gives also to the clinicians the possibility to know parameters that are usually hidden to the human eye, such as physiological parameters and exchanged forces.

The clinician will be able to evaluate, in an aggregated view, gestures, interactions with the environment and the person's physiological parameters via an immersive virtual reality framework. The main innovation is the fact that the system will go beyond the subjective view of the therapist being able to collect a quantitative and objective view that embodies not only the subject interactions with the environment but also the user internal status via physiological parameters thus allowing, for the first time in clinical rehabilitation protocols, an empathic observational experience. The data provided by the system are innumerable. The actual use for clinical protocols has still to be explored in the clinic context through the use of ad hoc rehabilitative protocols able to exploit the full potential of the new paradigm. Improvements are required to enhance the density of the 3D point clouds, because, in some cases, a loss in details for the reconstruction of movements of hands and fingers was noticed by the therapists that tested the interface. However, the first preliminary assessments show that the feedback of the therapists is generally positive. All the parameters provided by the

interface were evaluated as meaningful and useful for a better comprehension of the actions of the patient.

An important part of the thesis was devoted to studying the mechanism of stress and in particular the cognitive one (Ch. 3). The new paradigm of Network Physiology was used. An analysis of the information dynamics of physiological networks during different levels of mental stress, i.e. REST, MA and SG, was conducted (Sec. 3.6). The aim was to investigate the mechanisms underlying the processing of information that leads to complex multivariate dynamics such as those displayed by the different brain wave amplitudes on the one side, and the cardiovascular and respiratory variability on the other side. Interesting applications can also emerge in real-life scenarios thanks to the fact that wearable devices were used for the acquisition of the physiological signals. The results indicate that the characterization of these networks is possible, both in terms of the levels of information produced and stored at each network node and in terms of the amounts of information transferred within and between the brain and peripheral subnetworks. Such characterization was informative regarding the description of the mechanisms leading to the complexity of physiological dynamics and the interaction between different physiological systems in a resting condition, and regarding the alteration of these mechanisms during a cognitive task evoking mental stress. The distinction between the cognitive task and the sustained attention task resulted in being more difficult, likely as a consequence of the fact that such states provoke similar autonomic changes. However, the consideration of central and autonomic effects as they are reflected in the topology of brain-heart interactions provided additional characterization among the analysed states. The findings of this thesis can be helpful for a better comprehension of physiological mechanisms behind stress conditions.

Future studies will extend the analysis to the other electrode signals (indeed only the electrode F3 was used as already explained in Sec. 3.6.1) for a deeper investigation of the dynamics of the entire brain area during different levels of mental stress [118]. Indeed, the use of the other electrodes could reveal other coupling dynamics depending on the specific electrode location, increasing the potential of the presented approach. Limitations of the current study are the absence of randomization of the MA and SG phases and the absence of self-assessment measures reporting on the perceived stress level. Moreover, further analysis should focus on the comparison between the two rest phases before and after mental arithmetic or serious games to investigate possible effects remaining after the stressful tasks. Finally, it would be also important to advance the methodology adopted here investigating the presence of instantaneous (zero-lag) interactions, also in consideration of the fact that zero-lag correlations cannot be excluded among the observed physiological time series [45]. This aspect was not addressed in this study because a non-trivial modification

of the estimators adopted would have been needed. For example, the direction of zero-lag interactions cannot be inferred from physiological considerations in the data analysed in this study, and thus methods exploiting non-Gaussianity should be adopted [42, 134].

Classifiers were also implemented to assess mental stress (Sec. 3.7), using information theoretic measures, such as self-entropy, mutual information, and conditional mutual information. The best results were obtained by LR and RF classifiers with an accuracy of 84.6 %. An accuracy of 76.5 % was instead obtained by RF using only features provided by the cardio-respiratory signals. These results are comparable with the ones found in the literature (Tab. 3.7). With respect to the current state of the art, the novelty of the presented approach consisted in using the Network Physiology paradigm on signals acquired from “low-invasive” and consumer wearable devices to distinguish among different levels of mental stress. Future development will foresee the improvement of the classification accuracy, using only the devices related to the cardio-respiratory signals for their lower invasiveness. Further analyses are also needed to investigate if the lower classification accuracy without the EEG headset is due to a reduced number of features, or actual information related to EEG dynamics.

The developed algorithm for stress detection will be in the next future implemented and tested with the acquired data of patients that will make use of the AUSILIA infrastructure.

References

- [1] Acharya, U. R., Joseph, K. P., Kannathal, N., Min, L. C., and Suri, J. S. (2007). Heart rate variability. In *Advances in cardiac signal processing*, pages 121–165. Springer.
- [2] Ako, M., Kawara, T., Uchida, S., Miyazaki, S., Nishihara, K., Mukai, J., Hirao, K., Ako, J., and Okubo, Y. (2003). Correlation between electroencephalography and heart rate variability during sleep. *Psychiatry and clinical neurosciences*, 57(1):59–65.
- [3] AL-Khalidi, F. Q., Saatchi, R., Burke, D., Elphick, H., and Tan, S. (2011). Respiration rate monitoring methods: A review. *Pediatric pulmonology*, 46(6):523–529.
- [4] Aoki, H., Takemura, Y., Mimura, K., and Nakajima, M. (2001). Development of non-restrictive sensing system for sleeping person using fiber grating vision sensor. In *Microelectronics and Human Science, 2001. MHS 2001. Proceedings of 2001 International Symposium on*, pages 155–160. IEEE.
- [5] Arun, K. S., Huang, T. S., and Blostein, S. D. (1987). Least-squares fitting of two 3-d point sets. *IEEE Transactions on pattern analysis and machine intelligence*, (5):698–700.
- [6] B.-N. Sanders, E. (2002). From user-centered to participatory design approaches. In *Design and the social sciences: Making connections*, pages 1–8. CRC Press.
- [7] Barnett, L., Barrett, A. B., and Seth, A. K. (2009). Granger causality and transfer entropy are equivalent for gaussian variables. *Physical review letters*, 103(23):238701.
- [8] Barnett, L. and Seth, A. K. (2015). Granger causality for state-space models. *Physical Review E*, 91(4):040101.
- [9] Bartsch, R. P., Liu, K. K., Bashan, A., and Ivanov, P. C. (2015). Network physiology: how organ systems dynamically interact. *PloS one*, 10(11):e0142143.
- [10] Bashan, A., Bartsch, R. P., Kantelhardt, J. W., Havlin, S., and Ivanov, P. C. (2012). Network physiology reveals relations between network topology and physiological function. *Nature communications*, 3:702.
- [11] Behzadnia, A., Ghoshuni, M., and Chermahini, S. (2017). Eeg activities and the sustained attention performance. *Neurophysiology*, 49(3):226–233.
- [12] Benetazzo, F., Ferracuti, F., Freddi, A., Giantomassi, A., Iarlori, S., Longhi, S., Monteriù, A., and Ortenzi, D. (2015). Aal technologies for independent life of elderly people. In *Ambient Assisted Living*, pages 329–343. Springer.

- [13] Berntson, G. G., Cacioppo, J. T., and Quigley, K. S. (1993). Respiratory sinus arrhythmia: autonomic origins, physiological mechanisms, and psychophysiological implications. *Psychophysiology*, 30(2):183–196.
- [14] Birkfellner, W., Figl, M., Huber, K., Watzinger, F., Wanschitz, F., Hummel, J., Hanel, R., Greimel, W., Homolka, P., Ewers, R., et al. (2002). A head-mounted operating binocular for augmented reality visualization in medicine-design and initial evaluation. *IEEE Transactions on Medical Imaging*, 21(8):991–997.
- [15] Bishop, A. N., Fidan, B., Anderson, B. D., Doğançay, K., and Pathirana, P. N. (2010). Optimality analysis of sensor-target localization geometries. *Automatica*, 46(3):479–492.
- [16] Boucsein, W. (2012). *Electrodermal activity*. Springer Science & Business Media.
- [17] Brandenberger, G., Ehrhart, J., Piquard, F., and Simon, C. (2001). Inverse coupling between ultradian oscillations in delta wave activity and heart rate variability during sleep. *Clinical neurophysiology*, 112(6):992–996.
- [18] Broeren, J., Björkdahl, A., Pascher, R., and Rydmark, M. (2002). Virtual reality and haptics as an assessment device in the postacute phase after stroke. *CyberPsychology & Behavior*, 5(3):207–211.
- [19] Buitinck, L., Louppe, G., Blondel, M., Pedregosa, F., Mueller, A., Grisel, O., Niculae, V., Prettenhofer, P., Gramfort, A., Grobler, J., et al. (2013). Api design for machine learning software: experiences from the scikit-learn project. *arXiv preprint arXiv:1309.0238*.
- [20] Carswell, A., McColl, M. A., Baptiste, S., Law, M., Polatajko, H., and Pollock, N. (2004). The canadian occupational performance measure: a research and clinical literature review. *Canadian journal of occupational therapy*, 71(4):210–222.
- [21] Castaldo, R., Melillo, P., Bracale, U., Caserta, M., Triassi, M., and Pecchia, L. (2015). Acute mental stress assessment via short term hrv analysis in healthy adults: a systematic review with meta-analysis. *Biomedical Signal Processing and Control*, 18:370–377.
- [22] Celani, N. L., Ponce, S., Quintero, O. L., and Vargas-Bonilla, F. (2017). Improving quality of life: Home care for chronically ill and elderly people. In *Caregiving and Home Care*. IntechOpen.
- [23] Censi, A. (2007). An accurate closed-form estimate of icp’s covariance. In *Proceedings 2007 IEEE International Conference on Robotics and Automation*, pages 3167–3172. IEEE.
- [24] Cheung, K., Baker, S., and Kanade, T. (2003). Shape-from-silhouette of articulated objects and its use for human body kinematics estimation and motion capture. In *2003 IEEE Computer Society Conference on Computer Vision and Pattern Recognition, 2003. Proceedings.*, volume 1, pages I–I. IEEE.
- [25] Chrousos, G. P. (2009). Stress and disorders of the stress system. *Nature reviews endocrinology*, 5(7):374.
- [26] Cohen, S., Janicki-Deverts, D., and Miller, G. E. (2007). Psychological stress and disease. *Jama*, 298(14):1685–1687.

- [27] Confalonieri, M., Guandalini, G., Da Lio, M., and De Cecco, M. (2012). Force and touch make video games serious for dexterity rehabilitation. *pHealth*, pages 139–144.
- [28] Confalonieri, M., Tomasi, P., Depaul, M., Guandalini, G., Baldessari, M., Oss, D., Prada, F., Mazzalai, A., Da Lio, M., and De Cecco, M. (2013). Neuro-physical rehabilitation by means of novel touch technologies. *Stud. Health Technol. Inform.*, 189:158–163.
- [29] Corti, A., Giancola, S., Mainetti, G., and Sala, R. (2016). A metrological characterization of the kinect v2 time-of-flight camera. *Robotics and Autonomous Systems*, 75:584–594.
- [30] Cover, T. M. and Thomas, J. A. (2012). *Elements of information theory*. John Wiley & Sons.
- [31] Curtis, B. M. and O’Keefe Jr, J. H. (2002). Autonomic tone as a cardiovascular risk factor: the dangers of chronic fight or flight. In *Mayo Clinic Proceedings*, volume 77, pages 45–54. Elsevier.
- [32] Dawson, M. E., Schell, A. M., and Filion, D. L. (2007). The electrodermal system. *Handbook of psychophysiology*, 2:200–223.
- [33] De Cecco, M., Fornaser, A., Tomasin, P., Zanetti, M., Guandalini, G., Ianes, P., Pilla, F., Nollo, G., Valente, M., and Pisoni, T. (2017). Augmented reality to enhance the clinician’s observation during assessment of daily living activities. In *International Conference on Augmented Reality, Virtual Reality and Computer Graphics*, pages 3–21. Springer.
- [34] De Morree, H., Szabó, B., Rutten, G.-J., and Kop, W. (2013). Central nervous system involvement in the autonomic responses to psychological distress. *Netherlands Heart Journal*, 21(2):64–69.
- [35] Dellaert, F. (2012). Factor graphs and gtsam: A hands-on introduction.
- [36] Dobbs, S. E., Schmitt, N. M., and Ozemek, H. S. (1984). Qrs detection by template matching using real-time correlation on a microcomputer. *Journal of clinical engineering*, 9(3):197–212.
- [37] Dorrington, P., Wilkinson, C., Tasker, L., and Walters, A. (2016). User-centered design method for the design of assistive switch devices to improve user experience, accessibility, and independence. *Journal of Usability Studies*, 11(2):66–82.
- [38] Drinnan, M. J., Allen, J., and Murray, A. (2001). Relation between heart rate and pulse transit time during paced respiration. *Physiological measurement*, 22(3):425.
- [39] Eda, N., Ito, H., Shimizu, K., Suzuki, S., Lee, E., and Akama, T. (2017). Yoga stretching for improving salivary immune function and mental stress in middle-aged and older adults. *Journal of women & aging*, pages 1–15.
- [40] Esler, M. (2017). Mental stress and human cardiovascular disease. *Neuroscience & Biobehavioral Reviews*, 74:269–276.
- [41] Esteban, C. H. and Schmitt, F. (2004). Silhouette and stereo fusion for 3d object modeling. *Computer Vision and Image Understanding*, 96(3):367–392.

- [42] Faes, L., Erla, S., Porta, A., and Nollo, G. (2013). A framework for assessing frequency domain causality in physiological time series with instantaneous effects. *Philosophical Transactions of the Royal Society A: Mathematical, Physical and Engineering Sciences*, 371(1997):20110618.
- [43] Faes, L., Marinazzo, D., Jurysta, F., and Nollo, G. (2015a). Linear and non-linear brain–heart and brain–brain interactions during sleep. *Physiological measurement*, 36(4):683.
- [44] Faes, L., Marinazzo, D., and Stramaglia, S. (2017a). Multiscale information decomposition: exact computation for multivariate gaussian processes. *Entropy*, 19(8):408.
- [45] Faes, L. and Nollo, G. (2010). Extended causal modeling to assess partial directed coherence in multiple time series with significant instantaneous interactions. *Biological cybernetics*, 103(5):387–400.
- [46] Faes, L., Nollo, G., Jurysta, F., and Marinazzo, D. (2014). Information dynamics of brain–heart physiological networks during sleep. *New Journal of Physics*, 16(10):105005.
- [47] Faes, L., Nollo, G., and Porta, A. (2017b). Information decomposition: A tool to dissect cardiovascular and cardiorespiratory complexity. In *Complexity and Nonlinearity in Cardiovascular Signals*, pages 87–113. Springer.
- [48] Faes, L., Porta, A., Javorka, M., and Nollo, G. (2017c). Efficient computation of multiscale entropy over short biomedical time series based on linear state-space models. *Complexity*, 2017.
- [49] Faes, L., Porta, A., and Nollo, G. (2015b). Information decomposition in bivariate systems: theory and application to cardiorespiratory dynamics. *Entropy*, 17(1):277–303.
- [50] Faes, L., Porta, A., Nollo, G., and Javorka, M. (2016). Information decomposition in multivariate systems: definitions, implementation and application to cardiovascular networks. *Entropy*, 19(1):5.
- [51] Fernández, T., Harmony, T., Rodríguez, M., Bernal, J., Silva, J., Reyes, A., and Marosi, E. (1995). Eeg activation patterns during the performance of tasks involving different components of mental calculation. *Electroencephalography and clinical Neurophysiology*, 94(3):175–182.
- [52] Fischler, M. A. and Bolles, R. C. (1981). Random sample consensus: a paradigm for model fitting with applications to image analysis and automated cartography. *Communications of the ACM*, 24(6):381–395.
- [53] Fisher, A. G. and Jones, K. B. (2012). *Assessment of Motor and Process Skills Volume II-User Manual*. Three Star Press.
- [54] Fornaser, A., De Cecco, M., Tomasin, P., Zanetti, M., Guandalini, G., Gasperini, B., Ianes, P., Pilla, F., and Ghensi, R. (2018). Augmented virtualized observation of hidden physical quantities in occupational therapy. In *2018 International Conference on Cyberworlds (CW)*, pages 423–426. IEEE.

- [55] Fornaser, A., Tomasin, P., De Cecco, M., Tavernini, M., and Zanetti, M. (2017). Automatic graph based spatiotemporal extrinsic calibration of multiple kinect v2 tof cameras. *Robotics and Autonomous Systems*, 98:105–125.
- [56] Funnell, M. M. (2000). Helping patients take charge of their chronic illnesses. *Fam Pract Manag*, 7(3):47–51.
- [57] Gauche, R., Lima, R. M., Myers, J., Gadelha, A. B., Neri, S. G., Forjaz, C. L., and Vianna, L. C. (2017). Blood pressure reactivity to mental stress is attenuated following resistance exercise in older hypertensive women. *Clinical interventions in aging*, 12:793.
- [58] Gelfand, I. M. and Yaglom, A. (1959). *Calculation of the amount of information about a random function contained in another such function*. American Mathematical Society Providence.
- [59] Germán-Salló, Z. and Germán-Salló, M. (2016). Non-linear methods in hrv analysis. *Procedia technology*, 22:645–651.
- [60] Giannakakis, G., Grigoriadis, D., and Tsiknakis, M. (2015). Detection of stress/anxiety state from eeg features during video watching. In *Engineering in Medicine and Biology Society (EMBC), 2015 37th Annual International Conference of the IEEE*, pages 6034–6037. IEEE.
- [61] Glantz, K., Durlach, N. I., Barnett, R. C., and Aviles, W. A. (1997). Virtual reality (vr) and psychotherapy: Opportunities and challenges. *Presence: Teleoperators & Virtual Environments*, 6(1):87–105.
- [62] Goodman, C. S. (1998). Technology assessment: A tool for technology management and improved patient outcomes. *The Lewin Group*.
- [63] Greco, A., Benvenuti, S. M., Gentili, C., Palomba, D., Valenza, G., and Scilingo, E. P. (2017). Nonlinear analysis of heart rate variability for the assessment of dysphoria. In *2017 39th Annual International Conference of the IEEE Engineering in Medicine and Biology Society (EMBC)*, pages 3170–3173. IEEE.
- [64] Greco, A., Faes, L., Catrambone, V., Barbieri, R., Scilingo, E. P., and Valenza, G. (2019). Lateralization of directional brain-heart information transfer during visual emotional elicitation. *American Journal of Physiology-Regulatory, Integrative and Comparative Physiology*.
- [65] Greco, A., Valenza, G., Lanata, A., Scilingo, E. P., and Citi, L. (2016). cvxeda: A convex optimization approach to electrodermal activity processing. *IEEE Transactions on Biomedical Engineering*, 63(4):797–804.
- [66] Halton, J. (2008). Virtual rehabilitation with video games: A new frontier for occupational therapy. *Occupational therapy now*, 9(6):12–14.
- [67] Hanna, M. G., Ahmed, I., Nine, J., Prajapati, S., and Pantanowitz, L. (2018). Augmented reality technology using microsoft hololens in anatomic pathology. *Archives of pathology & laboratory medicine*, 142(5):638–644.

- [68] Harmo, P., Taipalus, T., Knuuttila, J., Vallet, J., and Halme, A. (2005). Needs and solutions-home automation and service robots for the elderly and disabled. In *Intelligent Robots and Systems, 2005.(IROS 2005). 2005 IEEE/RSJ International Conference on*, pages 3201–3206. IEEE.
- [69] Hassard, J., Teoh, K. R., Visockaite, G., Dewe, P., and Cox, T. (2017). The cost of work-related stress to society: A systematic review.
- [70] Hodges, L. F., Kooper, R., Meyer, T. C., Rothbaum, B. O., Opdyke, D., De Graaff, J. J., Williford, J. S., and North, M. M. (1995). Virtual environments for treating the fear of heights. *Computer*, 28(7):27–34.
- [71] Hodges, L. F., Watson, B. A., Kessler, G. D., Rothbaum, B. O., and Opdyke, D. (1996). Virtually conquering fear of flying. *IEEE Computer Graphics and Applications*, 16(6):42–49.
- [72] Horwitz, B. (2003). The elusive concept of brain connectivity. *Neuroimage*, 19(2):466–470.
- [73] Hou, X., Liu, Y., Sourina, O., Tan, Y. R. E., Wang, L., and Mueller-Wittig, W. (2015). Eeg based stress monitoring. In *Systems, Man, and Cybernetics (SMC), 2015 IEEE International Conference on*, pages 3110–3115. IEEE.
- [74] Hsu, C.-H. and Chow, J. C. (2005). Design and clinic monitoring of a newly developed non-attached infant apnea monitor. *Biomedical Engineering: Applications, Basis and Communications*, 17(03):126–134.
- [75] Huang, H., Wu, S., Cohen-Or, D., Gong, M., Zhang, H., Li, G., and Chen, B. (2013). L1-medial skeleton of point cloud. *ACM Trans. Graph.*, 32(4):65–1.
- [76] Huysmans, D., Smets, E., De Raedt, W., Van Hoof, C., Bogaerts, K., Van Diest, I., and Helic, D. (2018). Unsupervised learning for mental stress detection-exploration of self-organizing maps. Scitepress.
- [77] Ichinose, W., Reinkensmeyer, D., Aoyagi, D., Lin, J., Ngai, K., Edgerton, V. R., Harkema, S., and Bobrow, J. (2003). A robotic device for measuring and controlling pelvic motion during locomotor rehabilitation. In *Proceedings of the 25th Annual International Conference of the IEEE Engineering in Medicine and Biology Society (IEEE Cat. No. 03CH37439)*, volume 2, pages 1690–1693. IEEE.
- [78] JCGM (2008). 100: 2008 (GUM 1995 with minor corrections) Evaluation of measurement data - Guide to the expression of uncertainty in measurement. *Joint Committee for Guides in Metrology*.
- [79] Josman, N., Kizony, R., Hof, E., Goldenberg, K., Weiss, P. L., and Klinger, E. (2014). Using the virtual action planning-supermarket for evaluating executive functions in people with stroke. *Journal of Stroke and Cerebrovascular Diseases*, 23(5):879–887.
- [80] Kemeny, M. E. (2003). The psychobiology of stress. *Current directions in psychological science*, 12(4):124–129.

- [81] Kim, K., Kim, J., Ku, J., Kim, D. Y., Chang, W. H., Shin, D. I., Lee, J. H., Kim, I. Y., and Kim, S. I. (2004). A virtual reality assessment and training system for unilateral neglect. *Cyberpsychology & Behavior*, 7(6):742–749.
- [82] Koenig, A., Wellner, M., Köneke, S., Meyer-Heim, A., Lünenburger, L., and Riener, R. (2008). Virtual gait training for children with cerebral palsy using the lokomat gait orthosis. *Studies in health technology and informatics*, 132:204–209.
- [83] Kopyt, A., Zuzewicz, K., and Bartuzi, P. (2017). Experimental identification of a mathematical model of human operator working under mental stress. *Acta of Bioengineering & Biomechanics*, 19(3).
- [84] Krapp, K. (2002). Activities of daily living evaluation., encyclopedia of nursing & allied health. gale group. Inc: USA.
- [85] Kubota, Y., Sato, W., Toichi, M., Murai, T., Okada, T., Hayashi, A., and Sengoku, A. (2001). Frontal midline theta rhythm is correlated with cardiac autonomic activities during the performance of an attention demanding meditation procedure. *Cognitive Brain Research*, 11(2):281–287.
- [86] Kujala, S. (2003). User involvement: a review of the benefits and challenges. *Behaviour & information technology*, 22(1):1–16.
- [87] Kuo, T. B., Chen, C.-Y., Hsu, Y.-C., and Yang, C. C. (2016). Eeg beta power and heart rate variability describe the association between cortical and autonomic arousals across sleep. *Autonomic Neuroscience*, 194:32–37.
- [88] Lee, J. H., Ku, J., Cho, W., Hahn, W. Y., Kim, I. Y., Lee, S.-M., Kang, Y., Kim, D. Y., Yu, T., Wiederhold, B. K., et al. (2003). A virtual reality system for the assessment and rehabilitation of the activities of daily living. *CyberPsychology & Behavior*, 6(4):383–388.
- [89] Levy, R. M. (2012). The virtual reality revolution: The vision and the reality. In *Virtual Reality-Human Computer Interaction*. IntechOpen.
- [90] Li, W., Lam-Damji, S., Chau, T., and Fehlings, D. (2009). The development of a home-based virtual reality therapy system to promote upper extremity movement for children with hemiplegic cerebral palsy. *Technology and Disability*, 21(3):107–113.
- [91] Liu, L., Miyazaki, M., and Watson, B. (1999). Norms and validity of the drivr: A virtual reality driving assessment for persons with head injuries. *Cyberpsychology & Behavior*, 2(1):53–67.
- [92] Ljung, L. (1987). *System identification: theory for the user*. Prentice-hall.
- [93] Lopez, N. M., Ponce, S., Piccinini, D., Perez, E., and Roberti, M. (2016). From hospital to home care: Creating a domotic environment for elderly and disabled people. *IEEE pulse*, 7(3):38–41.
- [94] Malik, M., Bigger, J. T., Camm, A. J., Kleiger, R. E., Malliani, A., Moss, A. J., and Schwartz, P. J. (1996). Heart rate variability: Standards of measurement, physiological interpretation, and clinical use. *European heart journal*, 17(3):354–381.

- [95] Marín-Morales, J., Higuera-Trujillo, J. L., Greco, A., Guixeres, J., Llinares, C., Scilingo, E. P., Alcañiz, M., and Valenza, G. (2018). Affective computing in virtual reality: emotion recognition from brain and heartbeat dynamics using wearable sensors. *Scientific reports*, 8(1):13657.
- [96] MartíNez, S. and Bullo, F. (2006). Optimal sensor placement and motion coordination for target tracking. *Automatica*, 42(4):661–668.
- [97] Martini, R., Rios, J., Polatajko, H., Wolf, T., and McEwen, S. (2015). The performance quality rating scale (pqrs): reliability, convergent validity, and internal responsiveness for two scoring systems. *Disability and rehabilitation*, 37(3):231–238.
- [98] Masaoka, Y. and Homma, I. (1997). Anxiety and respiratory patterns: their relationship during mental stress and physical load. *International Journal of Psychophysiology*, 27(2):153–159.
- [99] Masè, M., Mattei, W., Cucino, R., Faes, L., and Nollo, G. (2011). Feasibility of cuff-free measurement of systolic and diastolic arterial blood pressure. *Journal of electrocardiology*, 44(2):201–207.
- [100] Maule, L., Fornaser, A., Leuci, M., Conci, N., Da Lio, M., and De Cecco, M. (2016). Development of innovative hmi strategies for eye controlled wheelchairs in virtual reality. In *International Conference on Augmented Reality, Virtual Reality and Computer Graphics*, pages 358–377. Springer.
- [101] Mayr, A., Kofler, M., Quirbach, E., Matzak, H., Fröhlich, K., and Saltuari, L. (2007). Prospective, blinded, randomized crossover study of gait rehabilitation in stroke patients using the lokomat gait orthosis. *Neurorehabilitation and neural repair*, 21(4):307–314.
- [102] Merino Monge, M., Gómez González, I. M., and Molina Cantero, A. J. (2015). Eeg feature variations under stress situations. In *EMBC 2015: 37th Annual International Conference of the IEEE Engineering in Medicine and Biology Society (2015)*, p 6700-6703, pages 6700–6703. IEEE Computer Society.
- [103] Miori, V. and Russo, D. (2017). Improving life quality for the elderly through the social internet of things (siot). In *Global Internet of Things Summit (GIoTS), 2017*, pages 1–6. IEEE.
- [104] Mohino-Herranz, I., Gil-Pita, R., Ferreira, J., Rosa-Zurera, M., and Seoane, F. (2015). Assessment of mental, emotional and physical stress through analysis of physiological signals using smartphones. *Sensors*, 15(10):25607–25627.
- [105] Moody, G. B., Mark, R. G., Bump, M. A., Weinstein, J. S., Berman, A. D., Mietus, J. E., and Goldberger, A. L. (1986). Clinical validation of the ecg-derived respiration (edr) technique. *Computers in cardiology*, 13:507–510.
- [106] Moon, S., Park, Y., Ko, D. W., and Suh, I. H. (2016). Multiple kinect sensor fusion for human skeleton tracking using kalman filtering. *International Journal of Advanced Robotic Systems*, 13(2):65.
- [107] Muthukumaraswamy, S. (2013). High-frequency brain activity and muscle artifacts in meg/eeg: a review and recommendations. *Frontiers in human neuroscience*, 7:138.

- [108] Noelker, L., Browdie, R., and Sidney Katz, M. (2013). A new paradigm for chronic illness and long-term care. *Gerontologist*, 8(6):1–8.
- [109] Nunez, P. L., Srinivasan, R., et al. (2006). *Electric fields of the brain: the neurophysics of EEG*. Oxford University Press, USA.
- [110] Orini, M., Citi, L., and Barbieri, R. (2012). Bivariate point process modeling and joint non-stationary analysis of pulse transit time and heart period. In *Engineering in Medicine and Biology Society (EMBC), 2012 Annual International Conference of the IEEE*, pages 2831–2834. IEEE.
- [111] Oweis, R. J. and Al-Tabbaa, B. O. (2014). Qrs detection and heart rate variability analysis: A survey. *Biomedical science and engineering*, 2(1):13–34.
- [112] Pagliari, D. and Pinto, L. (2015). Calibration of kinect for xbox one and comparison between the two generations of microsoft sensors. *Sensors*, 15(11):27569–27589.
- [113] Pandit, S. V. and Jalife, J. (2013). Rotors and the dynamics of cardiac fibrillation. *Circulation research*, 112(5):849–862.
- [114] Pantelopoulos, A. and Bourbakis, N. G. (2010). A survey on wearable sensor-based systems for health monitoring and prognosis. *Part C (Applications and Reviews) IEEE Transactions on Systems, Man, and Cybernetics*, 40(1):1–12.
- [115] Patel, S., Park, H., Bonato, P., Chan, L., and Rodgers, M. (2012). A review of wearable sensors and systems with application in rehabilitation. *Journal of NeuroEngineering and Rehabilitation*.
- [116] Pathirana, P. N., Li, S., Trinh, H. M., and Seneviratne, A. (2016). Robust real-time bio-kinematic movement tracking using multiple kinects for tele-rehabilitation. *IEEE Transactions on Industrial Electronics*, 63(3):1822–1833.
- [117] Pelargos, P. E., Nagasawa, D. T., Lagman, C., Tenn, S., Demos, J. V., Lee, S. J., Bui, T. T., Barnette, N. E., Bhatt, N. S., Ung, N., et al. (2017). Utilizing virtual and augmented reality for educational and clinical enhancements in neurosurgery. *Journal of Clinical Neuroscience*, 35:1–4.
- [118] Pernice, R., Zanetti, M., Nollo, G., De Cecco, M., Busacca, A., and Faes, L. (2019). Mutual information analysis of brain-body interactions during different levels of mental stress. In *IEEE EMBC 2019, Proceeding*. IEEE.
- [119] Pisoni, T., Conci, N., De Natale, F. G., De Cecco, M., Nollo, G., Frattari, A., and Guandalini, G. M. (2016). Ausilia: assisted unit for simulating independent living activities. In *2016 IEEE International Smart Cities Conference (ISC2)*, pages 1–4. IEEE.
- [120] Porta, A., D’Addio, G., Guzzetti, S., Lucini, D., and Pagani, M. (2004). Testing the presence of non stationarities in short heart rate variability series. In *Proc. Computers in Cardiology*, pages 645–648.
- [121] Porta, A., Faes, L., Nollo, G., Bari, V., Marchi, A., De Maria, B., Takahashi, A. C., and Catai, A. M. (2015). Conditional self-entropy and conditional joint transfer entropy in heart period variability during graded postural challenge. *PLoS One*, 10(7):e0132851.

- [122] Pratt, D. R., Zyda, M., and Kelleher, K. (1995). Virtual reality: in the mind of the beholder. *Computer*, (7):17–19.
- [123] Rashidi, P. and Mihailidis, A. (2013). A survey on ambient-assisted living tools for older adults. *IEEE journal of biomedical and health informatics*, 17(3):579–590.
- [124] Reyes del Paso, G. A., Langewitz, W., Mulder, L. J., Van Roon, A., and Duschek, S. (2013). The utility of low frequency heart rate variability as an index of sympathetic cardiac tone: a review with emphasis on a reanalysis of previous studies. *Psychophysiology*, 50(5):477–487.
- [125] Robinson, H., MacDonald, B., and Broadbent, E. (2014). The role of healthcare robots for older people at home: A review. *International Journal of Social Robotics*, 6(4):575–591.
- [126] Rothbaum, B. O., Hodges, L., Watson, B. A., Kessler, G. D., and Opdyke, D. (1996). Virtual reality exposure therapy in the treatment of fear of flying: A case report. *Behaviour Research and Therapy*, 34(5-6):477–481.
- [127] Rothmann, M. J., Danbjørg, D. B., Jensen, C. M., and Clemensen, J. (2016). Participatory design in health care: participation, power and knowledge. In *Proceedings of the 14th Participatory Design Conference: Short Papers, Interactive Exhibitions, Workshops-Volume 2*, pages 127–128. ACM.
- [128] Saeed, S. M. U., Anwar, S. M., Majid, M., and Bhatti, A. M. (2015). Psychological stress measurement using low cost single channel eeg headset. In *Signal Processing and Information Technology (ISSPIT), 2015 IEEE International Symposium on*, pages 581–585. IEEE.
- [129] Sanchez, R., Wolbrecht, E., Smith, R., Liu, J., Rao, S., Cramer, S., Rahman, T., Bobrow, J. E., and Reinkensmeyer, D. J. (2005). A pneumatic robot for re-training arm movement after stroke: Rationale and mechanical design. In *9th International Conference on Rehabilitation Robotics, 2005. ICORR 2005.*, pages 500–504. IEEE.
- [130] Sandulescu, V., Andrews, S., Ellis, D., Bellotto, N., and Mozos, O. M. (2015). Stress detection using wearable physiological sensors. In *International Work-Conference on the Interplay Between Natural and Artificial Computation*, pages 526–532. Springer.
- [131] Saposnik, G., Teasell, R., Mamdani, M., Hall, J., McIlroy, W., Cheung, D., Thorpe, K. E., Cohen, L. G., and Bayley, M. (2010). Effectiveness of virtual reality using wii gaming technology in stroke rehabilitation: a pilot randomized clinical trial and proof of principle. *Stroke*, 41(7):1477–1484.
- [132] Sarnoff, S. J. (1955). Myocardial contractility as described by ventricular function curves; observations on starling’s law of the heart. *Physiological reviews*, 35(1):107–122.
- [133] Schäfer, C., Rosenblum, M. G., Kurths, J., and Abel, H.-H. (1998). Heartbeat synchronized with ventilation. *nature*, 392(6673):239.
- [134] Schiatti, L., Nollo, G., Rossato, G., and Faes, L. (2015). Extended granger causality: a new tool to identify the structure of physiological networks. *Physiological measurement*, 36(4):827.

- [135] Schulz, S., Adochiei, F.-C., Edu, I.-R., Schroeder, R., Costin, H., Bär, K.-J., and Voss, A. (2013). Cardiovascular and cardiorespiratory coupling analyses: a review. *Philosophical Transactions of the Royal Society A: Mathematical, Physical and Engineering Sciences*, 371(1997):20120191.
- [136] Selye, H. (1976). Stress without distress. In *Psychopathology of human adaptation*, pages 137–146. Springer.
- [137] Seo, S.-H. and Lee, J.-T. (2010). Stress and eeg. In *Convergence and hybrid information technologies*. InTech.
- [138] Seoane, F., Mohino-Herranz, I., Ferreira, J., Alvarez, L., Buendia, R., Ayllón, D., Llerena, C., and Gil-Pita, R. (2014). Wearable biomedical measurement systems for assessment of mental stress of combatants in real time. *Sensors*, 14(4):7120–7141.
- [139] Shahidi, B., Haight, A., and Maluf, K. (2013). Differential effects of mental concentration and acute psychosocial stress on cervical muscle activity and posture. *Journal of electromyography and kinesiology*, 23(5):1082–1089.
- [140] Sharma, N. and Gedeon, T. (2012). Objective measures, sensors and computational techniques for stress recognition and classification: A survey. *Computer methods and programs in biomedicine*, 108(3):1287–1301.
- [141] Shotton, J., Sharp, T., Kipman, A., Fitzgibbon, A., Finocchio, M., Blake, A., Cook, M., and Moore, R. (2013). Real-time human pose recognition in parts from single depth images. *Communications of the ACM*, 56(1):116–124.
- [142] Shuhaiber, J. H. (2004). Augmented reality in surgery. *Archives of surgery*, 139(2):170–174.
- [143] Sinex, J. E. (1999). Pulse oximetry: principles and limitations. *The American journal of emergency medicine*, 17(1):59–66.
- [144] Singh, M. and Narang, M. (2014). Changes in brain wave rhythms during tasks involving attention and working memory. *International journal of information technology and knowledge management*, 7(2):71–97.
- [145] Singh, M. and Queyam, A. B. (2013). A novel method of stress detection using physiological measurements of automobile drivers. *International Journal of Electronics Engineering*, 5(2):13–20.
- [146] Sioni, R. and Chittaro, L. (2015). Stress detection using physiological sensors. *Computer*, 48(10):26–33.
- [147] Smets, E., Casale, P., Großekathöfer, U., Lamichhane, B., De Raedt, W., Bogaerts, K., Van Diest, I., and Van Hoof, C. (2015). Comparison of machine learning techniques for psychophysiological stress detection. In *International Symposium on Pervasive Computing Paradigms for Mental Health*, pages 13–22. Springer.
- [148] Speranza, G., Nollo, G., Ravelli, F., and Antolini, R. (1993). Beat-to-beat measurement and analysis of the rt interval in 24 h ecg holter recordings. *Medical and Biological Engineering and Computing*, 31(5):487–494.

- [149] Steinheuser, V., Ackermann, K., Schönfeld, P., and Schwabe, L. (2014). Stress and the city: impact of urban upbringing on the (re) activity of the hypothalamus-pituitary-adrenal axis. *Psychosomatic medicine*, 76(9):678–685.
- [150] Steward, J., Lichti, D., Chow, J., Ferber, R., and Osis, S. (2015). Performance assessment and calibration of the kinect 2.0 time-of-flight range camera for use in motion capture applications. *FIG Working Week 2015*, pages 1–14.
- [151] Subhani, A. R., Malik, A. S., Kamil, N., and Saad, M. N. M. (2016). Difference in brain dynamics during arithmetic task performed in stress and control conditions. In *Biomedical Engineering and Sciences (IECBES), 2016 IEEE EMBS Conference on*, pages 695–698. IEEE.
- [152] Subhani, A. R., Mumtaz, W., Saad, M. N. B. M., Kamel, N., and Malik, A. S. (2017). Machine learning framework for the detection of mental stress at multiple levels. *IEEE Access*, 5:13545–13556.
- [153] Sunagawa, K., Kawada, T., and Nakahara, T. (1998). Dynamic nonlinear vago-sympathetic interaction in regulating heart rate. *Heart and vessels*, 13(4):157–174.
- [154] Tang, Y., Li, Y., Wang, J., Tong, S., Li, H., and Yan, J. (2011). Induced gamma activity in eeg represents cognitive control during detecting emotional expressions. In *2011 Annual International Conference of the IEEE Engineering in Medicine and Biology Society*, pages 1717–1720. IEEE.
- [155] Tran, Y., Thuraisingham, R., Wijesuriya, N., Nguyen, H., and Craig, A. (2007). Detecting neural changes during stress and fatigue effectively: a comparison of spectral analysis and sample entropy. In *Neural Engineering, 2007. CNE'07. 3rd International IEEE/EMBS Conference on*, pages 350–353. IEEE.
- [156] Umeyama, S. (1991). Least-squares estimation of transformation parameters between two point patterns. *IEEE Transactions on pattern analysis and machine intelligence*, 13(4):376–380.
- [157] United Nations, Department of Economic and Social Affairs, Population Division (2015a). World population ageing 2015 (st/esa/ser. a/390).
- [158] United Nations, Department of Economic and Social Affairs, Population Division (2015b). World population prospects: The 2015 revision, key findings and advance tables. *Working Paper, No. ESA/P/WP. 241*.
- [159] Vaccarino, V., Sullivan, S., Hammadah, M., Wilmot, K., Al Mheid, I., Ramadan, R., Elon, L., Pimple, P. M., Garcia, E. V., Nye, J., et al. (2018). Mental stress-induced-myocardial ischemia in young patients with recent myocardial infarction: Sex differences and mechanisms. *Circulation*, 137(8):794–805.
- [160] Valente, M., Javorka, M., Porta, A., Bari, V., Krohova, J., Czippelova, B., Turianikova, Z., Nollo, G., and Faes, L. (2018). Univariate and multivariate conditional entropy measures for the characterization of short-term cardiovascular complexity under physiological stress. *Physiological measurement*, 39(1):014002.

- [161] Valente, M., Javorka, M., Turianikova, Z., Czippelova, B., Krohova, J., Nollo, G., and Faes, L. (2017). Cardiovascular and respiratory variability during orthostatic and mental stress: A comparison of entropy estimators. In *Engineering in Medicine and Biology Society (EMBC), 2017 39th Annual International Conference of the IEEE*, pages 3481–3484. IEEE.
- [162] Valenza, G., Citi, L., Saul, P., and Barbieri, R. (2018). Ecg-derived sympathetic and parasympathetic nervous system dynamics: A congestive heart failure study. In *CinC*.
- [163] Valenza, G., Lanata, A., and Scilingo, E. P. (2012). The role of nonlinear dynamics in affective valence and arousal recognition. *IEEE transactions on affective computing*, 3(2):237–249.
- [164] Valenza, G., Toschi, N., and Barbieri, R. (2016). Uncovering brain–heart information through advanced signal and image processing. *Philosophical transactions. Series A, Mathematical, physical, and engineering sciences*, 374(2067).
- [165] Van Diest, I., Bradley, M. M., Guerra, P., Van den Bergh, O., and Lang, P. J. (2009). Fear-conditioned respiration and its association to cardiac reactivity. *Biological psychology*, 80(2):212–217.
- [166] Vanitha, V. and Krishnan, P. (2016). Real time stress detection system based on eeg signals. *Biomedical Research*.
- [167] Visnovcova, Z., Mestanik, M., Javorka, M., Mokra, D., Gala, M., Jurko, A., Calkovska, A., and Tonhajzerova, I. (2014). Complexity and time asymmetry of heart rate variability are altered in acute mental stress. *Physiological measurement*, 35(7):1319.
- [168] Vlemincx, E., Taelman, J., De Peuter, S., Van Diest, I., and Van Den Bergh, O. (2011). Sigh rate and respiratory variability during mental load and sustained attention. *Psychophysiology*, 48(1):117–120.
- [169] Vlemincx, E., Van Diest, I., and Van den Bergh, O. (2012). A sigh following sustained attention and mental stress: effects on respiratory variability. *Physiology & behavior*, 107(1):1–6.
- [170] Wesseling, K. (1996). Finger arterial pressure measurement with finapres. *Zeitschrift fur Kardiologie*, 85:38–44.
- [171] Widjaja, D., Montalto, A., Vlemincx, E., Marinazzo, D., Van Huffel, S., and Faes, L. (2015). Cardiorespiratory information dynamics during mental arithmetic and sustained attention. *PLoS One*, 10(6):e0129112.
- [172] Wijsman, J., Grundlehner, B., Penders, J., and Hermens, H. (2010). Trapezius muscle emg as predictor of mental stress. In *Wireless Health 2010*, pages 155–163. ACM.
- [173] Wilson, P. (1997). Smart communities guidebook. *Governor of California, CA, USA*.
- [174] Xhyheri, B., Manfrini, O., Mazzolini, M., Pizzi, C., and Bugiardini, R. (2012). Heart rate variability today. *Progress in cardiovascular diseases*, 55(3):321–331.

- [175] Xiang, L., Echtler, F., Kerl, C., Wiedemeyer, T., Lars, hanyazou, Gordon, R., Facioni, F., laborer2008, Wareham, R., Goldhoorn, M., alberth, gaborpapp, Fuchs, S., jmtatsch, Blake, J., Federico, Jungkurth, H., Mingze, Y., vinouz, Coleman, D., Burns, B., Rawat, R., Mokhov, S., Reynolds, P., Viau, P., Fraissinet-Tachet, M., Ludique, Billingham, J., and Alistair (2016). libfreenect2: Release 0.2.
- [176] Yang, L., Zhang, L., Dong, H., Alelaiwi, A., and El Saddik, A. (2015). Evaluating and improving the depth accuracy of kinect for windows v2. *IEEE Sensors Journal*, 15(8):4275–4285.
- [177] Yang, S., Hwang, W.-H., Tsai, Y.-C., Liu, F.-K., Hsieh, L.-F., and Chern, J.-S. (2011). Improving balance skills in patients who had stroke through virtual reality treadmill training. *American journal of physical medicine & rehabilitation*, 90(12):969–978.
- [178] Ye, S.-y., Kim, G.-R., Jung, D.-K., Baik, S., and Jeon, G. (2010). Estimation of systolic and diastolic pressure using the pulse transit time. *World Academy of Science, Engineering and Technology*, 67:726–731.
- [179] Zanetti, M., Faes, L., De Cecco, M., Fornaser, A., Valente, M., Guandalini, G., and Nollo, G. (2018). Assessment of mental stress through the analysis of physiological signals acquired from wearable devices. In *Italian Forum of Ambient Assisted Living*, pages 243–256. Springer.
- [180] Zanetti, M., Faes, L., Nollo, G., De Cecco, M., Pernice, R., Maule, L., Pertile, M., and Fornaser, A. (2019). Information dynamics of the brain, cardiovascular and respiratory network during different levels of mental stress. *Entropy*, 21(3):275.
- [181] Zhang, L., Sturm, J., Cremers, D., and Lee, D. (2012). Real-time human motion tracking using multiple depth cameras. In *2012 IEEE/RSJ International Conference on Intelligent Robots and Systems*, pages 2389–2395. IEEE.
- [182] Zheng, R., Yamabe, S., Nakano, K., and Suda, Y. (2015). Biosignal analysis to assess mental stress in automatic driving of trucks: Palmar perspiration and masseter electromyography. *Sensors*, 15(3):5136–5150.